

Review

# Preparation and Photocatalytic Activities of TiO<sub>2</sub>-Based Composite Catalysts

Huaitao Yang<sup>1</sup>, Beibei Yang<sup>1</sup>, Wei Chen<sup>1</sup> and Junjiao Yang<sup>1,2,\*</sup><sup>1</sup> College of Chemistry, Beijing University of Chemical Technology, Beijing 100029, China<sup>2</sup> Analysis and Test Center of Beijing University of Chemical Technology, Beijing University of Chemical Technology, Beijing 100029, China

\* Correspondence: yangjj@mail.buct.edu.cn

**Abstract:** While modern industry has contributed to the prosperity of an increasingly urbanized society, it has also led to serious pollution problems, with discharged wastewater and exhaust gases causing significant environmental harm. Titanium dioxide (TiO<sub>2</sub>), which is an excellent photocatalyst, has received extensive attention because it is inexpensive and able to photocatalytically degrade pollutants in an environmentally friendly manner. TiO<sub>2</sub> has many advantages, including high chemical stability, low toxicity, low operating costs, and environmental friendliness. TiO<sub>2</sub> is an N-order semiconductor material with a bandgap of 3.2 eV. Only when the wavelength of ultraviolet light is less than or equal to 387.5 nm, the valence band electrons can obtain the energy of the photon and pass through the conduction band to form photoelectrons, meanwhile the valence band forms a photogenerated hole. And light in other wavelength regions does not excite this photogenerated electrons. The most common methods used to improve the photocatalytic efficiency of TiO<sub>2</sub> involve increasing its photoresponse range and reducing photogenerated-carrier coupling. The morphology, size, and structure of a heterojunction can be altered through element doping, leading to improved photocatalytic efficiency. Mainstream methods for preparing TiO<sub>2</sub> are reviewed in this paper, with several excellent preparation schemes for improving the photocatalytic efficiency of TiO<sub>2</sub> introduced. TiO<sub>2</sub> is mainly prepared using sol-gel, solvothermal, hydrothermal, anodic oxidation, microwave-assisted, CVD and PVD methods, and TiO<sub>2</sub> nanoparticles with excellent photocatalytic properties can also be prepared. Ti-containing materials are widely used to purify harmful gases, as well as contaminants from building materials, coatings, and daily necessities. Therefore, the preparation and applications of titanium materials have become globally popular research topics.

**Keywords:** titanium dioxide; titania preparation; composite catalyst; photodegradation

**Citation:** Yang, H.; Yang, B.; Chen, W.; Yang, J. Preparation and Photocatalytic Activities of TiO<sub>2</sub>-Based Composite Catalysts. *Catalysts* **2022**, *12*, 1263. <https://doi.org/10.3390/catal12101263>

Academic Editor: Magdalena Janus

Received: 25 September 2022

Accepted: 11 October 2022

Published: 17 October 2022

**Publisher's Note:** MDPI stays neutral with regard to jurisdictional claims in published maps and institutional affiliations.



**Copyright:** © 2022 by the authors. Licensee MDPI, Basel, Switzerland. This article is an open access article distributed under the terms and conditions of the Creative Commons Attribution (CC BY) license (<https://creativecommons.org/licenses/by/4.0/>).

## 1. Introduction

Several environmental pollution problems have become increasingly prominent since the beginning of the 21st century, a result of the rapid development of industry and technology, with air pollution attracting considerable attention as a societal problem [1]. Increasing quality-of-life demands have focused attention on the control and remediation of air pollution as urgent problems that need to be solved. Statistical surveys show that people spend more than 80% of their time in indoor spaces, such as office buildings, shopping malls, and residential buildings. Modern upholstery, adhesives, paints, and other building materials, as well as furniture, continuously release a variety of pollutants, especially volatile organic compounds (VOCs), including alkanes, aromatic hydrocarbons (such as toluene), esters, olefins, and aldehydes (such as formaldehyde) [2]. Humans can experience chest tightness, nausea, dry mouths, coughing, fatigue, dizziness, various cardiopulmonary diseases (in severe cases), and even cancer when exposed to polluted air for prolonged times [3–5].

In 1972, Fujishima and Honda first proposed that TiO<sub>2</sub> can be irradiated with light to split water and generate hydrogen [6]. TiO<sub>2</sub> photocatalysis has been extensively researched

over the ensuing decades, which has promoted the progress of TiO<sub>2</sub> photocatalysis technology. At the same time, this technology has been used to treat sewage and purify air [7], with photocatalytic oxidation technology used to degrade various pollutants and thoroughly mineralize organic matter, thereby avoiding secondary pollution; in addition, TiO<sub>2</sub> inhibits airborne bacteria. Continuous scientific exploration has led to photocatalysts that exhibit high pollutant-degradation efficiencies, are simple to maintain, are relatively cost-effective, and are widely applicable, which makes this technology promising as a purification method.

Photocatalysis effectively uses solar energy to degrade pollutants and reduce carbon dioxide, and it is a potential means of solving environmental problems, including the greenhouse effect [8–12]. Although many semiconductor materials are photocatalytically active, some semiconductor catalysts are poorly reactive, photocorrode, and exhibit other factors that limit their wide applicability; such semiconductor materials include TiO<sub>2</sub>, WO<sub>3</sub>, Fe<sub>x</sub>O<sub>y</sub>, V<sub>2</sub>O<sub>5</sub>, MnO<sub>2</sub>, ZnO, CdS, and PbS, among others [13–20]. Among the many photocatalytic semiconductor materials, TiO<sub>2</sub> materials have been widely studied and used to photocatalytically produce hydrogen and in photodegradation applications, which is ascribable to their excellent properties, including wide availability, chemical stability, high catalytic activity, resistance to photocorrosion, and lack of toxicity [21]. TiO<sub>2</sub> is considered to be one of the most promising materials in the photocatalysis field and has attracted significant attention [22–25].

Despite the outstanding advantages of TiO<sub>2</sub>, some disadvantages limit its air-purification applications. For example, TiO<sub>2</sub> has a wide bandgap and can only be excited by UV light, which results in a low visible light utilization rate. Secondly, the electrons and holes generated by the excitation of TiO<sub>2</sub> easily recombine, which results in a low quantum efficiency. The photocatalysis reaction is slow in practical applications, which leads to a low pollutant degradation efficiency. Many reports aimed at improving the photoresponse range and quantum efficiency of TiO<sub>2</sub> by compounding with non-metallic [26–29] and noble metal [30–36] dopants, or by modifying the morphology of TiO<sub>2</sub> [37–39], have appeared in the literature, along with other methods for improving the adsorption performance of the photocatalyst.

This paper mainly reviews research progress on titanium dioxide, in terms of its preparation and applications (as shown in Figure 1). Titanium dioxide photodegradation catalysts with specific electronic structures are prepared by doping, isomerization, particle-size control, and other means, and they are used to purify air by removing harmful gases, as well as contaminants from building material, medicines, and other daily necessities. Problems and challenges that face titanium dioxide research into air-pollution and water remediation are analyzed and discussed.

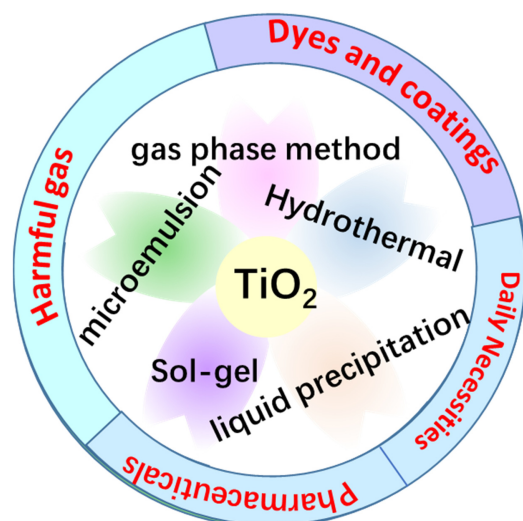
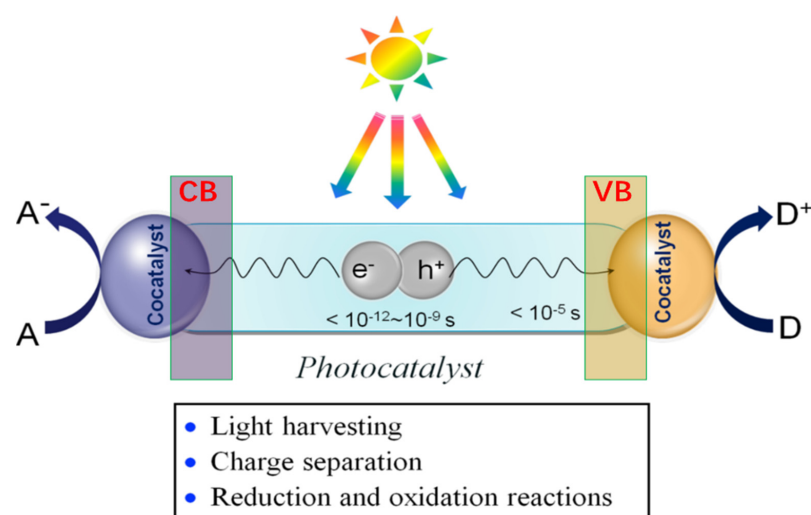


Figure 1. TiO<sub>2</sub> preparation methods and applications.

## 2. Photocatalysis Mechanism for TiO<sub>2</sub>

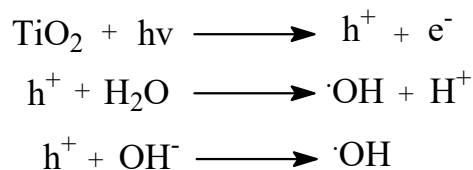
A photocatalysis reaction refers to a process in which the photocatalyst itself does not change when irradiated with light; rather, it converts light energy into chemical energy to promote the production or decomposition of compounds. While photosynthesis is the most representative example of photocatalysis in nature [40], the most widely studied and applied photocatalysts are semiconductor-based. A semiconductor is a material whose conductivity lies between that of a conductor and an insulator. The lowest energy level occupied by valence electrons in the electronic energy band structure of a semiconductor is referred to as the “valence band”, and the lowest unoccupied energy level is referred to as the “conduction band”. The energy region between the conduction and valence bands is referred to as the “forbidden band”, which is a discontinuous region whose width depends on crystal structure and interatomic relationships and is a characteristic parameter of a semiconductor material [41]. The energy band structure of a semiconductor affects light absorption and the photocatalytic performance of the material. When a photocatalyst is irradiated with photons with energies greater than the forbidden band width of the semiconductor, the electrons ( $e^-$ ) in the valence band are excited and transition to the conduction band, with holes ( $h^+$ ) simultaneously created in the valence band. Photogenerated electrons are reductive, and photogenerated holes are oxidative; these photogenerated carriers migrate to the catalyst surface to participate in catalytic redox reactions, as shown in the schematic diagram in Figure 2 [42]. The photocatalytic reaction initiates from the generation of electron–hole pairs upon light irradiation. When a semiconductor photocatalyst absorbs photons with energy equal to or greater than its  $E_g$ , the electrons in VB will be excited to CB, leaving the holes in VB. In contrast, photogenerated electrons and holes are trapped by defect sites in the bulk or surface of the catalyst, where they recombine to release photons or heat [43]. Carrier lifetime depends on the rate of photogenerated-carrier recombination; fast recombination leads to short lifetimes, which, in turn, limits the photochemical energy conversion efficiency of the catalyst.



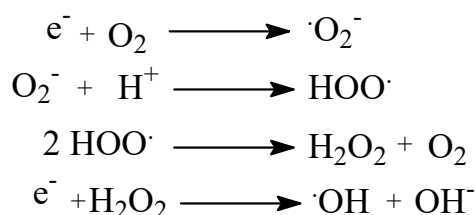
**Figure 2.** Proposed mechanism for a photocatalytic reaction on a semiconductor photocatalyst. Reprinted/adapted with permission from Ref. [42]. 2014, ACS publications.

As TiO<sub>2</sub> is a good semiconductor photocatalyst, its photocatalytic advantages, deficiencies, and preparation methods have been reviewed on many occasions [13,44–58]. Anatase TiO<sub>2</sub> has a forbidden bandwidth of 3.2 eV; therefore, energies greater than this bandwidth will excite electrons ( $e^-$ ) to the conduction band (CB), while leaving  $h^+$  in the top of the valence band (VB) to form electron–hole pairs. The photogenerated electrons and holes are effectively separated by the space-charge layer, with holes transferred to the TiO<sub>2</sub> surface. The photogenerated holes are the main photon energy-derived components that react with

the  $\text{H}_2\text{O}$  or  $\text{OH}^-$  adsorbed on the surface to form  $\cdot\text{OH}$  through strong oxidation [59–62], as shown in the following equation:



The photogenerated electrons can react with  $\text{O}_2$  on the surface to form superoxide radicals ( $\cdot\text{O}_2^-$ ) that are strongly oxidizing. The  $\cdot\text{OH}$  on the surface is also formed in a similar manner:



This reaction generates active free radicals ( $\cdot\text{OH}$ ,  $\cdot\text{O}_2^-$ , and  $\text{HOO}\cdot$ ) and strong oxidizing properties. These radicals can directly mineralize pollutants (mainly organic pollutants) into small inorganic molecules, such as  $\text{CO}_2$  and  $\text{H}_2\text{O}$ , by exploiting their strong oxidizing properties, which completes the water treatment process [63–70].

The diagram in Figure 3 shows a typical photocatalytic mechanism for the  $\text{TiO}_2$  semiconductor that includes several important processes, including the generation of electron–hole pairs, charge transfer, electron–hole-pair recombination on the body or surface, and chemical reactions promoted by electrons and holes on the surface. After electron–hole pair separation, only the separated electrons or holes that migrate to the surface successfully have opportunities to drive the reduction or oxidation reactions, respectively (processes 1 and 3 in Figure 3). However, most of the electrons and holes recombine on the surface or in the bulk, and the energy of the charge carriers is converted to vibrational energy of lattice atoms (phonons) or photons (processes 2 and 4 in Figure 3). Specifically, the entire process involves three steps: (I) the absorption of photons with energies greater than the bandgap energy to generate electron–hole pairs, (II) charge separation and migration to the surface, and (III) redox reactions involving charges and reactants adsorbed on the surface [71–77].

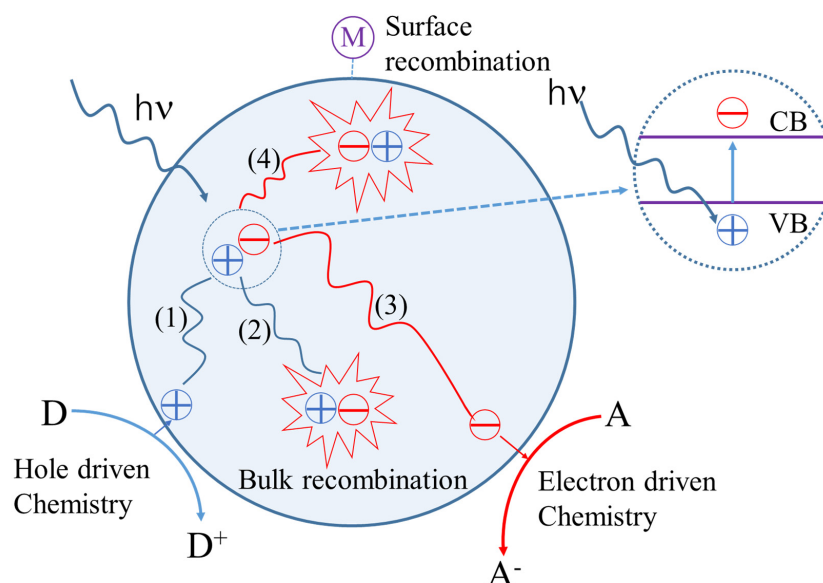


**Figure 3.** Photocatalytic mechanism associated with  $\text{TiO}_2$ .

### 3. Methods for Preparing TiO<sub>2</sub>

The low photocatalytic degradation efficiency of TiO<sub>2</sub> is somewhat limiting. The main factors that determine efficiency include light-absorption capacity, electron–hole separation efficiency, the surface catalytic reaction rate, adsorption capacity for the target reactants, and photochemical stability, and various methods for modifying TiO<sub>2</sub> have been studied with these factors in mind [78–81]. For example, highly crystalline TiO<sub>2</sub> can be prepared using hydrothermal or high-temperature calcination methods to improve the separation efficiency of photogenerated carriers [82,83]. Reducing the number of crystal defects and the photogenerated-carrier-recombination probability, or preparing one-dimensionally structured TiO<sub>2</sub> (i.e., TiO<sub>2</sub> nanobelts or nanowires), can improve the electron–hole separation efficiency.

Nanomaterials with various sizes, morphologies, and properties have been increasingly studied and used in various applications, due to the rapid development of nano-material preparation technologies [84–88]. TiO<sub>2</sub> photocatalysis mainly depends on the photocatalytic material and light source, based on the TiO<sub>2</sub> photocatalysis principles introduced above. Because the light source is an external condition, semiconductor TiO<sub>2</sub> photocatalysis research has focused on the photocatalytic material [89–91]. In this paper, the current methods used to prepare TiO<sub>2</sub> are briefly classified and reviewed to provide the reader with an understanding of how TiO<sub>2</sub> is prepared and how new high-performance photocatalytic materials are developed. TiO<sub>2</sub>-preparation processes are divided into three types, according to the medium used, namely solid-phase, gas-phase, and liquid-phase.

#### 3.1. Solid Phase

Solid-phase methods involve the preparation of raw materials, intermediates, and solid products and have been traditionally used to manufacture TiO<sub>2</sub> nanomaterials, with solid-phase synthesis and comminution techniques commonly used. Solid-phase methods are simple and suitable for mass production on the industrial scale. Although such methods are associated with disadvantages that include high energy consumption, the formation of large particles, and the introduction of impurities, they are still commonly used to prepare TiO<sub>2</sub> nanomaterials [92–94].

Abbas et al. used solid-state reaction technology to prepare Cu-doped TiO<sub>2</sub> by mixing various concentrations of Cu and TiO<sub>2</sub> nanoparticles, followed by calcination, and investigated the surface morphology, size, hardness, roughness, thermal conductivity, and other mechanical properties of each prepared pellet. The prepared Cu-doped TiO<sub>2</sub> contained particles that were approximately 20–30 nm in size [95]. A solid-state reaction method was used to synthesize G-C<sub>3</sub>N<sub>4</sub>/TiO<sub>2</sub> using graphite, carbon nitride, and titanate acid as raw materials. The G-C<sub>3</sub>N<sub>4</sub>/TiO<sub>2</sub> catalyst delivered a 59% methylene blue (MB) degradation rate when irradiated with a 300-W mercury lamp for 5 h [96].

#### 3.2. Gas Phase

Gas-phase methods use gaseous raw materials or convert raw materials into their gaseous states in various ways, after which solid nanoparticles are formed through condensation and deposition by physical or chemical methods. Gas-phase methods are divided into two types: physical and chemical. Gas-phase-prepared nano-TiO<sub>2</sub> is highly pure, contains small particles, and is well-dispersed [97–102].

Wang et al. used a gas-phase oxidation method to prepare TiO<sub>2</sub> nanoparticles by placing TiCl<sub>4</sub> in an oxidation reactor and the studied reaction conditions, such as the reaction temperature, residence time, and toluene flow rate. Larger TiO<sub>2</sub> particles were formed at higher toluene flow rates, higher reaction temperatures, and longer residence times. In addition, the TiO<sub>2</sub> particle size was effectively controlled by the addition of KCl during the reaction [103]. Yuan et al. prepared Ag/TiO<sub>2</sub> thin films using two different magnetron sputtering methods and by taking advantage of the characteristics of nano-TiO<sub>2</sub> films that are easily oxidized in air. The surface microstructure of the Ag/TiO<sub>2</sub> composite film deposited on a fabric surface was observed to be uniform, compact, and smoother than



### 3.3.3. Hydrothermal Synthesis

The hydrothermal synthesis method involves creating a high-temperature and high-pressure reaction environment by heating a reaction autoclave containing an aqueous solution as the reaction medium, which promotes the dissolution and recrystallization of ordinarily insoluble materials. The hydrothermal method is cost-efficient, requires simple equipment, and produces particles with narrow size distributions, which are advantages. However, the high reaction temperatures and pressures of the hydrothermal method require strict equipment safety protocols. The crystal structure and size of the TiO<sub>2</sub> particles are controlled by varying the reaction conditions. TiO<sub>2</sub> powder or a newly prepared titanate hydrolysis gel is often used as a precursor. On the one hand, crystal structure and performance can be further controlled by adjusting the hydrothermal conditions; on the other hand, the recrystallization step in the hydrothermal synthesis protocol produces highly pure products using relatively simple reaction processes and equipment. Yugan et al. studied the morphologies of TiO<sub>2</sub> particles formed at various hydrothermal reaction times, the results of which are shown in Figure 4 [114,115]. Xiao et al. prepared Ce<sup>2+</sup>-doped mesoporous TiO<sub>2</sub> nanomaterials with high specific surface areas using a hydrothermal method. Doping with Ce<sup>2+</sup> ions was found to not only increase the specific surface area of the mesoporous TiO<sub>2</sub> nanoparticles, but also effectively inhibit the mesoporous collapse and transformation of the anatase phase into the rutile phase [116]. Zhiru et al. prepared a graphene-TiO<sub>2</sub> photocatalytic material using a hydrothermal method, which delivered degradation rates of 89% and 91% for MB and rhodamine B (RhB) under xenon lamp light source (Xe300UV) within 60 min, respectively, which are higher than those of pure TiO<sub>2</sub> nanoparticles. Graphene, as a carrier, effectively improves the photodegradation performance of TiO<sub>2</sub> toward pollutants [117].

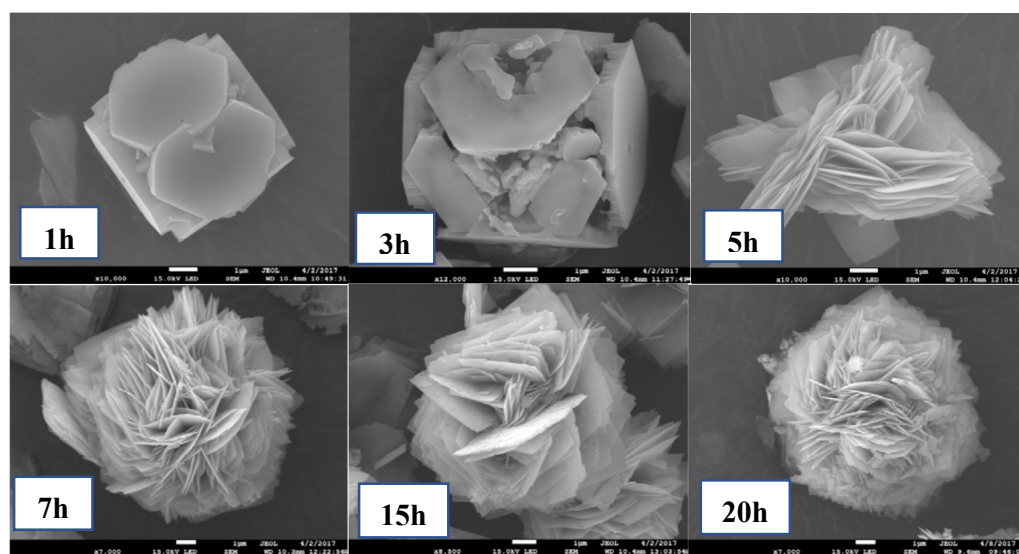


**Figure 4.** SEM images of products obtained in various reaction stages (1 h,3 h,5 h,7 h,15 h, 20 h) [114].

### 3.3.4. Microemulsion Method

The microemulsion method mainly uses emulsifiers, such as surfactants, weakly polar organics, and alcohols, to generate an immiscible emulsion that forms a homogeneous latex that then reacts to produce amorphous TiO<sub>2</sub>; subsequent calcination produces nano-TiO<sub>2</sub> particles. The microemulsion method can be divided into water-in-oil (O/W) and oil-in-water (W/O) micro-latex techniques [118,119]. The microemulsion method does not require heat, uses simple equipment, and produces controllable particles (etc.), which are advantages; however, the stability of the microemulsion is hard to control, and the post-treatment procedure requires washing with an organic solvent, which results in higher costs. Nanoparticles prepared by the microemulsion method are generally spherical or quasi-spherical in shape. Because surfactants and co-surfactants are adsorbed on the

surfaces of the TiO<sub>2</sub> particles, they find it difficult to agglomerate during high-temperature heat treatment, which is conducive to producing well-dispersed TiO<sub>2</sub> nanomaterials. This method produces small particles, is simple to operate, consumes little energy, and is stable, which are advantages; however, removing the organic substances from the surfaces of the particles is difficult because large amounts of surfactants are used. At present, the structures and properties of the microemulsions used in this method need further study, low-cost and easily recycled surfactants need to be sourced, and a production system suitable for industrialization needs to be established [120,121]. Karbasi et al. used the microemulsion method to prepare a series of uniformly shaped Si-TiO<sub>2</sub> particles with narrow particle-size distributions and high photocatalytic activities. Reducing the water content of the system was found to improve the photocatalytic activity of TiO<sub>2</sub>. Higher calcination temperatures led to higher crystallinities, larger particles, and higher MB degradation rates [122].

With the rapid development of scientific research, a variety of physical and chemical methods can be used to prepare TiO<sub>2</sub> particles. Table 1 summarizes the advantages and disadvantages of the common preparation methods of TiO<sub>2</sub>, and the corresponding synthesis methods can be adopted according to the use requirements.

**Table 1.** The advantages and disadvantages of preparation methods of TiO<sub>2</sub>.

Preparation Methods	Advantages	Disadvantages	
Solid phase	1. Simple process 2. Large scale production	1. High energy consumption, 2. Large particle size and uneven 3. Low purity	
Gas phase	1. High purity 2. Small particle size	1. Particles easy to agglomerate 2. High production cost	
Liquid phase	Sol-gel method	1. Simple process 2. Uniform chemical composition 3. Controllable microstructure	1. High raw material price 2. Long process time
	Precipitation method	1. Simple process 2. Large scale production	1. Low purity 2. Large particle size and uneven
	Hydrothermal synthesis	1. High purity 2. Good dispersion, good crystal shape and controllability	1. High equipment requirements 2. Technical difficulties 3. High costs 4. Difficulties in mass production
	Microemulsion method	1. Simple equipment 2. Controllable particles	1. Difficult process control 2. Difficulties in mass production 3. High cost

#### 4. Methods for Modifying TiO<sub>2</sub> Materials

Despite being a green and environmentally friendly photocatalytic material, TiO<sub>2</sub> has some limitations when used to photocatalytically degrade organic pollutants. Sunlight energy is essentially inexhaustible and can provide continuous light energy for oxidative photocatalytic degradation reactions; it is, therefore, an ideal and economical source of light. The energy in the solar spectrum is mainly concentrated in the visible light region, with the infrared region (wavelength: 400–700 nm) accounting for 50% of the total solar light, and the ultraviolet region accounting for approximately only 5%. Unfortunately, the bandgap width of TiO<sub>2</sub> means that it can only absorb ultraviolet photons; consequently, its photocatalytic activity is limited to the ultraviolet region, which leads to a very low solar energy utilization rate. Therefore, improving the responses of TiO<sub>2</sub> materials to visible light and stimulating high photocatalytic activity in the visible region have become research hotspots in the TiO<sub>2</sub> photocatalysis field.

Doping is a powerful method for improving the performance of TiO<sub>2</sub>; it can change the crystal and electronic structure of the metal, as well as the bandgap of the semiconductor, as a consequence. Generally speaking, doping is considered to be an effective strategy for promoting the absorption performance of visible light, as is mainly reflected in the following three points: (1) the bandgap redshifts to the visible region, (2) the band-edge absorption widens to include the visible region, and (3) a new visible-region absorption process is introduced. While doping typically enhances the abilities of metal oxides to absorb visible light, doping may promote aggregation of the photocatalyst, which reduces light absorption and increases charge recombination, thereby inhibiting catalytic performance. Excessive doping can lead to structural changes and Moss–Burstein transfer that widens the bandgap [123]. Therefore, optimizing the amount of dopant is very important. The energy band structure of TiO<sub>2</sub> can be adjusted by regulating defects, non-metal-ion doping, and transition-metal-ion doping, among others. Surface dye sensitization, noble-metal deposition, semiconductor recombination, and other means can also promote the absorption of light and the separation of photogenerated carriers by TiO<sub>2</sub>. In addition, the photogenerated carrier recombination efficiency can be improved by controlling the TiO<sub>2</sub> crystal structure, crystallinity, surface morphology, and grain size. Doping can increase the number of defects in the TiO<sub>2</sub> lattice, which changes the structure and properties of the TiO<sub>2</sub> photocatalyst surface, narrows the TiO<sub>2</sub> bandgap, and enhances the photocatalytic efficiency of TiO<sub>2</sub>. The methods used to modify TiO<sub>2</sub> can roughly be divided into categories that include excessive metal doping, noble-metal and rare-earth doping, non-metal doping, semiconductor recombination, organic dye photosensitization, and catalysis [124–128].

#### 4.1. Metal Doping

Metal doping can be categorized into transition-metal, noble-metal, and rare-earth-metal doping, according to the mechanism used by the metal-ion dopant to influence the photocatalytic activity of TiO<sub>2</sub>. An intermediate state energy level is typically introduced into the TiO<sub>2</sub> bandgap by metal doping, which changes the motional states of the carriers; consequently, the energy band structure of TiO<sub>2</sub> can be controlled by adjusting the distributed states of electrons and holes, in order to change the photocatalytic activity of TiO<sub>2</sub>. On the one hand, appropriate metal ions are selected to replace Ti<sup>4+</sup> in the TiO<sub>2</sub> lattice, and impurity energy levels are introduced near the conduction band. Hence, valence band electrons can be excited by photons with energies less than the original forbidden band width (3.2 eV) to impurity energy levels, and the photogenerated electrons in the conduction band can also transition to impurity energy levels, which promotes photogenerated electron–hole pair separation [129]. On the other hand, some transition metal ions act as electron traps and form intermediate valence ions after capturing electrons, which also realizes photogenerated electron–hole separation [113]. The energy levels of most dopant ions lie between the valence and conduction bands of TiO<sub>2</sub>; consequently, the introduction of dopant ions not only increases the electron–hole-pair capture rate in the crystal, but also prevents electron–hole recombination, thereby improving the photocatalytic ability of TiO<sub>2</sub> [130]. The introduction of metal dopants into the TiO<sub>2</sub> lattice leads to the formation of new energy states below the conduction band and above the valence band, and these new energy states act as charge-trapping sites that improve the charge-separation efficiency (Figure 5) [131]. However, the TiO<sub>2</sub> lattice becomes seriously distorted when the amount of dopant exceeds a certain level, which hinders further improvements in photocatalytic performance. Therefore, determining the optimal position and amount of the dopant element remains challenging.

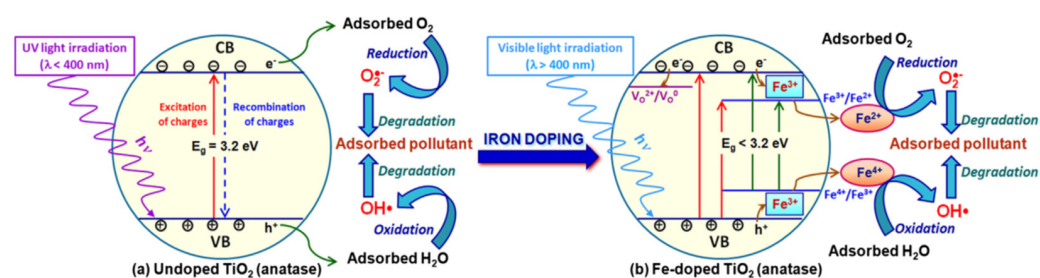


**Figure 5.** Schematic representation of the electronic band structure of (a) undoped anatase TiO<sub>2</sub> and (b) Fe-doped anatase TiO<sub>2</sub>. Reprinted/adapted with permission from Ref. [131]. 2018, Elsevier.

#### 4.1.1. Excessive Metal Doping

Metal doping helps to produce doped nanoparticles with fewer defects, and more recombination centers when the metal dopant is chemically similar to the metal in the metal oxide; therefore, the great potential of transition metals for modifying TiO<sub>2</sub> cannot be overlooked [44–50]. The addition of a transition metal can result in a shift in the TiO<sub>2</sub> absorption window to the visible region, with the transition metal creating a new energy level between the valence and conduction bands of TiO<sub>2</sub>. Doping with Mn [132], Cr [133], Fe [134–140], Cu [141–143], or V [112] effectively reduces the bandgap of TiO<sub>2</sub>, such that it responds to visible light. The type and amount of dopant ion are important factors that affect the photocatalytic oxidation activity of TiO<sub>2</sub>. While an appropriate amount of dopant ion can promote the separation of photogenerated electrons and holes, thereby enhancing visible light absorption, TiO<sub>2</sub> crystallinity is destroyed when excessively doped, and impurity ions become recombination centers for electrons and holes that reduce catalytic activity [144]. Mohammed et al. elucidated the photocatalytic mechanism of a 10% NiO/TiO<sub>2</sub> catalyst through the photodegradation of brilliant green (BG) and phenol; p–n heterojunctions are formed between the two oxides that effectively separate the photoinduced electrons and holes, thereby improving the light utilization efficiency. Figure 6 shows a photodegradation diagram for NiO/TiO<sub>2</sub> composite nanoparticles [145]. In a similar manner, Nadia et al. synthesized a bimetallically modified Cu–Ni/TiO<sub>2</sub> photodegradation catalyst and studied its photodegradation efficiency toward Orange II under various preparation conditions [146].

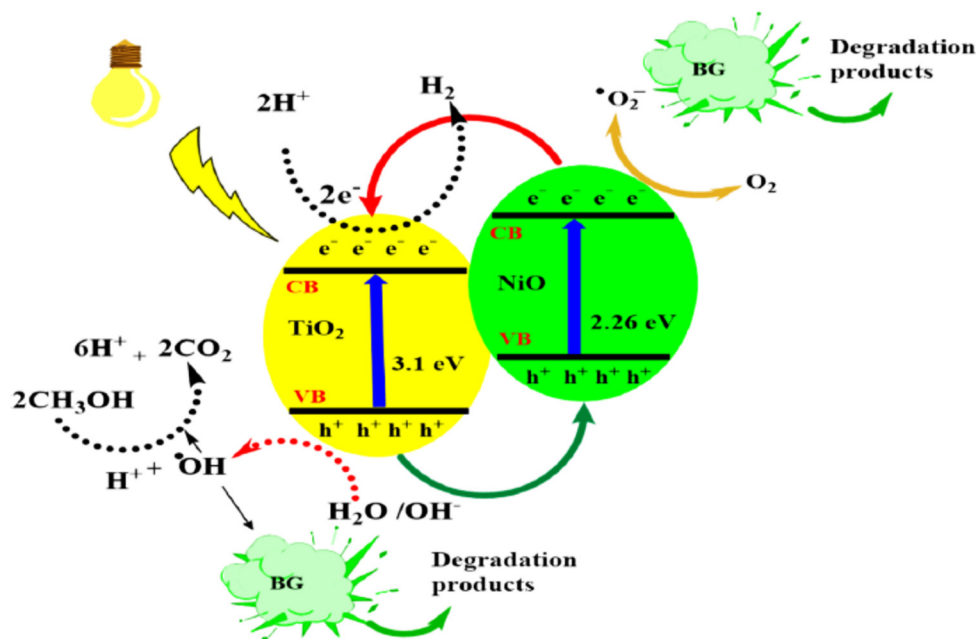
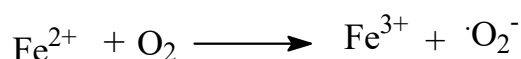
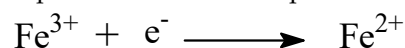


**Figure 6.** Postulated mechanism for electron transfer in NiO/TiO<sub>2</sub> nanoparticles [145]. Reprinted/adapted with permission from Ref. [131]. 2021, ACS Publications.

A small amount of Fe effectively reduces the TiO<sub>2</sub> bandgap width and promotes visible light absorption by TiO<sub>2</sub>. Doping with Fe<sup>3+</sup> effectively improves the catalytic activity of TiO<sub>2</sub>, which is mainly attributable to the fact that Fe<sup>3+</sup> is capable of capturing photogenerated electrons and holes to form intermediate Fe<sup>2+</sup>, as shown in Figure 7, thereby promoting photogenerated carrier separation [147]. In addition, Fe<sup>3+</sup> has an ionic radius of 0.63 Å, which is close to that of Ti<sup>4+</sup> (0.64 Å). Therefore, Fe<sup>3+</sup> becomes uniformly doped into the TiO<sub>2</sub> lattice without creating excessive distortion, thereby reducing the number of photogenerated electron–hole recombination centers [135]. The manner in which Fe<sup>3+</sup> traps electrons can be expressed as:



Yang et al. prepared an Fe-doped TiO<sub>2</sub> composite on glass fiber using the sol-gel method and studied the photodegradation performance of the composite toward benzene, toluene, ethylbenzene, and o-xylene. The GF-Fe-TiO<sub>2</sub> composite doped with 0.01 at% Fe exhibited better photocatalytic oxidation activity under visible light than the undoped GF-TiO<sub>2</sub> material [134]. Tieng et al. prepared an Fe<sup>3+</sup>-doped TiO<sub>2</sub> nanocoating and studied its photodegradation behavior toward ethylene gas. These authors believed that both photogenerated electrons and holes are captured by Fe<sup>3+</sup> and proposed an optimal size of approximately 8 nm for the TiO<sub>2</sub> nanocoating, based on the localization range of photogenerated electrons in the CB [148].

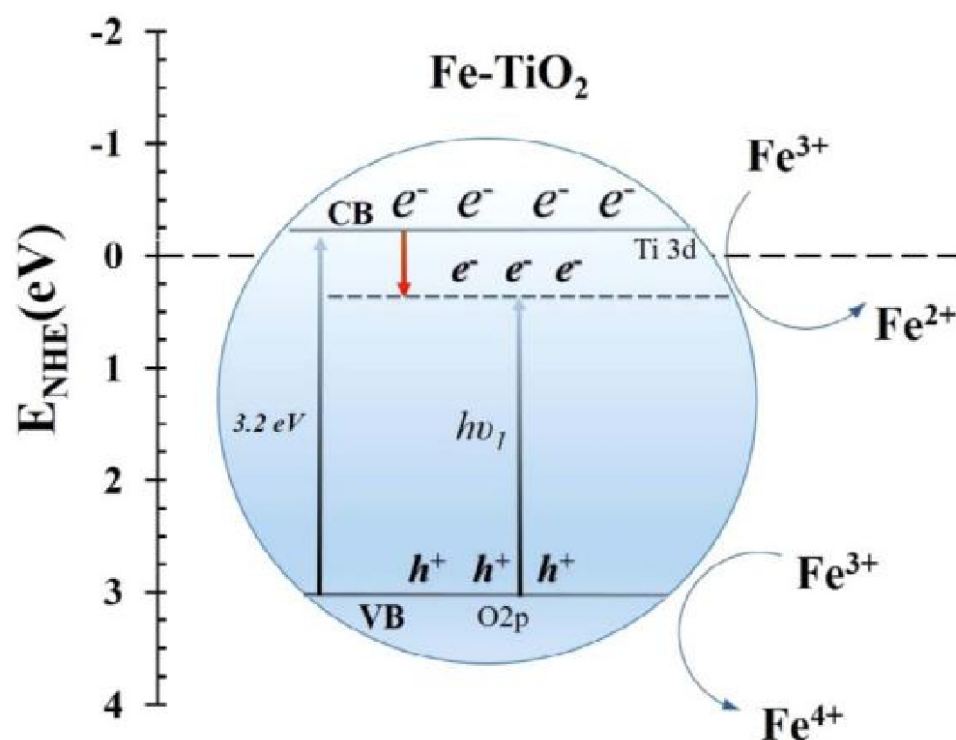


**Figure 7.** Schematic diagram showing the energy levels of TiO<sub>2</sub> doped with Fe (transition metal). Reprinted/adapted with permission from Ref. [147]. 2018, Elsevier.

Lu et al. synthesized a green Fe-doped TiO<sub>2</sub> photocatalyst on a Ti net by chemical impregnation and anodic oxidation and studied, in detail, the influence of the Fe content in the synthesized material on photocatalytic performance [149]. Compared with TiO<sub>2</sub>, the green Fe-doped TiO<sub>2</sub> photocatalyst absorbed more light, with a redshifted absorption peak and a narrower bandgap observed. Details of the charge-transfer and photocatalysis mechanisms are shown in Figure 8. Fe-doped TiO<sub>2</sub> exhibited a higher visible light response,

with an improved photodegradation rate of 87.9% for MB observed in a photocatalysis experiment with Fe-doped TiO<sub>2</sub> (0.6 wt%) under simulated sunlight irradiation for 2.5 h.

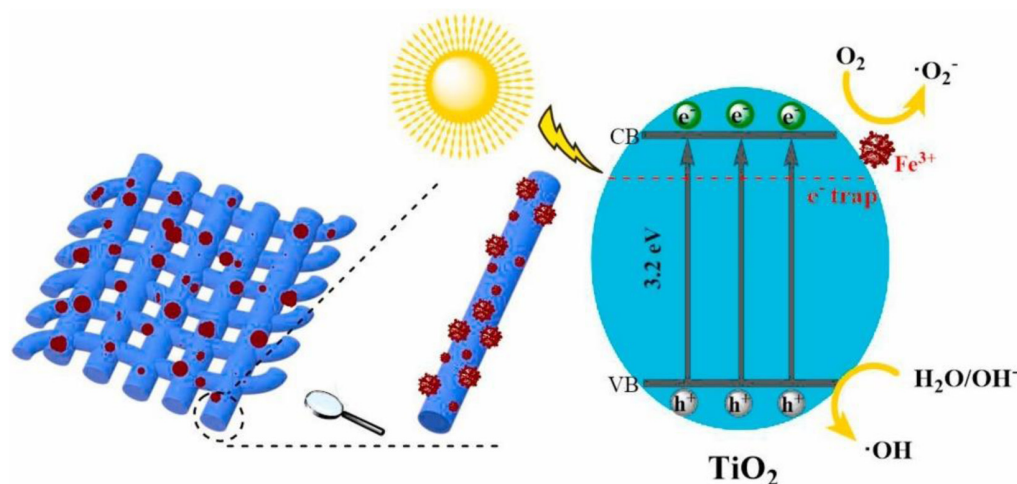


**Figure 8.** Simulated charge-transfer and photocatalysis mechanism for the Fe-doped TiO<sub>2</sub> photocatalyst. Reprinted/adapted with permission from Ref. [149]. 2021, Elsevier.

#### 4.1.2. Noble- and Rare-Earth-Metal Doping

The reported noble metals mainly include Pt [150], Ag [151–157], Ru [158,159], Ir [160], Pd [161–165], Au [166–172], and W [173], which are most commonly used and are strongly corrosion- and oxidation-resistant. Doping not only improves the photocatalytic activity of TiO<sub>2</sub>, but also increases its photochemical stability; consequently, noble-metal ions are ideal dopants. The Schottky barrier formed at the interface between the noble metal and TiO<sub>2</sub> promotes photogenerated electron transfer and reduces photogenerated carrier recombination [174]. Noble metal deposition on a semiconductor surface is considered to be an effective modification method for capturing excited electrons; it effectively reduces oxygen and improves photocatalytic activity. Noble metal deposition methods mainly include immersion reduction and photoreduction. The noble metal on the surface of a catalyst effectively forms a short-circuit microcell, with TiO<sub>2</sub> as the semiconductor and the metal as the electrode on the TiO<sub>2</sub> surface. The h<sup>+</sup> is generated by the TiO<sub>2</sub> electrode oxidizes organic matter in the liquid phase, whereas the e<sup>−</sup> flows to the metal electrode and reduces oxidized components in the liquid phase, thereby lowering the e<sup>−</sup>/h<sup>+</sup> ratio in the composite. Consequently, more ·OH and ·O<sub>2</sub><sup>−</sup> are produced on the TiO<sub>2</sub> surface, which improves catalytic activity [175,176].

Rare-earth metals, including Sc, Y, and the 15 lanthanide metals, have incomplete 4f and empty 5d orbitals. This electronic structure enables metal ions to act as intermediates that capture and transfer photogenerated electrons, which reduces photogenerated electron–hole recombination and improves photocatalytic activity [177,178]. Rare-earth metal-ion doping can also affect the activity of the catalyst by altering the phase structure, specific surface area, and surface morphology of TiO<sub>2</sub> during synthesis. The introduction of a rare-earth element into a TiO<sub>2</sub> crystal not only promotes crystal formation and lattice distortion, but also affects the crystal form, energy band structure, grain size, movement state, and photogenerated electron–hole-pair lifetimes in TiO<sub>2</sub> [179]. Doping with rare-earth elements also improves many properties of TiO<sub>2</sub>, including adsorption performance toward visible light and interfacial charge-transfer efficiency, with TiO<sub>2</sub> exhibiting an improved photocatalytic ability following this series of changes. Meng et al. prepared a Gd-La co-doped TiO<sub>2</sub> composite catalyst by simultaneously doping La<sub>2</sub>O<sub>3</sub> and Gd<sub>2</sub>O<sub>3</sub> into the TiO<sub>2</sub> lattice to generate abundant O vacancies and surface defects, which increased the absorption wavelength and improved the light-conversion efficiency of TiO<sub>2</sub> [180]. Wang et al. co-doped Fe and La into TiO<sub>2</sub>; the composite showed excellent photocatalytic

performance, compared to single-element-doped TiO<sub>2</sub> [181]. Li et al. simultaneously doped five elements, namely Co, Ce, La, Eu, and Sn, into the TiO<sub>2</sub> lattice to form a transition and rare earth element co-doped photodegradation catalyst [182]. Jiang et al. hydrothermally prepared anatase-TiO<sub>2</sub> photocatalysts co-doped with Pr, N, and P without post-sintering treatment; the material exhibited an improved UV-light-absorbing ability, owing to the high hydroxyl content on the surface, which also reduced photogenerated electron–hole recombination [183]. Eskandarloo et al. prepared a mixed catalyst by physically mixing and reheating TiO<sub>2</sub> and CeO<sub>2</sub> powders and studied the photodegradation performance of the catalyst for phenazopyridine [184]. Thiruppathi et al. doped Ce metal into a TiO<sub>2</sub> lattice to prepare Ce@TiO<sub>2</sub> nanocomposites and studied the photodegradation of diclofenac sodium [185]. Xu et al. synthesized TiO<sub>2</sub> catalysts co-doped with Y, Yb, and Tm and extended the light-sensitive range to the near-infrared region [186]. A (Yb<sup>3+</sup>, Er<sup>3+</sup>) co-doped TiO<sub>2</sub>/Ag<sub>3</sub>PO<sub>4</sub> hybrid composite that exhibited enhanced visible light photocatalytic activity was prepared; this composite degraded phenol when irradiated with visible or near-infrared (NIR) light. Possible intermediate products generated during the photodegradation of phenol were also investigated, and a plausible photodegradation pathway for phenol and a mechanism for the observed enhanced photocatalytic activity were proposed [187].

Doping the TiO<sub>2</sub> lattice with a rare-earth metal can also enhance the adsorption of organics on the catalyst surface, thereby improving the photocatalytic activity of TiO<sub>2</sub> [188]. Trujillo-Navarrete et al. prepared Nd<sup>3+</sup>-doped TiO<sub>2</sub> nanoparticles using the Stöber method and studied the effect of doping on the crystal structure and micromorphology of anatase TiO<sub>2</sub>. The addition of Nd<sup>3+</sup> was found to affect the Ti–O bond length and reduce octahedral distortion, with the TiO<sub>2</sub> structure found to be more stable after doping and more conducive to charge transfer [189]. Zhao et al. studied the degradation of phenolic compounds using Nd–TiO<sub>2</sub> photocatalysts [190], while Feng et al. synthesized a Gd–SiO<sub>2</sub>–TiO<sub>2</sub> catalyst using the sol-gel method; this catalyst exhibited a degradation efficiency of approximately 90% for MB under sunlight [191] for 150 min.

#### 4.2. Nonmetallic Doping

A non-metallic dopant can be substituted into an O site or a parent-metal-atom site, or it may exist as a gap dopant. The 2p orbital of a non-metallic dopant reduces the bandgap width and enhances visible light absorption [192–194], which is mainly ascribable to the generation of more mixing or local states near the edge of the valence or conduction band of the semiconductor. Therefore, doping with non-metallic elements has always been a TiO<sub>2</sub> modification research hotspot. Doping with N [195–199], C [200–205], S [206–208], B [209], F [75,114,115], I [210–212], and other elements has been shown to successfully expand the light-response range of TiO<sub>2</sub> to include the visible region. When doping non-metallic ions, the TiO<sub>2</sub> lattice is generally believed to change the energy-level structure of TiO<sub>2</sub> to form new doping levels near the valence band edge, which narrows the bandgap. S and N, as dopant examples, replace the lattice O in TiO<sub>2</sub> to form new energy bands through the hybrid mixing of the p and O 2p orbitals, which reduces the bandgap. Zhou et al. doped S into TiO<sub>2</sub> to narrow its bandgap and provided an effective method for improving the photocatalytic efficiency and expanding the absorption window of TiO<sub>2</sub> from ultraviolet to the visible region; they also showed that disulfide macro-rings (DSMs) are ideal candidates for highly doped TiO<sub>2</sub>. A series of characterization studies showed that S exists in its S<sup>6+</sup> form when it replaces Ti<sup>4+</sup> on the surface of the TiO<sub>2</sub> lattice to form SO<sub>4</sub><sup>2−</sup>. S–TiO<sub>2</sub> has a bandgap of 2.3 eV, which is less than that of the original TiO<sub>2</sub> (3.2 eV); hence, it absorbs in the visible region [213].

In addition, the doped state does not act as a charge carrier in a non-metallic-doped system; consequently, it does not become a photogenerated electron–hole recombination center in the lattice, unlike metal ions [214]. Therefore, non-metal-element doping is considered to be more effective than metal-element doping for improving the photocatalytic performance of TiO<sub>2</sub>. Research has favored non-metal-doped TiO<sub>2</sub>, especially using N, C, S, F, and other elements [215].

#### 4.2.1. N Doping

N doping endows TiO<sub>2</sub> with catalytic properties when irradiated with visible light and is, therefore, an important non-metal-doping subject. N has a low ionization potential and an ionic radius close to that of O; hence, N easily replaces O in the TiO<sub>2</sub> lattice [216]. N doping not only reduces the TiO<sub>2</sub> bandgap width, leading to a material that responds to visible light, but also changes the physical properties of TiO<sub>2</sub>, including its hardness, refractive index, conductivity, and elastic modulus [217]. Albrbar et al. proposed that the N in N-doped TiO<sub>2</sub> enters gaps in the TiO<sub>2</sub> lattice (gap type) or replaces lattice oxygens to become incorporated into the lattice (displacement type) [218]. Pandian et al. prepared three kinds of N-doped TiO<sub>2</sub> films (chemisorption, gap, and displacement) using DC magnetron sputtering technology at various oxygen partial pressures and studied their electronic energy band structures. They observed that displacement-type N has an acceptor level of 0.14 eV, which is above the valence band of TiO<sub>2</sub>, while that of gap-type N is 0.73 eV [216]. The N 2p orbitals of displacement-type N and the O 2p orbitals of the lattice oxygen are generally believed mix to form a localized N 2p state that lies above the valence band; visible light catalysis occurs because this localized state has a low electron-transition energy. In addition, the N 2p orbital of N and the S 2p orbitals of S can also mix. For example, N enters the lattice more easily when Ti<sup>4+</sup> is replaced by S<sup>4+</sup> or S<sup>6+</sup> to form (N, S)-co-doped anatase TiO<sub>2</sub> that exhibits photocatalytic activity under visible light [206]. Yang et al. prepared N-doped TiO<sub>2</sub>, loaded it onto carbon foam, and studied the photodegradation performance of the prepared catalyst toward phenol [219].

#### 4.2.2. C Doping

C-doping is also an effective method for modifying TiO<sub>2</sub>. C has been reported to not only reduce the bandgap by forming intermediate energy levels in the TiO<sub>2</sub> bandgap, but also promote the adsorption of organic substances and transport of photogenerated carriers within TiO<sub>2</sub> [220]. Valentin et al. studied the structure of C-doped TiO<sub>2</sub> using density function theory. A low C content and a lack of oxygen in the reaction is believed to facilitate the entry of C into the TiO<sub>2</sub> lattice by replacing lattice O. C is more likely to enter the lattice in the form of interstitial atoms or by substituting Ti atoms when insufficient O is present [221]. Chen et al. experimentally compared C-doped and N-doped TiO<sub>2</sub>, with the former exhibiting better photocatalytic activity for the degradation of MB under visible light. These researchers proposed that doping TiO<sub>2</sub> with C inhibits the growth of TiO<sub>2</sub> crystals, with active carbon materials or other carbides deposited on the surface of the catalyst, which help to adsorb organic pollutants [216]. Kavitha et al. prepared C-doped TiO<sub>2</sub> using anhydrous D-glucose as the carbon source and confirmed that the C atoms were mainly incorporated into the lattice gaps of TiO<sub>2</sub> through Ti–O–C bond and O–Ti–C bonds. The valence band edge was observed to move in the negative direction and increased the photogenerated-hole oxidation potential when the amount of the carbon concentration was increased [222]. Photodegradation performance toward 4-chlorophenol under ultraviolet and visible light revealed that that C-doped TiO<sub>2</sub> exhibited better catalytic activity under visible light because the carbon-containing compounds on the surface of the catalyst were removed under ultraviolet light, which weakened the catalytic synergy between the carbon-containing substances on the surface of the catalyst and the crystalline carbon. The selection of an appropriate amount of dopant can effectively improve the catalytic activity of TiO<sub>2</sub>. On the one hand, too much dopant leads to a large number of defects in the TiO<sub>2</sub> lattice, which inhibits the photogenerated carrier separation; on the other

hand, too many carbides are formed on the  $\text{TiO}_2$  surface, which affects light absorption, hides active sites, and reduces photocatalytic activity.

Depositing a C-point on the surface of the catalyst is equivalent to forming a short-circuit microcell with a semiconductor heterojunction and a carbon layer as the electrode. For example, Figure 9 shows the photodegradation catalysis mechanism that operates after doping a C-point with  $\text{ZnO}/\text{TiO}_2$ . The  $\text{h}^+$  generated by the  $\text{TiO}_2$  electrode oxidizes the organic matter in the liquid phase, while the  $\text{e}^-$  flows to the metal electrode and reduces the oxidized components in the liquid phase, thereby lessening the  $\text{e}^-/\text{h}^+$  recombination rate and improving the activity of the catalyst [223].

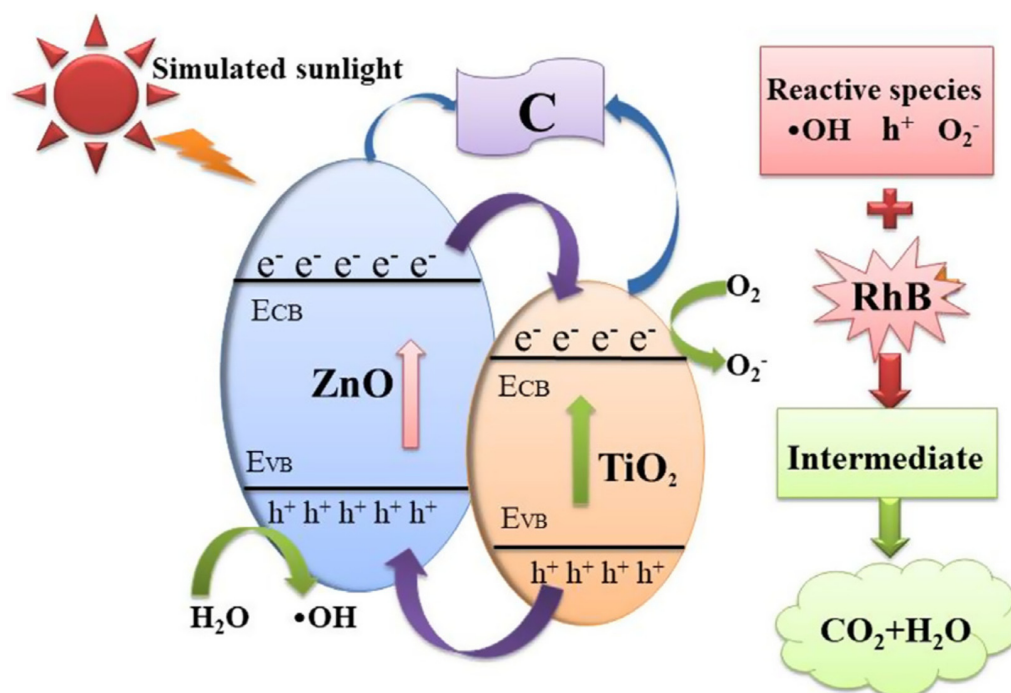


**Figure 9.** Schematic diagram showing the photocatalytic degradation mechanism associated with  $\text{Zn}/\text{Ti}$ -2%-MOF-600. Reprinted/adapted with permission from Ref. [223], 2021, Elsevier.

#### 4.3. Co-Doping

Modifying  $\text{TiO}_2$  by elemental co-doping can compensate for the shortcomings of single-element doping and has attracted significant attention in recent years as a consequence. Elemental co-doping can be divided into non-metal, metal/non-metal, and metal co-doping, among which, metal co-doping has been somewhat less studied.

##### 4.3.1. Nonmetallic Co-Doping

Non-metallic co-doping methods for modifying  $\text{TiO}_2$  have been widely studied to date. Mesoporous carbon nitride and titanium dioxide ( $\text{C}_3\text{N}_4\text{-TiO}_2$ ) nanocomposites were prepared using urea as the  $\text{C}_3\text{N}_4$  precursor and titanium tetraisopropoxide as the titanium source. The prepared nanocomposites were yellow, in contrast to the white  $\text{TiO}_2$  and  $\text{C}_3\text{N}_4$  nanomaterials. Tauc plots derived by UV-Vis absorption spectroscopy revealed that the  $\text{C}_3\text{N}_4\text{-TiO}_2$  nanocomposite has a significantly narrower bandgap energy, compared to that of the individual  $\text{TiO}_2$  (3.2 eV) and  $\text{C}_3\text{N}_4$  (2.8 eV) samples, leading to a high visible light response [224]. Using thiourea as a dopant, Lei et al. prepared NSC- $\text{TiO}_2$  co-doped with N, S, and C using the sol-gel method, followed by calcination. XPS revealed that the N in the product is mainly doped as Ti-O-N and Ti-N bonds, while S is mainly doped as Ti-O-S bonds, and C is mainly doped as Ti-O-C bonds. Elemental co-doping and the calcination temperature were found to significantly influence the  $\text{TiO}_2$  microstructure and size, with the catalytic activity of  $\text{TiO}_2$  under visible light improved, owing to N, S, and C doping synergy [225].

Li et al. used ammonium fluoride ( $\text{NH}_4\text{F}$ ) as a dopant and  $\text{TiCl}_4$  as the titanium source to prepare N and F co-doped  $\text{TiO}_2$  powder by spray pyrolysis and studied its photodegradation performance for gaseous acetaldehyde and trichloroethylene under visible light. Compared with samples doped with N or F alone, the co-doped  $\text{TiO}_2$  sample exhibited higher catalytic activity [226]. These researchers proposed that N doping promotes visible light absorption and that the formed oxygen vacancies promote the formation of  $\bullet\text{O}_2^-$ , while F doping affords more active  $\bullet\text{OH}$  sites. Therefore, catalysis through N and F co-doping synergy improves material performance. Pan et al. prepared N, N&S and N&F doped hierarchical macro-/mesoporous  $\text{TiO}_2$  with tetrabutyl titanate, urea, thiourea, and ammonium fluoride as raw materials. Morphological changes and RhB degradation were also studied [227]. Zeng et al. synthesized N-doped and B/N-co-doped  $\text{TiO}_2$  photocatalysts and  $\text{TiO}_2$  using a liquid-phase precipitation method combined with a solid-phase thermal-decomposition method. XPS revealed that B occupies the  $\text{TiO}_2$  gap position. In addition, the specific surface area of the  $\text{TiO}_2$  NPs was significantly higher, and their photocatalytic activity was enhanced by B/N co-doping [228]. He et al. synthesized F-doped  $\text{TiO}_2$  using HF as the raw material. The morphologies of  $\text{TiO}_2$  particles doped with various amounts of F were observed to be completely different, as shown in Figure 10. However,  $\text{TiO}_2$  prepared at different hydrothermal reaction temperatures exhibited different morphologies when the same addition amount of F was added, as shown in Figure 11.

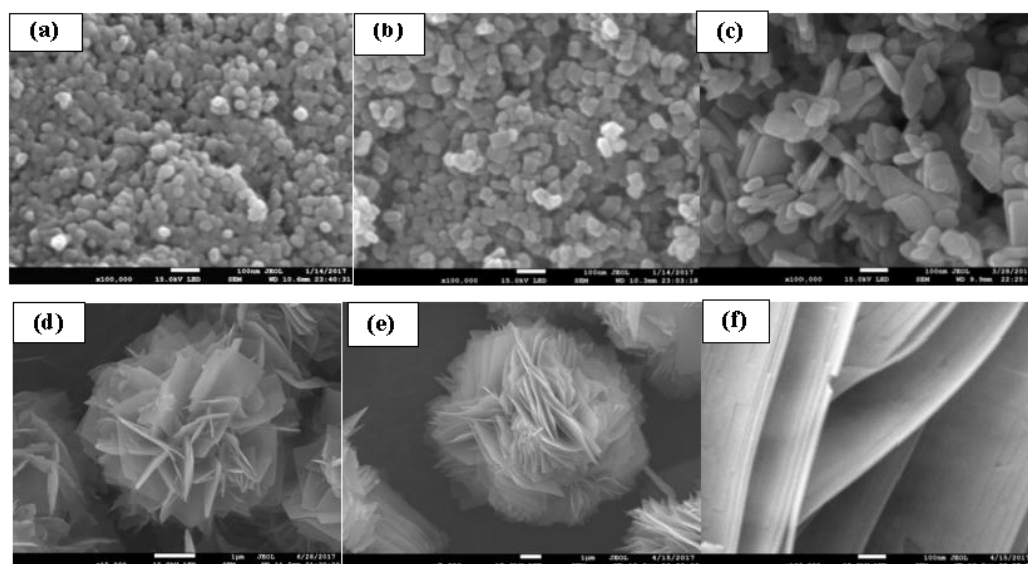


**Figure 10.** SEM images of  $\text{TiO}_2$  samples prepared with different amounts of HF: (a) pure- $\text{TiO}_2$ , (b) T-1F, (c) T-3F, (d) T-5F, (e) T-7F, and a high magnification image of (f) T-7F [114].

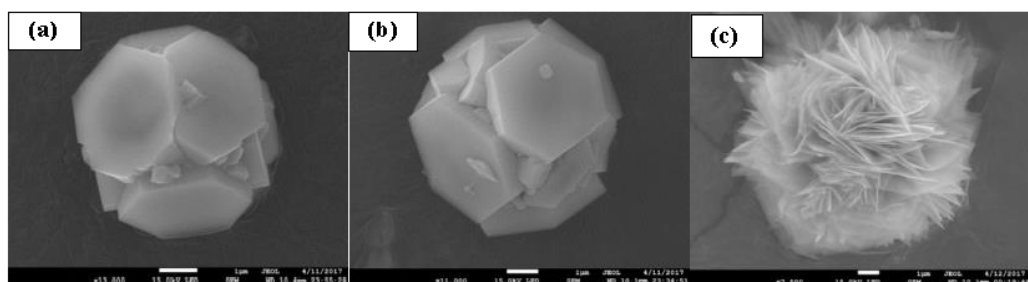


**Figure 11.** SEM images of T-7F hydrothermally prepared at various temperatures: (a) 150, (b) 170, and (c) 200 °C [114].

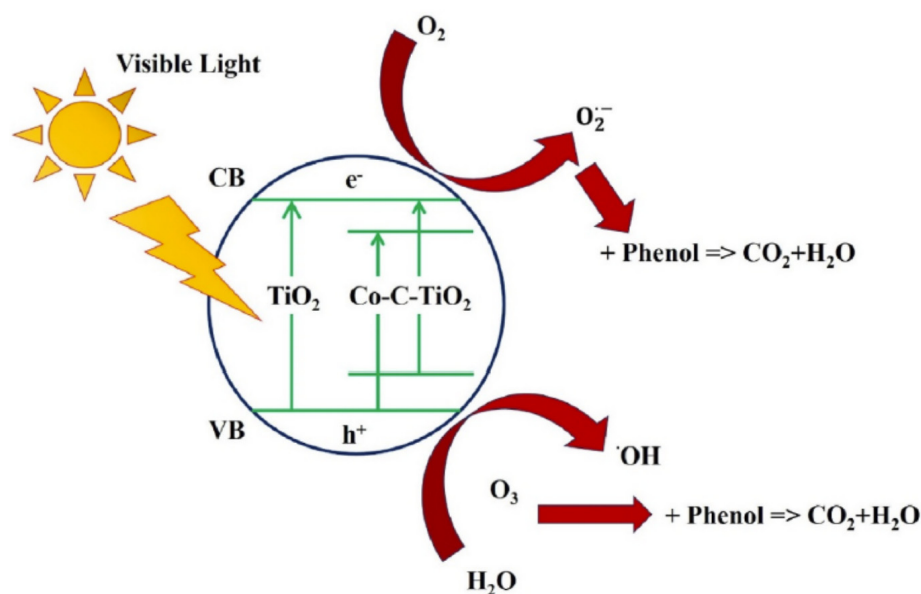
#### 4.3.2. Metal/Nonmetal Co-Doping

Table 2 can be controlled by metal/non-metal co-doping. Metal ion doping is believed to mainly replace Ti atoms to form an impurity level below the conduction band, whereas non-metal doping forms an impurity level near to, but above, the valence band. Therefore, co-doping with a metal and a non-metal can effectively reduce the TiO<sub>2</sub> bandgap width and improve its responsiveness to visible light. Fang et al. prepared Mo and C co-doped TiO<sub>2</sub> materials using a hydrothermal method involving pre-calcination. C was found to mainly exist on the surfaces of the TiO<sub>2</sub> particles, in the form of carbides, whereas the Mo was mainly present in the lattice in the form of Mo<sup>6+</sup> (replacing Ti<sup>4+</sup>). The Mo<sup>6+</sup>-formed impurity level was determined to lie at 0.4 eV, which is below the TiO<sub>2</sub> conduction band. This impurity level captures photogenerated electrons (Mo<sup>6+</sup>/Mo<sup>5+</sup>) and promotes carrier separation [229]. In addition, metal-ion/non-metal-element synergy promotes photogenerated carrier separation to a certain extent. Fan et al. prepared N and Fe co-doped TiO<sub>2</sub> using a two-step method, with Ti and N as precursors. Fe was found to mainly exist on the TiO<sub>2</sub> surface in the Fe<sup>3+</sup>/Fe<sup>2+</sup> form; the presence of Fe also enhanced the photochemical stability of the N dopant in the TiO<sub>2</sub>. Fe-N-TiO<sub>2</sub> was observed to be more stable and more catalytically active than N-TiO<sub>2</sub> toward the photodegradation of gas-phase toluene, with EPR and PL experiments showing that Fe<sup>3+</sup>/Fe<sup>2+</sup> is capable of effectively promoting photogenerated carrier separation [230].

**Table 2.** Summary of TiO<sub>2</sub> modification methods.

	Doping Type		Action Mechanism
Metal doping	Noble metal	Pt, Au, Ag, Pd, W, Ru, Re, Os, Ir, et al.	Schottky barrier formed between interfaces
	Rare earth metal	Ce, La, Eu, Pr, Y, Yb, Er, Nd, Sm, Tm, et al.	Changing TiO <sub>2</sub> crystal structure
	Transition metal	Fe, Mn, Cr, Cu, V, et al.	Changing TiO <sub>2</sub> crystal structure
Nonmetallic doping		C, N, S, B, F, I, et al.	Changing TiO <sub>2</sub> crystal structure
Co-doping	Nonmetallic co-doping	C-N, N-S-C, S-N, N-F, B-N, et al.	Changing TiO <sub>2</sub> crystal structure
	Metal metal co-doping	Gd-La, Yb-Er, Y-Yb-Tm, Yb-Er, Co-Ce-La-Eu-Sm, et al.	Changing TiO <sub>2</sub> crystal structure
	Nonmetal and metal co-doping	Pr-P-N, Mo-C, Fe-N, Co-N, et al.	Changing TiO <sub>2</sub> crystal structure
Semiconductor doping		ZnO, ZnS, CdS, Fe <sub>2</sub> O <sub>3</sub> , Fe <sub>3</sub> O <sub>4</sub> , MoS <sub>2</sub> , ZrO <sub>2</sub> , SnO <sub>2</sub> , Al <sub>2</sub> O <sub>3</sub> , WO <sub>3</sub> , et al.	Forming semiconductor heterojunction
Photosensitization of organic dyes		Anthocyanins, Red sandalwood pigments, Carotenoids, Porphyrins, Tetracarboxy phthalocyanines, Squaraine dye, polyaniline, et al.	Improve the absorption of sunlight

Carbon and iron doping were found to modify the absorption edge of the TiO<sub>2</sub> photocatalyst, which shifted toward the visible region. Fe<sup>3+</sup> can be doped into the TiO<sub>2</sub> matrix, which hinders the recombination of excited electrons/holes. The carbon- and iron-modified TiO<sub>2</sub> was observed to exhibit superior photocatalytic activity for the decomposition of Acid Orange 7 under visible light [231]. The cobalt and carbon co-dopants in TiO<sub>2</sub> act in synergy to lower the bandgap energy level to 2.81 eV, which encompasses the visible light region. At the same time, it stimulates electron-hole-pair separation to produce more •OH, thereby improving the light-conversion efficiency, as shown in Figure 12 [232]. Similarly, iron and carbon co doped TiO<sub>2</sub> photocatalysts have obtained similar conclusions [233]. The cobalt and sulphur doped TiO<sub>2</sub> photocatalysts shows stronger photocatalytic degradation ability than the pure TiO<sub>2</sub> [234].



**Figure 12.** Schematic representation of the proposed photocatalytic degradation mechanism of TiO<sub>2</sub> co-doped with Co and C under visible light [233]. Reprinted/adapted with permission from Ref. [233]. 2021, Elsevier.

#### 4.4. Semiconductor Recombination

Two semiconductor structures can be coupled to form a semiconductor heterojunction. Photogenerated electrons and holes are separated at the heterojunction interface, owing to the different energy band structures of the two semiconductors. Photogenerated electrons transfer from the semiconductor with the higher conduction band to the semiconductor with the lower conduction band, while photogenerated holes transfer from the semiconductor with a lower valence band to the semiconductor with the higher valence band [235]. Heterogeneous photocatalysts mostly use TiO<sub>2</sub>, ZnO, ZnS, CdS, and Fe<sub>2</sub>O<sub>3</sub>, with two semiconductors with matched energy band structures combined to reduce electron–hole recombination, improve the light-absorption range, and promote photogenerated carrier migration [236]. Many types of heterojunctions have been studied, with the aim of effectively improving the photoactivity of the material. The mechanism associated with heterojunction photocatalysis can be divided into three steps: (1) photons absorption on the surface to generate electron–hole pairs, (2) the separation and transfer of photogenerated electron–hole pairs, and (3) redox chemistry involving adsorbed reactants and the carriers [237].

Figure 13 show a plausible visible light-driven reaction mechanism for the photodegradation of bisphenol A(BPA) by the p–n heterojunction of the ZnFe<sub>2</sub>O<sub>4</sub>–TiO<sub>2</sub> nanocomposite when irradiated with 465 nm (visible) light. Electrons in the VB of ZnFe<sub>2</sub>O<sub>4</sub> are photoexcited to the CB to produce electron–hole pairs when exposed to visible light (pathway 1). The excited electrons in ZnFe<sub>2</sub>O<sub>4</sub> easily transfer across the nanocomposite interface to the CB of anatase TiO<sub>2</sub> because the redox potential of the CB of ZnFe<sub>2</sub>O<sub>4</sub> (1.54 eV) is higher than that of anatase TiO<sub>2</sub> (0.29 eV), leaving holes in the ZnFe<sub>2</sub>O<sub>4</sub> VB (pathway 2). Therefore, p-type ZnFe<sub>2</sub>O<sub>4</sub> and n-type TiO<sub>2</sub> coupling effectively reduces the electron–hole recombination rate, which lowers the internal resistance and enhances interfacial charge-transfer efficiency as a consequence. Therefore, the photogenerated holes (h<sup>+</sup>) in the VB of ZnFe<sub>2</sub>O<sub>4</sub> directly photodegrade BPA when irradiated with 465 nm (visible light) (pathway 3) [238].

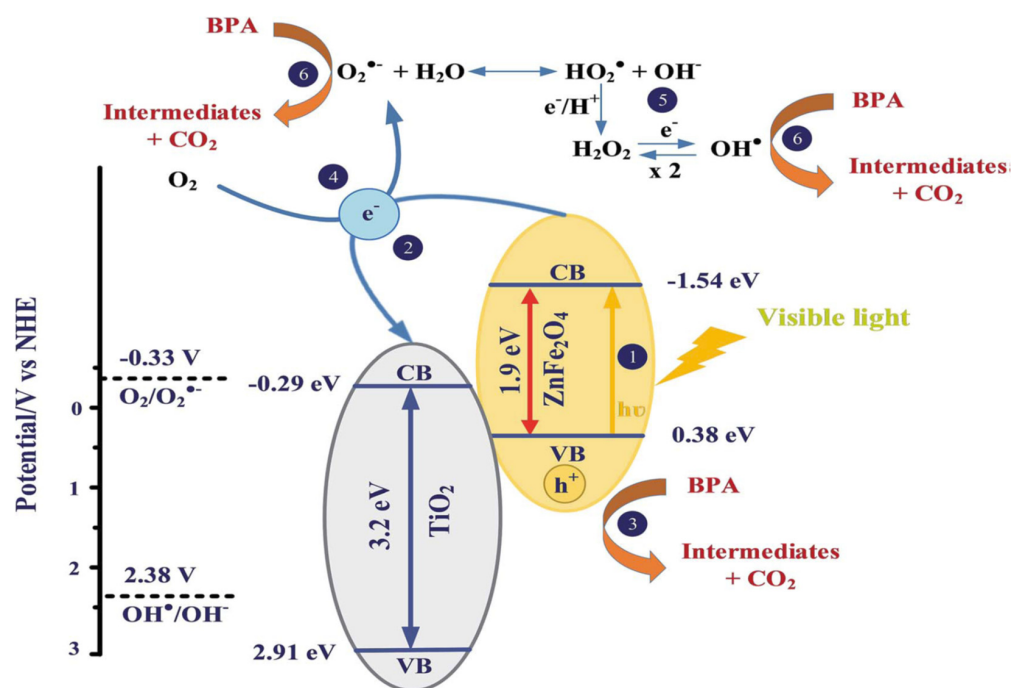


**Figure 13.** Schematic illustrating the visible light-driven photodegradation of BPA by a  $\text{ZnFe}_2\text{O}_4\text{-TiO}_2$  photocatalyst under visible light [238].

Photogenerated electron–hole recombination is another important factor that affects photocatalytic activity because electron–hole pairs generated by photoexcitation very easily recombine; hence, reducing the photogenerated carrier recombination rate also improves photocatalytic efficiency. Other types of semiconductor material can also improve photogenerated carrier separation efficiency and the light-absorption rate when combined with  $\text{TiO}_2$ , thereby improving photocatalytic efficiency. The semiconductor composite is essentially  $\text{TiO}_2$  modified by another particle. Studies have shown that composite semiconductors have many advantages, including: (1) the bandgap and spectral-absorption range of the semiconductor are easily controlled by adjusting the particle size, (2) the light absorption of semiconductor particles is a banded edge, which benefits effective sunlight collection, and (3) photostability is improved by surface-modifying the particles [239]. Further studies have shown that the energy bands of the two semiconductors bend at the heterojunction interface, which creates a strong internal electric field between the interfaces and separates photogenerated carriers. Hu et al. built a heterojunction that expanded the response range of the material to include the visible region (>450 nm) by combining  $\text{TiO}_2$  with a small amount of  $\text{BiVO}_4$ , which increased the degradation efficiency for gaseous benzene by a factor of three. The high degradation efficiencies of heterojunction materials can be maintained for more than 50 h [240]. Using molybdenum disulfide as a raw material, Hunge et al. prepared a composite  $\text{MoS}_2/\text{TiO}_2$  catalyst with various  $\text{MoS}_2$  contents using a hydrothermal method; one of the catalysts exhibited a photodegradation rate of 84% for 10 mg/L tetracycline within 100 min under 400 W metal halide lamp used as the UV–Vis light source [241]. Lu et al. prepared a  $\text{Bi}_2\text{Mo}_6/\text{GQDs}/\text{TiO}_2$  double-heterojunction-structured material with an expanded absorption-wavelength range and limited photogenerated electron–hole recombination, thereby improving the solar-energy conversion efficiency [242]. Yang et al. showed that  $\text{TiO}_2\text{-ZnO}$  composite particles attached to diatomite surfaces exhibit a higher absorption wavelength than pure  $\text{ZnO}/\text{diatomite}$  [243]. Modification with  $\text{ZnO}$  was shown to move the absorption window of  $\text{TiO}_2$  to the visible region, with improved light conversion efficiency also observed [244,245]. Similar behavior was also reported for  $\text{CdS}/\text{TiO}_2$  [246],  $\text{CoSe}/\text{TiO}_2$  [247],  $\text{SnO}_2/\text{TiO}_2$  [248,249],  $\text{ZrO}_2/\text{TiO}_2$  [250–253],  $\text{Ag}_2\text{S}/\text{TiO}_2$  [254],  $\text{Fe}_3\text{O}_4/\text{TiO}_2$  [255,256],  $\text{Co}_3\text{O}_4/\text{TiO}_2$  [257],  $\text{WO}_3/\text{TiO}_2$  [258,259],  $\text{TiO}_2/\text{Bi}_2\text{O}_3/\text{TiO}_2$  [260],  $\text{BiOXs}/\text{TiO}_2$  [261],  $\text{TiO}_2\text{-WO}_3\text{-Bi}_2\text{O}_3/\text{SiO}_2$  [262],  $\text{SiO}_2/\text{TiO}_2$  [263–266], and

$\text{Al}_2\text{O}_3/\text{TiO}_2$  [267], among others, with the formed heterojunction also observed to improve the absorption wavelength and light-conversion efficiency of each composite material.

#### 4.5. Photosensitizing Organic Dyes

$\text{TiO}_2$  only absorbs approximately 4% of the solar spectrum; consequently, extending the excitation wavelength of the catalyst material is an important photocatalysis research topic. Colored organic or inorganic compounds can be chemically or physically adsorbed by a  $\text{TiO}_2$  semiconductor material with a high specific surface area to sensitize the wide-energy-gap semiconductor surface. On the one hand, the surface of a  $\text{TiO}_2$  thin film adsorbs a single layer of sensitizer molecules, while the interior of the sponge-like film adsorbs additional sensitizer molecules; consequently, sunlight that is reflected many times on the rough surface is repeatedly absorbed by the sensitizer molecules, which improves the sunlight utilization rate [268]. On the other hand, sensitization increases the efficiency of the light-excitation process and expands the excitation wavelength window to the visible region, thereby improving the photoelectric energy-conversion efficiency, which is the purpose of the sensitizer. In this sense, dye molecules act as semiconductors. The ground state is equivalent to the valence band of the semiconductor, while the excited state is equivalent to the conduction band, with the following specific process adhered to: dye molecules are excited when the photon energy is less than that of the forbidden bandwidth of the semiconductor. Dye-excited electrons are injected into and transported by the semiconductor, which is a long-distance electron-transport system. The electron-trapping agent finally captures the electrons on the surface of the semiconductor to realize electron–hole separation; the carriers then become involved in photocatalysis chemistry. Photosensitizing a catalytic semiconductor material involves the physical or chemical adsorption of active compounds on the semiconductor surface. Sensitizing materials can be divided into pure-organic and metal-organic dyes; the former does not contain central metal ions and includes polymethyl chuan, oxazolium, and some natural dyes, such as anthocyanins, red sandalwood pigments, and carotenoids. These substances have large excitation factors toward visible light, which results in the excited state exhibiting a more negative potential than that of the conduction band of the semiconductor; consequently, the excitation factor is injected into the conduction band of the semiconductor material, thereby expanding the excitation wavelength range of the semiconductor and improving sunlight utilization [269,270]. Porphyrins [271,272], tetracarboxyphthalocyanines [273], squaraine dyes [274], and other organic dyes are especially chemically stable and have outstanding redox properties, good excited-state reaction activities, long emission lifetimes, exhibit good luminescence performance, and strongly affect energy and electron transport through photosensitization. Maximizing dye loading on the semiconductor surface does not always lead to improved performance; consequently, the influence of dye concentration on the photocatalytic performance of a semiconductor needs to be screened [275–277]. The tris(2,2'-bipyridyl)dichlororuthenium composite with titanium-pillared saponite increases the specific surface area and pore size of  $\text{TiO}_2$ , with photocatalytic activity extending to the visible region as a consequence [159]. Samuel et al. sensitized  $\text{TiO}_2$  using a dye sensitization method and a variety of natural dyes. The use of chlorophyll was shown to lead to the best degradation effect, with a degradation rate of 60% for MB recorded [278]. Koodali et al. used an iron(III)-phthalocyanine-modified  $\text{TiO}_2$  catalyst to study the photodegradation of p-aminobenzoic acid, p-nitrobenzoic acid, p-chlorophenoxyacetic acid, salicylic acid, and aniline and found that synergy between iron(III) phthalocyanine and  $\text{TiO}_2$  contributes to the production of  $\bullet\text{OH}$  [279]. The optical bandgap energy of  $\text{TiO}_2$  surface-modified with polyaniline (PANI) was observed to decrease with increasing amounts of PANI.  $\text{TiO}_2$ -PANI loaded onto polystyrene ( $\text{TiO}_2$ -PANI-PS) exhibited an appreciably accelerated photodegradation rate, compared to the PS- $\text{TiO}_2$  composite and pristine PS, when irradiated with UV light [280].

The doping can change the crystal and electronic structure of  $\text{TiO}_2$ , inhibit the recombination rate of photogenerated electron-hole pairs to improve its quantum efficiency, and

broaden the response range of light wavelength, which is a powerful factor for improving the photocatalytic performance of TiO<sub>2</sub>. The summary of different TiO<sub>2</sub> modifications is shown in Table 2.

## 5. Applications

Emissions generated by economic development and human activity have greatly polluted the air that we all rely on. Processes used to fabricate products, tail gases from vehicles, emissions from indoor decorations, and oil smoke from catering activities, among others, have all contributed to a decline in air quality. In addition, water is arguably the most valuable resource offered to life by nature; it plays an integral role in the lives of all living organisms and is an essential material for life itself. However, economic development and population increases have seriously polluted water resources through the massive use of pesticides, the discharge of pharmaceuticals and their metabolites, and the seemingly unlimited use of dyes. Consequently, organic pollutants in water are a problem that needs to be urgently addressed, with TiO<sub>2</sub> photocatalysts widely studied and used in water-treatment applications.

TiO<sub>2</sub> photocatalysis is an energy-saving and environmentally friendly technology for the highly efficient catalytic oxidation of organic pollutants. It uses the energy of solar radiation to excite photoelectron–hole pairs on the TiO<sub>2</sub> surface, which results in the generation of highly reactive radicals, such as superoxide ( $\bullet\text{O}_2^-$ ) and hydroxyl ( $\bullet\text{OH}$ ), and the oxidation of organic gases, liquids, and other pollutants into carbon dioxide and water. The selective photocatalysis field has undergone rapid development in recent years and now extends to include several new applications. This review focuses on the overall strategies that improve photocatalysis selectivity and encompasses a wide variety of photocatalysts and their modifications, as well as the vital related processes of industrial significance, such as the reduction and oxidation of organics and inorganics and transformation of CO<sub>2</sub>. After optimizing various procedures, the ultimate challenge of this field involves the use of natural sunlight to remediate real wastewater [281–284].

### 5.1. Volatile Organic Compounds (VOCs)

VOCs are common outdoor and indoor air pollutants, and their levels determine air quality. People in developed countries spend more than 90% of their lives indoors; however, the construction and assembly of synthetic materials has resulted in serious VOC pollution problems that directly affect human health. Therefore, indoor air treatment is receiving increasing levels of attention. Formaldehyde is a prominent air pollutant in a newly decorated room; it ranks second in the list of controlled toxic chemical, with only dioxin (strong carcinogen) above it in the list. Formaldehyde is referred to the “first killer” of the indoor environment. Long-term exposure to formaldehyde (even small amounts) can greatly harm the human body. Various measures have been taken to remove formaldehyde from indoor air, mainly through the use of the ventilation, filtration, adsorption, and catalytic purification methods [285,286]. However, these methods are associated with disadvantages that include ease of saturation during adsorption, regular adsorbent replacement, harsh conditions, high costs, and very limited formaldehyde-removal abilities. Recent studies have shown that photocatalytic methods can effectively degrade formaldehyde to harmless CO<sub>2</sub> and H<sub>2</sub>O in indoor air. Such methods use little energy, are simple to operate, use mild reaction conditions, and produce no secondary pollution. Pure semiconductor TiO<sub>2</sub> only generates electron–hole pairs when excited by ultraviolet light, with low light-conversion efficiency. Narrow-bandgap TiO<sub>2</sub> (after modification) can be excited by visible light, with delayed charge carrier recombination improving the light-utilization rate, thereby improving photocatalytic activity and the formaldehyde-degradation rate [287–289].

Song et al. prepared a composite photodegradation catalyst by loading Au–Pt alloy nanoparticles onto TiO<sub>2</sub> and examining indoor formaldehyde degradation [290]. Lama et al. prepared a Cr/TiO<sub>2</sub> photocatalyst and investigated its performance for the photocatalytic degradation of formaldehyde gas using singly polluted air flowing through Cr/TiO<sub>2</sub> [85].

Lan et al. studied the photodegradation of formaldehyde at 65 °C using TiO<sub>2</sub>-M (M = Cu, In, Pd, and Pt) catalysts and proposed the degradation mechanism shown in Figure 14 [291]. Korologos et al. studied the photocatalytic oxidation performance of 0.25% (w/w) Pt-, Fe-, and Ce-doped TiO<sub>2</sub> materials toward gas-phase benzene, toluene, ethylbenzene, and m-xylene under various UV-irradiation conditions. Ce-doped TiO<sub>2</sub> was shown to exhibit the best degradation activity for benzene and ethylbenzene [292]. The erbium in an Er-doped TiO<sub>2</sub> material occupies the Ti sites in the crystal lattice, which leads to the formation of oxygen vacancies (VO) and Ti<sup>3+</sup> that significantly enhance the photocatalytic performance of the catalyst. The presence of Er<sub>2</sub>O<sub>3</sub> also increases the specific surface area, which also improves the VOC-adsorption capacity of the catalyst. Moreover,  $\bullet\text{O}_2^-$  was found to play a dominant role in the degradation of acetaldehyde and ethylene, with  $\bullet\text{OH}$  being the dominant species responsible for the degradation of xylene [293].

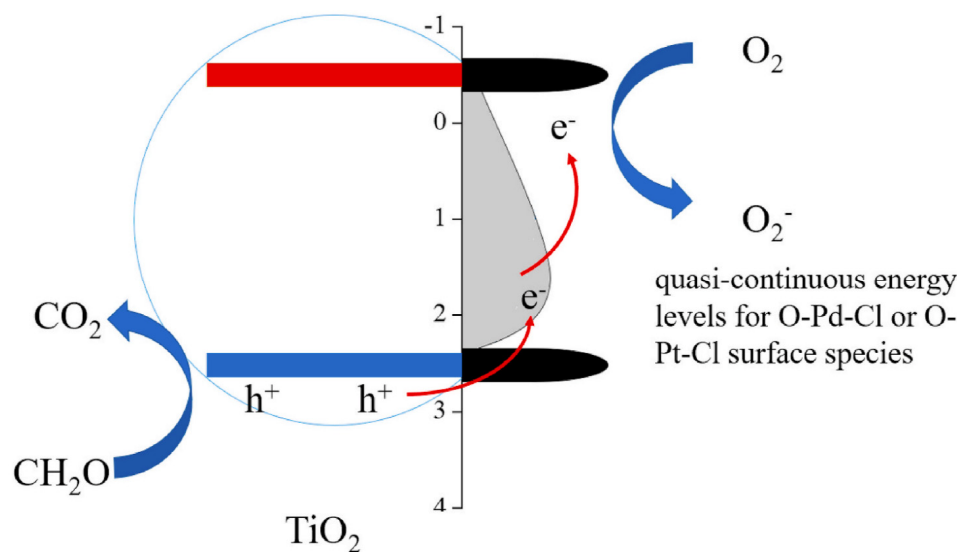


**Figure 14.** Schematic diagram depicting the thermal catalysis mechanism of a TiO<sub>2</sub>-M (M = Cu, In, Pd, and Pt) catalyst. Reprinted/adapted with permission from Ref. [291]. 2021, Elsevier.

Rao et al. used the sol-gel method to prepare Tm<sup>3+</sup>-modified TiO<sub>2</sub> nanoparticles that exhibited improved photoinduced electron-hole separation efficiency, higher hydrophilicity, increased adsorption capacities for acetaldehyde and o-xylene, and better photocatalytic activities than pure TiO<sub>2</sub> for the gas-phase degradation of acetaldehyde, o-xylene, and their mixtures [294]. The 0.5 mol% Tm-TiO<sub>2</sub> sample showed the highest photodegradation efficiency (>90.0%) for the abovementioned vapors, thereby providing an effective method for the degradation of VOCs using a TiO<sub>2</sub>-based catalyst, and it has important guiding significance for the future design of photocatalysts that degrade mixed VOCs. Ji et al. prepared mesoporous TiO<sub>2</sub> using a one-step hydrolysis method and various calcination temperatures and used it to photocatalytically degrade gaseous benzene. Mesoporous TiO<sub>2</sub> is more catalytically active and degradation stable toward benzene [67]; the use of mesoporous TiO<sub>2</sub> in a VUV environment is a promising and efficient benzene-removal method that reliably and conveniently degrades indoor organic pollutants. Mahmood et al. prepared carbon-quantum-dot-decorated TiO<sub>2</sub> (CQDs/TiO<sub>2</sub>) nanocomposites and proposed the photodegradation mechanism shown in Figure 15 [295]. The CQDs adsorbed on the TiO<sub>2</sub> facilitates strong hybridization between the TiO<sub>2</sub> CB, and the  $\pi$  electrons of the aromatic rings present in the CQD framework, which increases the light-absorption capacity. In addition, the C 2p states of the CQDs incorporate new energy states within the lower CB that shrink the bandgap; therefore, the CQDs/TiO<sub>2</sub> bandgap is narrower than that of pure TiO<sub>2</sub>. The new states within the CB act as reservoirs for the photoinduced electrons in the nanocomposite, which improves the charge-separation process. The CQDs improve the charge-separation and light-harvesting properties of TiO<sub>2</sub>. CQDs/TiO<sub>2</sub> showed

significantly different photodegradation efficiencies toward benzene, xylene, and toluene in photodegradation experiments.

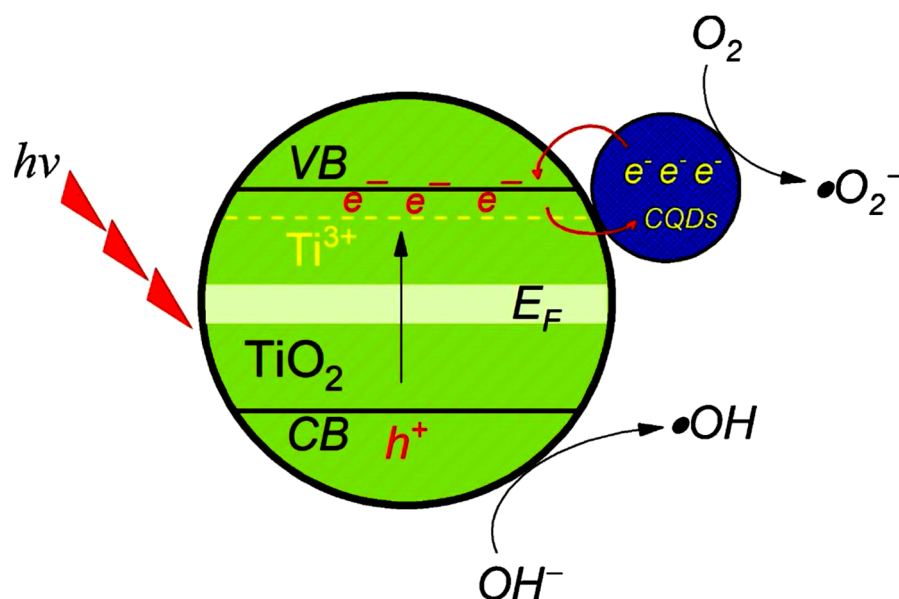


**Figure 15.** Schematic illustration depicting the surface interactions between CQDs and TiO<sub>2</sub> NPs. Illumination with light excites charges in TiO<sub>2</sub> that transfer to the CQDs. Reprinted/adapted with permission from Ref. [295]. 2021, Elsevier.

## 5.2. Dyes and Coatings

Ceramic matrices have become preferred substrates for TiO<sub>2</sub> thin-film coatings because they are resistant to high temperatures, very chemically stable, and corrosion resistant, and self-cleaning ceramic films are becoming increasingly researched. The Toto Company in Japan began plating metallic (Ag and Cu) layers on ceramic surfaces loaded with TiO<sub>2</sub> in the 1980s; the products exhibited good antibacterial properties when irradiated with visible light or in the dark and were commercially produced from 1994 onwards. The United States, South Korea, and other countries are also following the lead of Japan by investing in self-cleaning ceramics. China is a large country, in terms of ceramic production and use, and the pollution of ceramic products and their cleaning have also received extensive attention. A TiO<sub>2</sub> film-layer coating on a ceramic surface can decompose VOCs; such coatings are mainly used for air purification (nitrogen oxide, sulfur oxide, alcohols, aldehydes, etc.), anti-fogging, self-cleaning, decontamination, sterilization, and disinfection purposes [296].

Antibiotic residues and toxic organic molecules from the chemical, textile, and pharmaceutical industries are extremely toxic to aquatic ecosystems and human health. Semiconductor-based photocatalysts have been shown to provide significant advantages, owing to the simple methods used to prepare them, their cost-effectiveness, and lack of toxicity, etc., which improves their yields and utilization rates in practical applications [125]. Dyes may be carcinogenic and/or mutagenic and can impact humans, water-balance systems, and animals in the long-term [60]. Therefore, methods for degrading organic dyes are of paramount importance. Although membrane separation technology has been widely used in water treatment [297], photocatalytic treatment is among the best methods for reducing water pollution from colored dyes used in the textile industry [120,298–300]. Anila et al. reviewed dye pollution, dye classification, and dye decolorization/degradation strategies and introduced the degradation mechanism associated with the well-known TiO<sub>2</sub> photocatalyst, while concurrently discussing the latest research into metal-, non-metal-, transition-metal-, noble-metal-, and lanthanide-ion-doped TiO<sub>2</sub> aimed at improving photocatalytic efficiency. Structurally modified TiO<sub>2</sub> photocatalysts have become a flexible, economical, and effective commercial dye-treatment technology and represent the best catalytic materials for the degradation of various pollutants and sustainable environmental

remediation. Such catalysts are expected to be widely used in dye photodegradation research [9], with dyes such as methyl orange [301–305], MB [306–315], and RhB [316–326] having already been studied. Mohamed et al. compared the degradation efficiencies of mesoporous TiO<sub>2</sub> nanoparticles and commercially available P25 TiO<sub>2</sub> for the photodegradation of organic pollutants [327]. Perfluorooctanoic acid was photodegraded by 99.5% (100 mg/L) using spherical BiOBr-modified TiO<sub>2</sub>, which maintained a high h<sup>+</sup> content on the photocatalyst surface [328].

A heterojunction structure is formed when TiO<sub>2</sub> is grown on a diatomite carrier, which generates Si-O-Ti active sites in the boundary space between TiO<sub>2</sub> and the diatomite, thereby improving the charge-transfer process, as well as the photocatalytic degradation activity for dyes as a consequence [94,329]. Yang et al. grafted TiO<sub>2</sub> onto the inner wall of a quartz capillary, followed RhB-degradation products by mass spectrometry, and studied the mechanism responsible for the photocatalytic degradation of RhB (see Figure 16) [330]. Singh et al. prepared zinc oxide nanosheets (ZNFs) functionalized with TiO<sub>2</sub> nanoparticles (TNPs) and studied their abilities to detoxify molecular solutions of MB, rhodamine 6G, and oxytetracycline. The ZnO-TiO<sub>2</sub> nano-hybrid material exhibited excellent 3D photodegradation performance, which is ascribable to charge separation and TNP/ZNF synergy that increases the electron density in the conductive band. This study provided a simple method for preparing a ZnO-TiO<sub>2</sub> heterojunction photocatalyst capable of significantly photodegrading organic azo dyes and medical waste [125].

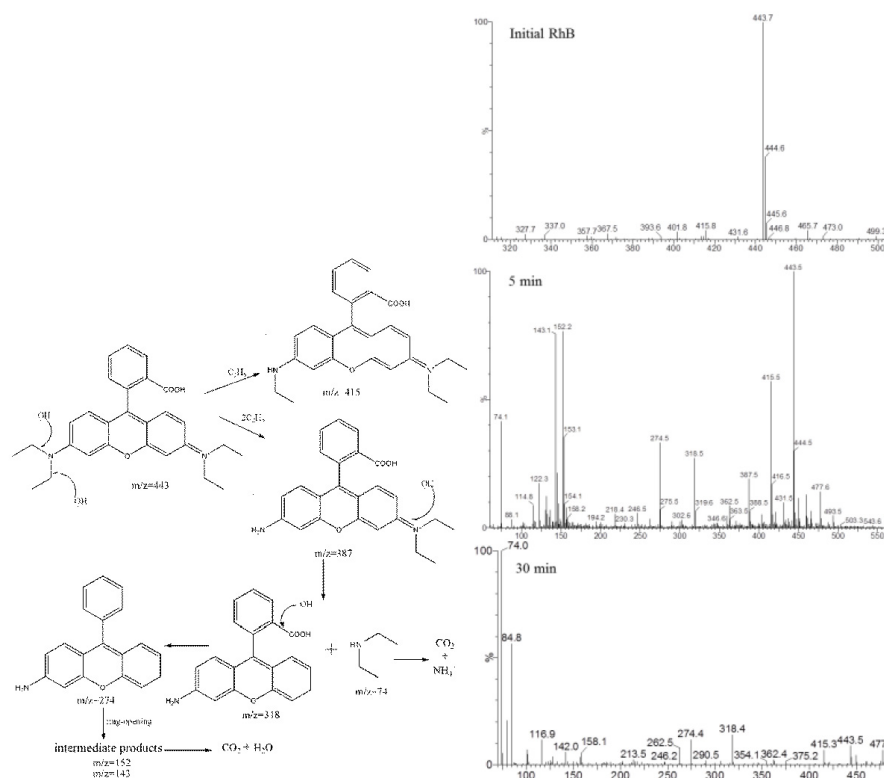


**Figure 16.** Investigating the mechanism responsible for the degradation of RhB by subjecting an initial RhB solution and solutions containing degradation products formed after 5 and 30 min to mass spectrometry [330].

### 5.3. Drugs and Daily Necessities

The production and use of medical drugs and their metabolites, psychotropic drugs, other abusive drugs, and agricultural drugs are continually increasing. These compounds greatly impact the aquatic ecosystem, with significant toxic side effects exhibited by microorganisms, algae, invertebrates, and vertebrates in the environment. Among these drugs, sulfamethoxazole [331–337], metronidazole [338–343], carbamazepine [344], ciprofloxacin [242,345], and

tetracycline [346–348], etc., and hormones such as  $17\alpha$ -methyltestosterone [349], have been most researched from a photodegradation perspective. Awfa et al. reviewed the use of carbon–TiO<sub>2</sub> composites as catalysts that photodegrade drugs and personal care products in aqueous media [350].

Mouele et al. used mass spectrometry to study the mechanism associated with the degradation of sulfamethoxazole drugs by a Ti/C-N-TiO<sub>2</sub> catalyst [351], while Hoi et al. used mass spectrometry to study the intermediates formed by the degradation of sulfamethoxazole drugs using a TiO<sub>2</sub> ceramic catalyst [330]. Eskandarian et al. studied the decomposition of acetaminophen, diclofenac, ibuprofen, sulfamethoxazole, and other model drugs by direct photolysis and TiO<sub>2</sub> photocatalysis and investigated the effect of the UV–LED wavelength on their decomposition [22]. The UV wavelength was found to be a more important parameter in the decomposition process than the light intensity. The decomposition effect of shorter-wavelength UV light followed the order: UVC > UVB > UVA. Photocatalytic decomposition was observed to be much more significant than direct photolysis. The results of this study are expected to promote the use of UV–LEDs for the treatment of water polluted by toxic chemicals that are difficult to degrade. Akter et al. optimized UV/TiO<sub>2</sub> photodegradation processes for metronidazole, ciprofloxacin, and sulfamethoxazole in aqueous solutions and determined their kinetics. The UV/TiO<sub>2</sub> photodegradation process was found to be applicable to the treatment of wastewater contaminated with pharmaceuticals [334].

Several issues associated with the photocatalytic degradation of antibiotics need to be resolved. Firstly, many antibiotics are not completely degraded into nontoxic substances. More effort needs to be directed toward evaluating eco-toxicity and designing photocatalysts with higher redox activities for antibiotic photodegradation. Secondly, more attention needs to be paid to recycling and regenerating photocatalysts, particularly for practical applications. Thirdly, previous studies into antibiotic photodegradation were mainly laboratory-based; therefore, larger-scale systems need to be evaluated to increase their applicability to real wastewater treatment projects [352].

## 6. Conclusions

Photocatalysis is a green and safe technology that converts light into chemical energy and has broad prospects for solving two global problems, namely environmental pollution and the energy crisis. TiO<sub>2</sub>-based photocatalysts show significant developmental potential and have many advantages, including high chemical stabilities, low costs, low toxicities, abundance, and high catalytic activities. Such catalysts have been widely used to photocatalytically degrade pollutants and purify harmful gases, coatings, and other daily necessities.

This paper reviewed TiO<sub>2</sub>-preparation methods and discussed the advantages and disadvantages of various methods, and several methods for modifying TiO<sub>2</sub> were also introduced. Finally, the use of these materials to degrade harmful gases, coatings, dyes, drugs, and daily necessities were summarized. To conclude, TiO<sub>2</sub>, as a typical representative photocatalytic semiconductor, has many advantages and shows great potential for further development and modification. Future scientific research is expected to result in further major solar photocatalytic technology breakthroughs that will benefit mankind, while also realizing a low-carbon economy.

**Author Contributions:** Conceptualization, H.Y. and J.Y.; methodology, H.Y.; software, B.Y.; validation, B.Y. and W.C.; formal analysis, W.C.; investigation, W.C.; resources, B.Y.; data curation, B.Y.; writing—original draft preparation, H.Y.; writing—review and editing, J.Y.; visualization, H.Y.; supervision, J.Y.; project administration, J.Y.; funding acquisition, J.Y. All authors have read and agreed to the published version of the manuscript.

**Funding:** This research received no external funding.

**Conflicts of Interest:** The authors declare no conflict of interest.

## References

1. Chow, J.C. Introduction to the A&WMA 2006 Critical Review—Health effects of fine particulate air pollution: Lines that connect. *J. Air Waste Manag. Assoc.* **2006**, *56*, 707–708. [[PubMed](#)]
2. Zhang, J.J.; Smith, K.R. Household air pollution from coal and biomass fuels in China: Measurements, health impacts, and interventions. *Env. Health Perspect.* **2007**, *115*, 848–855. [[CrossRef](#)] [[PubMed](#)]
3. Jones, A.P. Indoor air quality and health. *Atmos. Environ.* **1999**, *33*, 4535–4564. [[CrossRef](#)]
4. Mumford, J.L.; He, X.Z.; Chapman, R. S.; Cao, S.R.; Harris, D.B.; Li, X.M.; Xian, Y.L.; Jiang, W.Z.; Xu, C.W.; Chuang, J.C.; et al. Lung-cancer and indoor air-pollution in Xuan Wei, China. *Science* **1987**, *235*, 217–220. [[CrossRef](#)] [[PubMed](#)]
5. Pope, C.A.; Burnett, R.T.; Thun, M.J.; Calle, E.E.; Krewski, D.; Ito, K.; Thurston, G.D. Lung cancer, cardiopulmonary mortality, and long-term exposure to fine particulate air pollution. *JAMA* **2002**, *287*, 1132–1141. [[CrossRef](#)] [[PubMed](#)]
6. Fujishima, A.; Honda, K. Electrochemical photolysis of water at a semiconductor electrode. *Nature* **1972**, *238*, 37–38. [[CrossRef](#)] [[PubMed](#)]
7. Gaya, U.I.; Abdullah, A.H. Heterogeneous photocatalytic degradation of organic contaminants over titanium dioxide: A review of fundamentals, progress and problems. *J. Photochem. Photobiol. C* **2008**, *9*, 1–12. [[CrossRef](#)]
8. Liu, S.; Yu, J.; Jaroniec, M. Tunable Photocatalytic Selectivity of Hollow TiO<sub>2</sub> Microspheres Composed of Anatase Polyhedra with Exposed{001} Facets. *J. Am. Chem. Soc.* **2010**, *132*, 11914–11916. [[CrossRef](#)]
9. Ajmal, A.; Majeed, I.; Malik, R.N.; Idriss, H.; Nadeem, M.A. Principles and mechanisms of photocatalytic dye degradation on TiO<sub>2</sub> based photocatalysts: A comparative overview. *RSC Adv.* **2014**, *4*, 37003–37026. [[CrossRef](#)]
10. Akhtar, J.; Tahir, M.B.; Sagir, M.; Bamufleh, H.S. Improved photocatalytic performance of Gd and Nd co-doped ZnO nanorods for the degradation of methylene blue. *Ceram. Int.* **2020**, *46*, 11955–11961. [[CrossRef](#)]
11. Ani, I.J.; Akpan, U.G.; Olutoye, M.A.; Hameed, B.H. Photocatalytic degradation of pollutants in petroleum refinery wastewater by TiO<sub>2</sub>- and ZnO-based photocatalysts: Recent development. *J. Clean. Prod.* **2018**, *205*, 930–954. [[CrossRef](#)]
12. Azarang, M.; Shuhaimi, A.; Yousefi, R.; Golsheikh, A.M.; Sookhajian, M. Synthesis and characterization of ZnO NPs/reduced graphene oxide nanocomposite prepared in gelatin medium as highly efficient photo-degradation of MB. *Ceram. Int.* **2014**, *40*, 10217–10221. [[CrossRef](#)]
13. Linsebigler, A.L.; Lu, G.; Yates, J.T. Photocatalysis on TiO<sub>2</sub> Surfaces: Principles, Mechanisms, and Selected Results. *Chem. Rev.* **1995**, *95*, 735–758. [[CrossRef](#)]
14. Azzouz, I.; Habba, Y.G.; Capochichi-Gnambodoe, M.; Marty, F.; Vial, J.; Leprince-Wang, Y.; Bourouina, T. Zinc oxide nano-enabled microfluidic reactor for water purification and its applicability to volatile organic compounds. *Microsyst. Nanoeng.* **2018**, *4*, 17093. [[CrossRef](#)]
15. Chen, Y.; Liu, K. RETRACTED: Preparation of granulated N-doped TiO<sub>2</sub>/diatomite composite and its applications of visible light degradation and disinfection. *Powder Technol.* **2016**, *303*, 176–191. [[CrossRef](#)]
16. Chen, Y.; Zhang, C.; Huang, W.; Huang, W.; Situ, Y.; Huang, H. Multimorphologies nano-ZnO preparing through a simple solvothermal method for photocatalytic application. *Mater. Lett.* **2015**, *141*, 294–297. [[CrossRef](#)]
17. Kondamareddy, K.K.; Bin, H.; Lu, D.; Kumar, P.; Dwivedi, R.K.; Pelenovich, V.O.; Zhao, X.Z.; Gao, W.; Fu, D. Enhanced visible light photodegradation activity of RhB/MB from aqueous solution using nanosized novel Fe-Cd co-modified ZnO. *Sci. Rep.* **2018**, *8*, 10691.
18. Deng, X.Q.; Zhu, X.; Sun, Z.G.; Li, X.S.; Liu, J.L.; Shi, C.; Zhu, A.M. Exceptional activity for photocatalytic mineralization of formaldehyde over amorphous titania nanofilms. *Chem. Eng. J.* **2016**, *306*, 1001–1009. [[CrossRef](#)]
19. Dong, H.; Zeng, G.; Tang, L.; Fan, C.; Zhang, C.; He, X.; He, Y. An overview on limitations of TiO<sub>2</sub>-based particles for photocatalytic degradation of organic pollutants and the corresponding countermeasures. *Water Res.* **2015**, *79*, 128–146. [[CrossRef](#)]
20. Wenderich, K.; Mul, G. Methods, Mechanism, and Applications of Photodeposition in Photocatalysis: A Review. *Chem. Rev.* **2016**, *116*, 14587–14619. [[CrossRef](#)]
21. Hoffmann, M.R.; Martin, S.T.; Choi, W.; Bahnemann, D.W. Environmental applications of semiconductor photocatalysis. *Chem. Rev.* **1995**, *95*, 69–96. [[CrossRef](#)]
22. Eskandarian, M.R.; Choi, H.; Fazli, M.; Rasoulifard, M.H. Effect of UV-LED wavelengths on direct photolytic and TiO<sub>2</sub> photocatalytic degradation of emerging contaminants in water. *Chem. Eng. J.* **2016**, *300*, 414–422. [[CrossRef](#)]
23. Firdaus, C.M.; Rizam, M.S.; Rusop, M.; Hidayah, S.R. Characterization of ZnO and ZnO: TiO<sub>2</sub> Thin Films Prepared by Sol-Gel Spray-Spin Coating Technique. *Procedia Eng.* **2012**, *41*, 1367–1373. [[CrossRef](#)]
24. Fu, P.; Zhang, P. Characterization of Pt-TiO<sub>2</sub> film used in three formaldehyde photocatalytic degradation systems: UV254 nm, O<sub>3</sub>+UV254 nm and UV254+185 nm via X-ray photoelectron spectroscopy. *Chin. J. Catal.* **2014**, *35*, 210–218. [[CrossRef](#)]
25. Gandhi, V.G.; Mishra, M.K.; Joshi, P.A. A study on deactivation and regeneration of titanium dioxide during photocatalytic degradation of phthalic acid. *J. Ind. Eng. Chem.* **2012**, *18*, 1902–1907. [[CrossRef](#)]
26. Asahi, R.; Morikawa, T.; Ohwaki, T.; Aoki, K.; Taga, Y. Visible-light photocatalysis in nitrogen-doped titanium oxides. *Science* **2001**, *293*, 269–271. [[CrossRef](#)]
27. Choi, W.Y.; Termin, A.; Hoffmann, M.R. The role of metal-ion dopants in quantum-sized TiO<sub>2</sub>-correlation between photoreactivity and charge-carrier recombination dynamics. *J. Phys. Chem.* **1994**, *98*, 13669–13679. [[CrossRef](#)]
28. Serpone, N. Is the band gap of pristine TiO<sub>2</sub> narrowed by anion and cation-doping of titanium dioxide in second-generation photocatalysts. *J. Phys. Chem. B* **2006**, *110*, 24287–24293. [[CrossRef](#)]

29. Zhou, W.J.; Yin, Z.Y.; Du, Y.P.; Huang, X.; Zeng, Z.; Fan, Z.; Liu, H.; Wang, J.; Zhang, H. Synthesis of few-layer MoS<sub>2</sub> nanosheet-coated TiO<sub>2</sub> nanobelt heterostructures for enhanced photocatalytic activities. *Small* **2013**, *9*, 140–147. [[CrossRef](#)]
30. Dvoranova, D.; Brezova, V.; Mazur, M.; Malati, M.A. Investigations of metal-doped titanium dioxide photocatalysts. *Appl. Catal. B* **2002**, *37*, 91–105. [[CrossRef](#)]
31. Enache, D.I.; Edwards, J.K.; Landon, P.; Solsona-Espriu, B.; Carley, A.F.; Herzing, A.A.; Watanabe, M.; Kiely, C.J.; Knight, D.W.; Hutchings, G.J. Solvent-free oxidation of primary alcohols to aldehydes using Au-Pd/TiO<sub>2</sub> catalysts. *Science* **2006**, *311*, 362–365. [[CrossRef](#)] [[PubMed](#)]
32. Chen, M.S.; Goodman, D.W. The structure of catalytically active gold on titania. *Science* **2004**, *306*, 252–255. [[CrossRef](#)] [[PubMed](#)]
33. Siripala, W.; Ivanovskaya, A.; Jaramillo, T.F.; Baeck, S.H.; McFarland, E.W. A Cu<sub>2</sub>O/TiO<sub>2</sub> heterojunction thin film cathode for photoelectrocatalysis. *Sol. Energy Mater. Sol. Cells* **2003**, *77*, 229–237. [[CrossRef](#)]
34. Yao, W.F.; Zhang, B.; Huang, C.P.; Ma, C.; Song, X.; Xu, Q. Synthesis and characterization of high efficiency and stable Ag<sub>3</sub>PO<sub>4</sub>/TiO<sub>2</sub> visible light photocatalyst for the degradation of methylene blue and rhodamine B solutions. *J. Mater. Chem. A* **2012**, *22*, 4050–4055. [[CrossRef](#)]
35. Zhou, W.J.; Liu, H.; Wang, J.Y.; Liu, D.; Du, G.; Cui, J. Ag<sub>2</sub>O/TiO<sub>2</sub> Nanobelts Heterostructure with enhanced ultraviolet and visible photocatalytic activity. *ACS Appl. Mater. Interfaces* **2010**, *2*, 2385–2392. [[CrossRef](#)] [[PubMed](#)]
36. Anpo, M.; Takeuchi, M. The design and development of highly reactive titanium oxide photocatalysts operating under visible light irradiation. *J. Catal.* **2003**, *216*, 505–516. [[CrossRef](#)]
37. Wang, G.M.; Wang, H.Y.; Ling, Y.C.; Tang, Y.; Yang, X. Hydrogen-treated TiO<sub>2</sub> nanowire arrays for photoelectrochemical water splitting. *Nano Lett.* **2011**, *11*, 3026–3033. [[CrossRef](#)]
38. Ye, J.F.; Liu, W.; Cai, J.G.; Chen, S.; Zhao, X.; Zhou, H.; Qi, L. Nanoporous anatase TiO<sub>2</sub> mesocrystals: Additive-free synthesis, remarkable crystalline-phase stability, and improved lithium insertion behavior. *J. ACS* **2011**, *133*, 933–940. [[CrossRef](#)]
39. Kasuga, T.; Hiramatsu, M.; Hoson, A.; Sekino, T.; Niihara, K. Formation of titanium oxide nanotube. *Langmuir* **1998**, *14*, 3160–3163. [[CrossRef](#)]
40. Fox, M.A.; Dulay, M.T. Heterogeneous photocatalysis. *Chem. Rev.* **1993**, *93*, 341–357. [[CrossRef](#)]
41. Bartkowski, S.; Neumann, M.; Kurmaev, E.Z.; Fedorenko, V.V.; Shamin, S.N.; Cherkashenko, V.M.; Nemnonov, S.N.; Winiarski, A.; Rubie, D.C. Electronic structure of titanium monoxide. *Phys. Rev. B* **1997**, *56*, 10656–10667. [[CrossRef](#)]
42. Ma, Y.; Wang, X.L.; Jia, Y.S.; Chen, X.; Han, H.; Li, C. Titanium dioxide-based nanomaterials for photocatalytic fuel generations. *Chem. Rev.* **2014**, *114*, 9987–10043. [[CrossRef](#)]
43. Carp, O.; Huisman, C.L.; Reller, A. Photoinduced reactivity of titanium dioxide. *Prog. Solid State Chem.* **2004**, *32*, 33–177. [[CrossRef](#)]
44. Liu, G.; Yang, H.G.; Pan, J.; Yang, Y.Q.; Lu, G.Q.; Cheng, H.M. Titanium Dioxide Crystals with Tailored Facets. *Chem. Rev.* **2014**, *114*, 9559–9612. [[CrossRef](#)]
45. Chen, X.; Mao, S.S. Titanium Dioxide Nanomaterials: Synthesis, Properties, Modifications, and Applications. *Chem. Rev.* **2007**, *107*, 2891–2959. [[CrossRef](#)]
46. Noman, M.T.; Ashraf, M.A.; Ali, A. Synthesis and applications of nano-TiO<sub>2</sub>: A review. *Environ. Sci. Pollut. Res.* **2019**, *26*, 3262–3291. [[CrossRef](#)] [[PubMed](#)]
47. Li, Z.; Li, Z.; Zuo, C.; Fang, X. Application of Nanostructured TiO<sub>2</sub> in UV Photodetectors: A Review. *Adv. Mater.* **2022**, *34*, 2109083. [[CrossRef](#)]
48. Park, H.; Park, Y.; Kim, W.; Choi, W. Surface modification of TiO<sub>2</sub> photocatalyst for environmental applications. *J. Photochem. Photobiol. C* **2013**, *15*, 1–20. [[CrossRef](#)]
49. Kumar, S.G.; Devi, L.G. Review on Modified TiO<sub>2</sub> Photocatalysis under UV/Visible Light: Selected Results and Related Mechanisms on Interfacial Charge Carrier Transfer Dynamics. *J. Phys. Chem. A* **2011**, *115*, 13211–13241. [[CrossRef](#)]
50. Arora, I.; Chawla, H.; Chandra, A.; Sagadevan, S.; Garg, S. Advances in the strategies for enhancing the photocatalytic activity of TiO<sub>2</sub>: Conversion from UV-light active to visible-light active photocatalyst. *Inorg. Chem. Commun.* **2022**, *143*, 109700. [[CrossRef](#)]
51. Xia, C.; Nguyen, T.C.; Nguyen, X.C.; Nguyen, C.X.; Kim, S.Y.; Nguyen, D.; Le, T.; Raizada, P.; Singh, R.; Nguyen, V.-H.; et al. Emerging cocatalysts in TiO<sub>2</sub>-based photocatalysts for light-driven catalytic hydrogen evolution: Progress and perspectives. *Fuel* **2022**, *307*, 121745. [[CrossRef](#)]
52. Daghrir, R.; Drogui, P.; Robert, D. Modified TiO<sub>2</sub> For Environmental Photocatalytic Applications: A Review. *Ind. Eng. Chem. Res.* **2013**, *52*, 3581–3599. [[CrossRef](#)]
53. Nakata, K.; Fujishima, A. TiO<sub>2</sub> photocatalysis: Design and applications. *J. Photochem. Photobiol. C* **2012**, *13*, 169–189. [[CrossRef](#)]
54. Sang, L.; Zhao, Y.; Burda, C. TiO<sub>2</sub> Nanoparticles as Functional Building Blocks. *Chem. Rev.* **2014**, *114*, 9283–9318. [[CrossRef](#)]
55. Schneider, J.; Matsuoka, M.; Takeuchi, M.; Zhang, J.; Horiuchi, Y.; Anpo, M.; Bahnemann, D.W. Understanding TiO<sub>2</sub> Photocatalysis: Mechanisms and Materials. *Chem. Rev.* **2014**, *114*, 9919–9986. [[CrossRef](#)]
56. Henderson, M.A.; Lyubinetsky, I. Molecular-Level Insights into Photocatalysis from Scanning Probe Microscopy Studies on TiO<sub>2</sub>. *Chem. Rev.* **2013**, *113*, 4428–4455. [[CrossRef](#)]
57. Kapilashrami, M.; Zhang, Y.; Liu, Y.-S.; Hagfeldt, A.; Guo, J. Probing the Optical Property and Electronic Structure of TiO<sub>2</sub> Nanomaterials for Renewable Energy Applications. *Chem. Rev.* **2014**, *114*, 9662–9707. [[CrossRef](#)]
58. Humayun, M.; Raziq, F.; Khan, A.; Luo, W. Modification strategies of TiO<sub>2</sub> for potential applications in photocatalysis: A critical review. *Green Chem. Lett. Rev.* **2018**, *11*, 86–102. [[CrossRef](#)]

59. Gao, R.-Q.; Sun, Q.; Fang, Z.; Li, G.-T.; Jia, M.-Z.; Hou, X.-M. Preparation of nano-TiO<sub>2</sub>/diatomite-based porous ceramics and their photocatalytic kinetics for formaldehyde degradation. *Int. J. Min. Met. Mater.* **2018**, *25*, 73–79. [[CrossRef](#)]
60. Gnanaprakasam, A.; Sivakumar, V.M.; Sivayogavalli, P.L.; Thirumarimurugan, M. Characterization of TiO<sub>2</sub> and ZnO nanoparticles and their applications in photocatalytic degradation of azodyes. *Ecotoxicol. Environ. Saf.* **2015**, *121*, 121–125. [[CrossRef](#)]
61. Guo, Q.; Zhou, C.; Ma, Z.; Yang, X. Fundamentals of TiO<sub>2</sub> Photocatalysis: Concepts, Mechanisms, and Challenges. *Adv. Mater.* **2019**, *31*, e1901997. [[CrossRef](#)]
62. He, H.; Luo, Z.; Yu, C. Diatomite-anchored g-C<sub>3</sub>N<sub>4</sub> nanosheets for selective removal of organic dyes. *J. Alloys Compd.* **2020**, *816*, 152652. [[CrossRef](#)]
63. Hua, C.; Liu, X.; Ren, S.; Zhang, G.; Liu, W. Preparation of visible light-responsive photocatalytic paper containing BiVO<sub>4</sub>@diatomite/MCC/PVBCFs for degradation of organic pollutants. *Ecotoxicol. Environ. Saf.* **2020**, *202*, 110897. [[CrossRef](#)] [[PubMed](#)]
64. Jatav, N.; Kuntail, J.; Khan, D.; Kumar De, A.; Sinha, I. AgI/CuWO<sub>4</sub> Z-scheme photocatalyst for the degradation of organic pollutants: Experimental and molecular dynamics studies. *J. Colloid Interface Sci.* **2021**, *599*, 717–729. [[CrossRef](#)] [[PubMed](#)]
65. Jeong, J.; Sekiguchi, K.; Sakamoto, K. Photochemical and photocatalytic degradation of gaseous toluene using short-wavelength UV irradiation with TiO<sub>2</sub> catalyst: Comparison of three UV sources. *Chemosphere* **2004**, *57*, 663–671. [[CrossRef](#)] [[PubMed](#)]
66. Jeong, K.; Deshmukh, P.R.; Park, J.; Sohn, Y.; Shin, W.G. ZnO-TiO<sub>2</sub> Core-Shell Nanowires: A Sustainable Photoanode for Enhanced Photoelectrochemical Water Splitting. *ACS Sustain. Chem. Eng.* **2018**, *6*, 6518–6526. [[CrossRef](#)]
67. Ji, J.; Xu, Y.; Huang, H.; He, M.; Liu, S.; Liu, G.; Xie, R.; Feng, Q.; Shu, Y.; Zhan, Y.; et al. Mesoporous TiO<sub>2</sub> under VUV irradiation: Enhanced photocatalytic oxidation for VOCs degradation at room temperature. *Chem. Eng. J.* **2017**, *327*, 490–499. [[CrossRef](#)]
68. Chen, C.; Ma, W.; Zhao, J. Semiconductor-mediated photodegradation of pollutants under visible-light irradiation. *Chem. Soc. Rev.* **2010**, *39*, 4206–4219. [[CrossRef](#)]
69. Florez, F.L.E.; Hiers, R.D.; Larson, P.; Johnson, M.; O'Rear, E.; Rondinone, A.J.; Khajotia, S.S. Antibacterial dental adhesive resins containing nitrogen-doped titanium dioxide nanoparticles. *Mater. Sci. Eng. C* **2018**, *93*, 931–943. [[CrossRef](#)]
70. Nosaka, Y.; Nosaka, A.Y. Generation and Detection of Reactive Oxygen Species in Photocatalysis. *Chem. Rev.* **2017**, *117*, 11302–11336. [[CrossRef](#)] [[PubMed](#)]
71. Kang, Y.; Yang, Y.; Yin, L.-C.; Kang, X.; Wang, L.; Liu, G.; Cheng, H.-M. Selective Breaking of Hydrogen Bonds of Layered Carbon Nitride for Visible Light Photocatalysis. *Adv. Mater.* **2016**, *28*, 6471–6477. [[CrossRef](#)] [[PubMed](#)]
72. Kanjwal, M.A.; Leung, W.W.-F. Titanium based composite-graphene nanofibers as high-performance photocatalyst for formaldehyde gas purification. *Ceram. Int.* **2019**, *45*, 5617–5626. [[CrossRef](#)]
73. Kaur, J.; Singhal, S. Facile synthesis of ZnO and transition metal doped ZnO nanoparticles for the photocatalytic degradation of Methyl Orange. *Ceram. Int.* **2014**, *40*, 7417–7424. [[CrossRef](#)]
74. Khalid, N.R.; Hammad, A.; Tahir, M.B.; Rafique, M.; Iqbal, T.; Nabi, G.; Hussain, M.K. Enhanced photocatalytic activity of Al and Fe co-doped ZnO nanorods for methylene blue degradation. *Ceram. Int.* **2019**, *45*, 21430–21435. [[CrossRef](#)]
75. Khalilzadeh, A.; Fatemi, S. Spouted bed reactor for VOC removal by modified nano-TiO<sub>2</sub> photocatalytic particles. *Chem. Eng. Res. Des.* **2016**, *115*, 241–250. [[CrossRef](#)]
76. Kim, J.; Zhang, P.; Li, J.; Wang, J.; Fu, P. Photocatalytic degradation of gaseous toluene and ozone under UV254+185 nm irradiation using a Pd-deposited TiO<sub>2</sub> film. *Chem. Eng. J.* **2014**, *252*, 337–345. [[CrossRef](#)]
77. Krichevskaya, M.; Preis, S.; Moiseev, A.; Pronina, N.; Deubener, J. Gas-phase photocatalytic oxidation of refractory VOCs mixtures: Through the net of process limitations. *Catal. Today* **2017**, *280*, 93–98. [[CrossRef](#)]
78. Dahl, M.; Liu, Y.; Yin, Y. Composite Titanium Dioxide Nanomaterials. *Chem. Rev.* **2014**, *114*, 9853–9889. [[CrossRef](#)] [[PubMed](#)]
79. Lv, C.; Lan, X.; Wang, L.; Yu, Q.; Zhang, M.; Sun, H.; Shi, J. Alkaline-earth-metal-doped TiO<sub>2</sub> for enhanced photodegradation and H<sub>2</sub> evolution: Insights into the mechanisms. *Catal. Sci. Technol.* **2019**, *9*, 6124–6135. [[CrossRef](#)]
80. Jia, J.; Zhang, J.; Wang, F.; Han, L.; Zhou, J.-Z.; Mao, B.-W.; Zhan, D. Synergetic effect enhanced photoelectrocatalysis. *Chem. Commun.* **2015**, *51*, 17700–17703. [[CrossRef](#)]
81. Gao, M.; Zhu, L.; Ong, W.L.; Wang, J.; Ho, G.W. Structural design of TiO<sub>2</sub>-based photocatalyst for H<sub>2</sub> production and degradation applications. *Catal. Sci. Technol.* **2015**, *5*, 4703–4726. [[CrossRef](#)]
82. Kim, D.S.; Kwak, S.Y. The hydrothermal synthesis of mesoporous TiO<sub>2</sub> with high crystallinity, thermal stability, large surface area and enhanced photocatalytic activity. *Appl. Catal. A Gen.* **2007**, *323*, 110–118. [[CrossRef](#)]
83. Tian, G.H.; Fu, H.G.; Jing, L.Q.; Xin, B.F.; Pan, K. Preparation and characterization of stable biphasic TiO<sub>2</sub> photocatalyst with high crystallinity, large surface area, and enhanced photoactivity. *J. Phys. Chem. C* **2008**, *112*, 3083–3089. [[CrossRef](#)]
84. Kumar, S.; Kaushik, R.D.; Purohit, L.P. Novel ZnO tetrapod-reduced graphene oxide nanocomposites for enhanced photocatalytic degradation of phenolic compounds and MB dye. *J. Mol. Liq.* **2021**, *327*, 114814. [[CrossRef](#)]
85. Lam, R.C.W.; Leung, M.K.H.; Leung, D.Y.C.; Vrijmoed, L.L.P.; Yam, W.C.; Ng, S.P. Visible-light-assisted photocatalytic degradation of gaseous formaldehyde by parallel-plate reactor coated with Cr ion-implanted TiO<sub>2</sub> thin film. *Sol. Energy Mater. Sol. Cells* **2007**, *91*, 54–61. [[CrossRef](#)]
86. Wang, J.; Wang, Z.; Wang, W.; Wang, Y.; Hu, X.; Liu, J.; Gong, X.; Miao, W.; Ding, L.; Li, X.; et al. Synthesis, modification and application of titanium dioxide nanoparticles: A review. *Nanoscale* **2022**, *14*, 6709–6734. [[CrossRef](#)]
87. Ismail Adel, A.; Bahnmann Detlef, W. Mesoporous titania photocatalysts: Preparation, characterization and reaction mechanisms. *J. Mater. Chem.* **2011**, *21*, 11686–11707. [[CrossRef](#)]

88. Bianchi, C.L.; Pirola, C.; Galli, F.; Stucchi, M.; Morandi, S.; Cerrato, G.; Capucci, V. Nano and micro-TiO<sub>2</sub> for the photodegradation of ethanol: Experimental data and kinetic modelling. *RSC Adv.* **2015**, *5*, 53419–53425. [[CrossRef](#)]
89. Lee, S.Y.; Kang, D.; Jeong, S.; Do, T.H.; Kin, J.H. Photocatalytic Degradation of Rhodamine B Dye by TiO<sub>2</sub> and Gold Nanoparticles Supported on a Floating Porous Polydimethylsiloxane Sponge under Ultraviolet and Visible Light Irradiation. *ACS Omega* **2020**, *5*, 4233–4241. [[CrossRef](#)]
90. Li, B.; Huang, H.; Guo, Y.; Zhang, Y. Diatomite-immobilized BiOI hybrid photocatalyst: Facile deposition synthesis and enhanced photocatalytic activity. *Appl. Surf. Sci.* **2015**, *353*, 1179–1185. [[CrossRef](#)]
91. Li, M.; Lu, B.; Ke, Q.F.; Guo, Y.-J.; Guo, Y.-P. Synergetic effect between adsorption and photodegradation on nanostructured TiO<sub>2</sub>/activated carbon fiber felt porous composites for toluene removal. *J. Hazard. Mater.* **2017**, *333*, 88–98. [[CrossRef](#)] [[PubMed](#)]
92. Liang, L.; Meng, Y.; Shi, L.; Ma, J.; Sun, J. Enhanced photocatalytic performance of novel visible light-driven Ag-TiO<sub>2</sub>/SBA-15 photocatalyst. *Superlattices Microstruct.* **2014**, *73*, 60–70. [[CrossRef](#)]
93. Liao, Q.; Pan, W.; Zou, D.; Shen, R.; Sheng, G.; Li, X.; Zhu, Y.; Dong, L.; Asiri, A.M.; Alamry, K.A.; et al. Using of g-C<sub>3</sub>N<sub>4</sub> nanosheets for the highly efficient scavenging of heavy metals at environmental relevant concentrations. *J. Mol. Liq.* **2018**, *261*, 32–40. [[CrossRef](#)]
94. Liu, X.; He, Y.; Yang, B.; Yan, Q.; Yang, J. Highly Efficient Photo-Degradation of Gaseous Organic Pollutants Catalyzed by Diatomite-Supported Titanium Dioxide. *Catalysts* **2020**, *10*, 380. [[CrossRef](#)]
95. Abbas, M.M.; Rasheed, M. Solid State Reaction Synthesis and Characterization of Cu doped TiO<sub>2</sub> Nanomaterials. *J. Phys. Conf. Ser.* **2021**, *1795*, 012059.
96. Xin, G.; Pan, H.; Chen, D.; Zhang, Z.; Wen, B. Synthesis and photocatalytic activity of N-doped TiO<sub>2</sub> produced in a solid phase reaction. *J. Phys. Chem. Solids* **2013**, *74*, 286–290. [[CrossRef](#)]
97. Liu, Z.S.; Liu, Z.L.; Liu, J.L.; Zhang, J.W.; Zhou, T.F.; Ji, X. Enhanced photocatalytic performance of Er-doped Bi<sub>24</sub>O<sub>31</sub>Br<sub>10</sub>: Facile synthesis and photocatalytic mechanism. *Mater. Res. Bull.* **2016**, *76*, 256–263. [[CrossRef](#)]
98. Lopes, F.V.S.; Monteiro, R.A.R.; Silva, A.M.T.; Silva, G.V.; Faria, J.L.; Mendes, A.M.; Vilar, V.J.P.; Boaventura, R.A.R. Insights into UV-TiO<sub>2</sub> photocatalytic degradation of PCE for air decontamination systems. *Chem. Eng. J.* **2012**, *204–206*, 244–257. [[CrossRef](#)]
99. Mendoza, J.A.; Lee, D.H.; Kang, J.H. Photocatalytic removal of gaseous nitrogen oxides using WO<sub>3</sub>/TiO<sub>2</sub> particles under visible light irradiation: Effect of surface modification. *Chemosphere* **2017**, *182*, 539–546. [[CrossRef](#)]
100. Mo, J.; Zhang, Y.; Xu, Q. Effect of water vapor on the by-products and decomposition rate of ppb-level toluene by photocatalytic oxidation. *Appl. Catal. B* **2013**, *132–133*, 212–218. [[CrossRef](#)]
101. Mosleh, S.; Rahimi, M.R.; Ghaedi, M.; Dashtian, K. Sonophotocatalytic degradation of trypan blue and vesuvine dyes in the presence of blue light active photocatalyst of Ag<sub>3</sub>PO<sub>4</sub>/Bi<sub>2</sub>S<sub>3</sub>-HKUST-1-MOF: Central composite optimization and synergistic effect study. *Ultrason. Sonochem.* **2016**, *32*, 387–397. [[CrossRef](#)] [[PubMed](#)]
102. Nasr, M.; Balme, S.; Eid, C.; Habchi, R.; Miele, P.; Bechelany, M. Enhanced Visible-Light Photocatalytic Performance of Electrospun rGO/TiO<sub>2</sub> Composite Nanofibers. *J. Phys. Chem. C* **2016**, *121*, 261–269. [[CrossRef](#)]
103. Wang, Y.; Li, J.; Zhang, B. Study on particle size control of TiO<sub>2</sub> particles prepared by gas phase oxidation of TiCl<sub>4</sub>. *Henan Sci.* **2016**, *34*, 662–666.
104. Yuan, X.; Liang, S.; Ke, H.; Wei, Q.; Huang, Z.; Chen, D. Photocatalytic property of polyester fabrics coated with Ag/TiO<sub>2</sub> composite films by magnetron sputtering. *Vacuum* **2020**, *172*, 109103. [[CrossRef](#)]
105. Wang, Y.; Li, X.; Liu, Y. Preparation of TiO<sub>2</sub> Sol by Sol-gel Method. *Chin. Syn Chem.* **2008**, *16*, 705–708.
106. Liu, S. Synthesis of TiO<sub>2</sub>-gel by Sol-gel Method. *Shandong Chem. Ind.* **2015**, *20*, 3–5.
107. Shi, J.-W.; Cui, H.-J.; Chen, J.-W.; Fu, M.-L.; Xu, B.; Luo, H.-Y.; Ye, Z.-L. TiO<sub>2</sub>/activated carbon fibers photocatalyst: Effects of coating procedures on the microstructure, adhesion property, and photocatalytic ability. *J. Colloid Interface Sci.* **2012**, *388*, 201–208. [[CrossRef](#)]
108. Ahmad, M.M.; Mushtaq, S.; Qahtani, S.; Al, H.; Sedky, A.; Alam, M.W. Investigation of TiO<sub>2</sub> Nanoparticles Synthesized by Sol-Gel Method for Effectual Photodegradation, Oxidation and Reduction Reaction. *Crystals* **2021**, *11*, 1456. [[CrossRef](#)]
109. Ni, Q.; Cheng, H.; Ma, J.; Kong, Y.; Komarneni, S. Efficient degradation of orange II by ZnMn<sub>2</sub>O<sub>4</sub> in a novel photo-chemical catalysis system. *Front. Chem. Sci. Eng.* **2020**, *14*, 956–966. [[CrossRef](#)]
110. Pant, B.; Park, M.; Park, S. Recent Advances in TiO<sub>2</sub> Films Prepared by Sol-gel Methods for Photocatalytic Degradation of Organic Pollutants and Antibacterial Activities. *Coatings* **2019**, *9*, 613. [[CrossRef](#)]
111. Pant, B.; Ojha, G.P.; Kuk, Y.S.; Kwon, O.H.; Park, Y.W.; Park, M. Synthesis and Characterization of ZnO-TiO<sub>2</sub>/Carbon Fiber Composite with Enhanced Photocatalytic Properties. *Nanomaterials* **2020**, *10*, 1960. [[CrossRef](#)] [[PubMed](#)]
112. Pham, T.D.; Lee, B.K. Novel adsorption and photocatalytic oxidation for removal of gaseous toluene by V-doped TiO<sub>2</sub>/PU under visible light. *J. Hazard. Mater.* **2015**, *300*, 493–503. [[CrossRef](#)] [[PubMed](#)]
113. Pham, T.-D.; Lee, B.-K. Selective removal of polar VOCs by novel photocatalytic activity of metals co-doped TiO<sub>2</sub>/PU under visible light. *Chem. Eng. J.* **2017**, *307*, 63–73. [[CrossRef](#)]
114. He, Y.G.; Yan, Q.; Chang, X.Y.; Zhu, M.; Wang, W.; Dong, M.; Song, L.; Yang, J.; Huang, Y. Solvothermal Synthesis of Novel 3D Peony-Like TiO<sub>2</sub> Microstructures and its Enhanced Photocatalytic Activity. *NANO Brief Rep. Rev.* **2018**, *13*, 18500576. [[CrossRef](#)]
115. He, Y.; Yan, Q.; Liu, X.; Dong, M.; Yang, J.J. Effect of annealing on the structure, morphology and photocatalytic activity of surface-fluorinated TiO<sub>2</sub> with dominant {001} facets. *J. Photoch. Photobio. A* **2020**, *393*, 112400. [[CrossRef](#)]

116. Xiao, J.R.; Peng, T.Y.; Li, R.; Peng, Z.; Yan, C. Preparation, phase transformation and photocatalytic activities of cerium-doped mesoporous titania nanoparticles. *J. Solid State Chem.* **2006**, *179*, 1161–1170. [[CrossRef](#)]
117. Yang, Z.; He, Z.; Wu, W.; Zhou, Y. Preparation of graphene-TiO<sub>2</sub> photocatalysis materials by laser-induced hydrothermal method. *Colloids Interface Sci. Commun.* **2021**, *42*, 100408. [[CrossRef](#)]
118. Yamashita, H.; Harada, M.; Tani, A. Preparation of efficient titanium oxide photocatalysts by an ionized cluster beam (ICB) method and their photocatalytic reactivities for the purification of water. *Catal. Today* **2000**, *63*, 3–69. [[CrossRef](#)]
119. Pizem, H.; Sukenik, C.N.; Sampathkumaran, U.; McIlwain, A.K.; De Cuire, M.R. Effects of substrate surface unctonality on solution-deposited titania films. *Chem. Mater.* **2002**, *14*, 76–2485. [[CrossRef](#)]
120. Saravanan, R.; Gupta, V.K.; Narayanan, V.; Stephen, A. Comparative study on photocatalytic activity of ZnO prepared by different methods. *J. Mol. Liq.* **2013**, *181*, 133–141. [[CrossRef](#)]
121. Senthilraja, A.; Subash, B.; Krishnakumar, B.; Rajamanickam, D.; Swaminathan, M.; Shanthi, M. Synthesis, characterization and catalytic activity of co-doped Ag–Au–ZnO for MB dye degradation under UV-A light. *Mater. Sci. Semicond. Process.* **2014**, *22*, 83–91. [[CrossRef](#)]
122. Karbassi, M.; Zarrintaj, P.; Ghafarinazari, A.; Saeb, M.R.; Mohammadi, M.R.; Yazdanpanah, A.; Rajadas, J.; Mozafari, M. Microemulsion-based synthesis of a visible-light-responsive Si-doped TiO<sub>2</sub> photocatalyst and its photodegradation efficiency potential. *Mater. Chem. Phys.* **2018**, *220*, 374–382. [[CrossRef](#)]
123. Medhi, R.; Marquez, M.D.; Lee, T.R. Visible-Light-Active Doped Metal Oxide Nanoparticles: Review of their Synthesis, Properties, and Applications. *ACS Appl. Nano Mater.* **2020**, *3*, 6156–6185. [[CrossRef](#)]
124. Singh, J.; Arora, A.; Basu, S. Synthesis of coral like WO<sub>3</sub>/g-C<sub>3</sub>N<sub>4</sub> nanocomposites for the removal of hazardous dyes under visible light. *J. Alloys Compd.* **2019**, *808*, 151734. [[CrossRef](#)]
125. Singh, J.; Kumar, S.; Rishikesh; Manna, A.K.; Soni, R.K. Fabrication of ZnO–TiO<sub>2</sub> nanohybrids for rapid sunlight driven photodegradation of textile dyes and antibiotic residue molecules. *Opt. Mater.* **2020**, *107*, 110138. [[CrossRef](#)]
126. Son, H.K.; Sivakumar, S.; Rood, M.J.; Kim, B.J. Electrothermal adsorption and desorption of volatile organic compounds on activated carbon fiber cloth. *J. Hazard. Mater.* **2016**, *301*, 27–34. [[CrossRef](#)]
127. Takeuchi, M.; Hidaka, M.; Anpo, M. Efficient removal of toluene and benzene in gas phase by the TiO<sub>2</sub>/Y-zeolite hybrid photocatalyst. *J. Hazard. Mater.* **2012**, *237–238*, 133–139. [[CrossRef](#)]
128. Kochuveedu, S.T.; Jang, Y.H.; Kim, D.H. A study on the mechanism for the interaction of light with noble metal-metal oxide semiconductor nanostructures for various photophysical applications. *Chem. Soc. Rev.* **2013**, *42*, 8467–8493. [[CrossRef](#)]
129. Hernandez, J.V.; Coste, S.; Murillo, A.G.; Romo, F.C.; Kassiba, A. Effects of metal doping (Cu, Ag, Eu) on the electronic and optical behavior of nanostructured TiO<sub>2</sub>. *J. Alloys Compd.* **2017**, *710*, 355–363. [[CrossRef](#)]
130. Tejasvi, R.; Sharma, M.; Upadhyay, K. Passive photo-catalytic destruction of air-borne VOCs in high traffic areas using TiO<sub>2</sub>-coated flexible PVC sheet. *Chem. Eng. J.* **2015**, *262*, 875–881. [[CrossRef](#)]
131. Crişan, M.; Mardare, D.; Ianculescu, A.; Dragan, N.; Nitoi, I.; Grisan, D.; Voicescu, M.; Todan, L.; Oancea, P.; Adomnitei, G. Iron doped TiO<sub>2</sub> films and their photoactivity in nitrobenzene removal from water. *Appl. Surf. Sci.* **2018**, *45*, 201–215. [[CrossRef](#)]
132. Tseng, H.-H.; Wei, M.-C.; Hsiung, S.-F.; Chiou, C.-W. Degradation of xylene vapor over Ni-doped TiO<sub>2</sub> photocatalysts prepared by polyol-mediated synthesis. *Chem. Eng. J.* **2009**, *150*, 160–167. [[CrossRef](#)]
133. Koh, P.W.; Hatta MH, M.; Ong, S.T.; Yuliati, L.; Lee, S.L. Photocatalytic degradation of photosensitizing and non-photosensitizing dyes over chromium doped titania photocatalysts under visible light. *J. Photoch. Photobiol. A* **2017**, *332*, 215–223. [[CrossRef](#)]
134. Yang, S.B.; Chun, H.H.; Tayade, R.J.; Jo, W.-K. Iron-functionalized titanium dioxide on flexible glass fibers for photocatalysis of benzene, toluene, ethylbenzene, and o-xylene(BTEX) under visible- or ultraviolet-light irradiation. *J. Air Waste Manag. A* **2015**, *65*, 365–373. [[CrossRef](#)] [[PubMed](#)]
135. Hung, W.C.; Chen, Y.C.; Chu, H.; Tseng, T.-K. Synthesis and characterization of TiO<sub>2</sub> and Fe/TiO<sub>2</sub> nanoparticles and their performance for photocatalytic degradation of 1,2-dichloroethane. *Appl. Surf. Sci.* **2008**, *255*, 2205–2213. [[CrossRef](#)]
136. Saroj, S.; Singh, L.; Singh, S.V. Photodegradation of Direct Blue-199 in carpet industry wastewater using iron-doped TiO<sub>2</sub> nanoparticles and regenerated photocatalyst. *Int. J. Chem. Kinet.* **2019**, *51*, 189–205. [[CrossRef](#)]
137. Wang, J.; Liu, Z.; Cai, R. A New Role for Fe<sup>3+</sup> in TiO<sub>2</sub> Hydrosol: Accelerated Photodegradation of Dyes under Visible Light. *Environ. Sci. Technol.* **2008**, *42*, 5759–5764. [[CrossRef](#)]
138. Yu, H.; Irie, H.; Shimodaira, Y.; Hosogi, Y.; Kuroda, Y.; Mlyauch, M.; Hashimoto, K. An Efficient Visible-Light-Sensitive Fe(III)-Grafted TiO<sub>2</sub> Photocatalyst. *J. Phys. Chem. C* **2010**, *114*, 16481–16487. [[CrossRef](#)]
139. Sun, H.; Dong, B.; Song, L.; Du, J.; Gao, R.; Su, G.; Gao, L. High photodegradation ability of dyes by Fe(III)-tartrate/TiO<sub>2</sub> nanotubular photocatalyst supported via photo-Fenton reaction. *J. Photoch. Photobiol. A* **2017**, *334*, 20–25. [[CrossRef](#)]
140. Kapridaki, C.; Xynidis, N.; Vazgiouraki, E.; Kallithrakas-Kontos, N.; Marvelaki-Kalaizaki, P. Characterization of Photoactive Fe-TiO<sub>2</sub> Lime Coatings for Building Protection: The Role of Iron Content. *Materials* **2019**, *12*, 1847. [[CrossRef](#)]
141. Pham, T.D.; Lee, B.K.; Lee, C.H. The advanced removal of benzene from aerosols by photocatalytic oxidation and adsorption of Cu-TiO<sub>2</sub>/PU under visible light irradiation. *Appl. Catal. B* **2016**, *182*, 172–183. [[CrossRef](#)]
142. Reddy, N.L.; Emin, S.; Kumari, V.D.; Muthukonda Venkatakrishnan, S. CuO Quantum Dots Decorated TiO<sub>2</sub> Nanocomposite Photocatalyst for Stable Hydrogen Generation. *Ind. Eng. Chem. Res.* **2018**, *57*, 568–577. [[CrossRef](#)]
143. Mertah, O.; El Hajjaji, K.; El Amrani, S.; Tanji, K.; Goncharova, I.; Kherbeche, A. Visible-light Cu/TiO<sub>2</sub>@Ag<sub>3</sub>PO<sub>4</sub> heterostructure photocatalyst for selective nitrate reduction and antimicrobial activity. *Opt. Mater.* **2022**, *129*, 112549. [[CrossRef](#)]

144. Tseng, T.K.; Lin, Y.S.; Chen, Y.J.; Chu, H. A review of photocatalysts prepared by sol-gel method for VOCs removal. *Int. J. Mol. Sci.* **2010**, *11*, 2336–2361. [[CrossRef](#)] [[PubMed](#)]
145. Mohammed, A.M.; Khaled, F.Q.; Fares, T.A.; Salah, M.E.; Reda, S.S. Role of NiO Nanoparticles in Enhancing Structure Properties of TiO<sub>2</sub> and Its Applications in Photodegradation and Hydrogen Evolution. *ACS Omega* **2021**, *6*, 30386–30400.
146. Riaz, N.; Chong, F.K.; Man, Z.B.; Khan, M.S.; Dutta, B.K. Photodegradation of Orange II under Visible Light Using Cu–Ni/TiO<sub>2</sub>: Influence of Cu: Ni Mass Composition, Preparation, and Calcination Temperature. *Ind. Eng. Chem. Res.* **2013**, *52*, 4491–4503. [[CrossRef](#)]
147. Shayegan, Z.; Lee, C.S.; Haghghat, F. TiO<sub>2</sub> photocatalyst for removal of volatile organic compounds in gas phase—A review. *Chem. Eng. J.* **2018**, *334*, 2408–2439. [[CrossRef](#)]
148. Tieng, S.T.; Kanaev, A.; Chhor, K. New homogeneously doped Fe(III)-TiO<sub>2</sub> photocatalyst for gaseous pollutant degradation. *Appl. Catal. A Gen.* **2011**, *399*, 191–197. [[CrossRef](#)]
149. Lu, Y.; Huang, B.; Xu, X.; Liu, Y.; Cheng, A.; Hou, J. Construction and characteristics of a novel green photocatalyst: iron (III) doped titania nanomesh. *Chem. Eng. J.* **2021**, *47*, 23497–23506. [[CrossRef](#)]
150. Murcia, J.J.; Hidalgo, M.C.; Navio, J.A.; Vaiano, V.; Sannino, D.; Ciambelli, P. Cyclohexane photocatalytic oxidation on Pt/TiO<sub>2</sub> catalysts. *Catal. Today* **2013**, *209*, 164–169. [[CrossRef](#)]
151. Li, X.Y.; Zou, X.J.; Qu, Z.P.; Zhao, Q.; Wang, L. Photocatalytic degradation of gaseous toluene over Ag-doping TiO<sub>2</sub> nanotube powder prepared by anodization coupled with impregnation method. *Chemosphere* **2011**, *83*, 674–679. [[CrossRef](#)]
152. Lima, K.V.; Emídio, E.S.; Pupo Nogueira, R.F.; Vasconcelos, N.D.S.L.; Araújo, A.B. Application of a stable Ag/TiO<sub>2</sub> film in the simultaneous photodegradation of hormones. *J. Chem. Technol. Biotechnol.* **2020**, *95*, 2656–2663.
153. Lopes, F.C.S.M.R.; da Rocha, M.G.C.; Bargiel, P.; Ferreira, H.S.; Pires, C.A.M. Ag/TiO<sub>2</sub> photocatalyst immobilized onto modified natural fibers for photodegradation of anthracene. *Chem. Eng. Sci.* **2020**, *227*, 115939. [[CrossRef](#)]
154. Nguyen, T.H.; Hoang, N.H.; Tran, C.V.; Nguyen, P.T.M.; Dang, T.-D.; Chung, W.J.; Chang, S.W.; Nguyen, D.D.; Kumar, P.S.; La, D.D. Green synthesis of a photocatalyst Ag/TiO<sub>2</sub> nanocomposite using *Cleistanax operculatus* leaf extract for degradation of organic dye. *Chemosphere* **2022**, *306*, 135474. [[CrossRef](#)]
155. Gang, R.; Xia, Y.; Xu, L.; Zhang, L.; Ju, S.; Wang, Z.; Koppala, S. Size controlled Ag decorated TiO<sub>2</sub> plasmonic photocatalysts for tetracycline degradation under visible light. *Surf. Interfaces* **2022**, *31*, 102018. [[CrossRef](#)]
156. Wang, Y.; Zhao, S.; Yang, Y.; Rodriguez, R.D.; Lipovka, A.; Lu, Y.; Huang, H.; Chen, J. Ag nanoparticle-decorated Bi<sub>2</sub>O<sub>3</sub>-TiO<sub>2</sub> heterogeneous nanotubular photocatalysts for enhanced degradation of organic contaminants. *Colloids Surf. A Physicochem. Eng. Asp.* **2022**, *648*, 129233. [[CrossRef](#)]
157. Zhou, Y.; Zhao, D.; Cao, F.; Luo, Q.; Xiang, Y.; Deng, Y. Highly photoactive Ag-based urchin-like E-g-C<sub>3</sub>N<sub>4</sub>/TiO<sub>2</sub> ternary composite photocatalyst. *Micro Nano Lett.* **2019**, *14*, 154–157. [[CrossRef](#)]
158. Houskova, V.; Stengl, V.; Bakardjieva, S.; Murafa, N.; Tyrpekl, V. Efficient gas phase photodecomposition of acetone by Ru-doped Titania. *Appl. Catal. B* **2009**, *89*, 613–619. [[CrossRef](#)]
159. Fatimah, I.; Nurillahi, R.; Sahroni, I.; Muraza, O. TiO<sub>2</sub>-pillared saponite and photosensitization using a ruthenium complex for photocatalytic enhancement of the photodegradation of bromophenol blue. *Appl. Clay Sci.* **2019**, *183*, 105302. [[CrossRef](#)]
160. Menendez-Flores, V.M.; Ohno, T. High visible-light active Ir-doped-TiO<sub>2</sub> brookite photocatalyst synthesized by hydrothermal microwave-assisted process. *Catal. Today* **2014**, *230*, 214–220. [[CrossRef](#)]
161. Wu, Q.; Ye, J.; Qiao, W.; Li, Y.; Niemantsverdriet, J.W.; Richards, E.; Pan, F.; Su, R. Inhibit the formation of toxic methylphenolic by-products in photo-decomposition of formaldehyde–toluene/xylene mixtures by Pd cocatalyst on TiO<sub>2</sub>. *Appl. Catal. B* **2021**, *291*, 120118. [[CrossRef](#)]
162. Michael, B.; Andrew, M. Photonic efficiency and selectivity study of M (M=Pt, Pd, Au and Ag)/TiO<sub>2</sub> photocatalysts for methanol reforming in the gas phase. *J. Photochem. Photobiol. A Chem.* **2020**, *389*, 112257.
163. Sharma, S.; Mittal, A.; Chauhan, N.S.; Saini, S.; Yadav, J.; Kushwaha, M.; Chakraborty, R.; Sengupta, S.; Kumari, K.; Kumar, N. Mechanistic investigation of RhB photodegradation under low power visible LEDs using a Pd-modified TiO<sub>2</sub>/Bi<sub>2</sub>O<sub>3</sub> photocatalyst: Experimental and DFT studies. *J. Phys. Chem. Solids* **2022**, *162*, 110510. [[CrossRef](#)]
164. Cristina, L.; Pietro, A.; Teresa, F.M.; Pirri, G.; Poerio, T.; Molinari, R. Pd/TiO<sub>2</sub> doped faujasite photocatalysts for acetophenone transfer hydrogenation in a photocatalytic membrane reactor. *J. Catal.* **2017**, *353*, 152–161.
165. Al-Azri, Z.H.N.; Chen, W.-T.; Chan, A.; Jovic, V.; Ina, T.; Idriss, H.; Waerhouse, G.I.N. The roles of metal co-catalysts and reaction media in photocatalytic hydrogen production: Performance evaluation of M/TiO<sub>2</sub> photocatalysts (M = Pd, Pt, Au) in different alcohol–water mixtures. *J. Catal.* **2015**, *329*, 355–367. [[CrossRef](#)]
166. Jin, K.; Qin, M.; Li, X.; Wang, R.; Zhao, Y.; Wang, H. Z-scheme Au@TiO<sub>2</sub>/Bi<sub>2</sub>WO<sub>6</sub> heterojunction as efficient visible-light photocatalyst for degradation of antibiotics. *J. Mol. Liq.* **2022**, *364*, 120017. [[CrossRef](#)]
167. Pradeepta, B.; Soumya, R.D.; Kulamani, P. Mechanistic insight the visible light driven hydrogen generation by plasmonic Au-Cu alloy mounted on TiO<sub>2</sub>@B-doped g-C<sub>3</sub>N<sub>4</sub> heterojunction photocatalyst. *J. Alloys Compd.* **2022**, *909*, 164754.
168. Al-Hajji, L.A.; Ismail, A.A.; Bumajdad, A.; Alsaidi, M.; Ahmed, S.A.; Al-Hazza, A.; Ahmed, N. Photodegradation of powerful five estrogens collected from waste water treatment plant over visible-light-driven Au/TiO<sub>2</sub> photocatalyst. *Environ. Technol. Innov.* **2021**, *24*, 101958. [[CrossRef](#)]
169. Yu, X.; Qiu, H.; Wang, B.; Meng, Q.; Sun, S.; Tang, Y.; Zhao, K. A ternary photocatalyst of all-solid-state Z-scheme TiO<sub>2</sub>-Au-BiOBr for efficiently degrading various dyes. *J. Alloys Compd.* **2020**, *839*, 155597. [[CrossRef](#)]

170. Luna, M.; Gatica, J.M.; Vidal, H.; Mosquera, M.J. One-pot synthesis of Au/N-TiO<sub>2</sub> photocatalysts for environmental applications: Enhancement of dyes and NO<sub>x</sub> photodegradation. *Powder Technol.* **2019**, *355*, 793–807. [CrossRef]
171. Alsaidi, M.; Azeez, F.A.; Al-Hajji, L.A.; Ismail, A.A. Impact of reaction parameters for photodegradation pharmaceuticals in wastewater over gold/titania photocatalyst synthesized by pyrolysis of NH<sub>2</sub>-MIL-125(Ti). *J. Environ. Manag.* **2022**, *314*, 115047. [CrossRef] [PubMed]
172. Wu, Y.; Liu, H.; Zhang, J.; Chen, F. Enhanced Photocatalytic Activity of Nitrogen-Doped Titania by Deposited with Gold. *J. Phys. Chem. C* **2009**, *113*, 14689–14695. [CrossRef]
173. Mayoufi, A.; Nsib, M.F.; Houas, A. Doping level effect on visible-light irradiation W-doped TiO<sub>2</sub>-anatase photocatalysts for Congo red photodegradation. *Comptes Rendus Chim.* **2014**, *17*, 818–823. [CrossRef]
174. Mogal, S.I.; Gandhi, V.G.; Mishra, M.; Ttipathi, S.; Shripathi, T.; Joshi, P.A.; Shah, D.O. Single-step synthesis of silver-doped titanium dioxide: Influence of silver on structural, textural, and photocatalytic properties. *Ind. Eng. Chem. Res.* **2014**, *53*, 5749–5758. [CrossRef]
175. Ellouzi, I.; Bouddouch, A.; Bakiz, B.; Benlhachemi, A.; Oualid, H.A. Glucose-assisted ball milling preparation of silver-doped biphasic TiO<sub>2</sub> for efficient photodegradation of Rhodamine B: Effect of silver-dopant loading. *Chem. Phys. Lett.* **2021**, *770*, 138456. [CrossRef]
176. Alamelu, K.; Jaffar Ali, B.M. TiO<sub>2</sub>-Pt composite photocatalyst for photodegradation and chemical reduction of recalcitrant organic pollutants. *J. Environ. Chem. Eng.* **2018**, *6*, 5720–5731.
177. Wu, Y.; Gong, Y.; Liu, J.; Zhang, Z.; Xu, Y.; Ren, H.; Li, C.; Niu, L. B and Y co-doped TiO<sub>2</sub> photocatalyst with enhanced photodegradation efficiency. *J. Alloys Compd.* **2017**, *695*, 1462–1469. [CrossRef]
178. Erik, C.; Elisa, G.; Paola, C.; Cristina, P.M. The role of Cerium, Europium and Erbium doped TiO<sub>2</sub> photocatalysts in water treatment: A mini-review. *Chem. Eng. J. Adv.* **2022**, *10*, 100268.
179. Thi, V.H.T.; Lee, B.K. Effective photocatalytic degradation of paracetamol using La-doped ZnO photocatalyst under visible light irradiation. *Mater. Res. Bull.* **2017**, *96*, 171–182. [CrossRef]
180. Wang, M.; Xu, X.; Lin, L.; He, D. Gd–La codoped TiO<sub>2</sub> nanoparticles as solar photocatalysts. *Mater. Int.* **2015**, *125*, 6–11. [CrossRef]
181. Wang, Q.; Xu, S.; Shen, F. Preparation and Characterization of TiO<sub>2</sub> photocatalysts co-doped with iron(III) and lanthanum for the degradation of organic pollutants. *App. Sur. Sci.* **2011**, *257*, 7671–7677. [CrossRef]
182. Li, S.; Yang, Y.; Su, Q.; Liu, X.; Zhao, H.; Zhao, Z.; Li, J.; Jin, C. Synthesis and photocatalytic activity of transition metal and rare earth element co-doped TiO<sub>2</sub> nano particles. *Mater. Lett.* **2019**, *252*, 123–125. [CrossRef]
183. Jiang, H.; Wang, Q.; Zang, S.; Li, J.; Wang, X. Hydrothermal synthesis of high-efficiency Pr, N, P-tridoped TiO<sub>2</sub> from TiCl<sub>4</sub> hydrolysis and mechanism of its enhanced photoactivity. *J. Alloys Compd.* **2014**, *600*, 34–42. [CrossRef]
184. Eskandarloo, H.; Badiei, A.; Behnajady, M.A. TiO<sub>2</sub>/CeO<sub>2</sub> Hybrid Photocatalyst with Enhanced Photocatalytic Activity: Optimization of Synthesis Variables. *Ind. Eng. Chem. Res.* **2014**, *53*, 7847–7855. [CrossRef]
185. Thirupathi, M.; Kumar, P.S.; Devendran, P.; Ramalingan, C.; Swaminathan, M.; Nagarajan, E.R. Ce@TiO<sub>2</sub> nanocomposites: An efficient, stable and affordable photocatalyst for the photodegradation of diclofenac sodium. *J. Alloys Compd.* **2018**, *735*, 728–734. [CrossRef]
186. Xu, D.-X.; Lian, Z.-W.; Fu, M.-L.; Yuan, B.; Shi, J.-W.; Cui, H.-J. Advanced near-infrared-driven photocatalyst: Fabrication, characterization, and photocatalytic performance of NaYF<sub>4</sub>:Yb<sup>3+</sup>, Tm<sup>3+</sup>@TiO<sub>2</sub> core@shell microcrystals. *Appl. Catal. B* **2013**, *142–143*, 377–386. [CrossRef]
187. Liu, Y.; Wang, W.; Si, M.; Yu, Y.; Zhang, H. (Yb<sup>3+</sup>, Er<sup>3+</sup>) co-doped TiO<sub>2</sub>/Ag<sub>3</sub>PO<sub>4</sub> hybrid photocatalyst with enhanced activity for photodegradation of phenol. *Appl. Surf. Sci.* **2019**, *463*, 159–168. [CrossRef]
188. Cheng, Z.W.; Gu, Z.Q.; Chen, J.M.; Yu, J.; Zhou, L. Synthesis, characterization, and photocatalytic activity of porous La-N-co-doped TiO<sub>2</sub> nanotubes for gaseous chlorobenzene oxidation. *J. Environ. Sci.* **2016**, *46*, 203–213. [CrossRef]
189. Trujillo-Navarrete, B.; Haro-Vazquez, M.P.; Felix-Navarro, R.M.; Paraguay-Delgado, F.; Alvarez-Huerta, H.; Perez-Sicairos, S.; Reynoso-Soto, E.A. Effect of Nd<sup>3+</sup> doping on structure, microstructure, lattice distortion and electronic properties of TiO<sub>2</sub> nanoparticles. *J. Rare Earths* **2017**, *35*, 259–270. [CrossRef]
190. Zhao, Z.; Liu, J.; Sa, G.; Xu, A. Electronic properties and photodegradation ability of Nd-TiO<sub>2</sub> for Phenol. *J. Rare Earths* **2022**, *40*, 1063–1072. [CrossRef]
191. Feng, H.; Xu, H.; Feng, H.; Gao, Y.; Jin, X. The sol-gel synthesis and photocatalytic activity of Gd-SiO<sub>2</sub>-TiO<sub>2</sub> photocatalyst. *Chem. Phys. Lett.* **2019**, *733*, 136676. [CrossRef]
192. Marschall, R.; Wang, L. Non-metal doping of transition metal oxides for visible-light photocatalysis. *Catal. Today* **2014**, *22*, 111–135. [CrossRef]
193. Yu, L.; Li, J.; Lin, Y. Research progress in photocatalytic performance of non-metallic doped nano-TiO<sub>2</sub>. *Appl. Chem. Ind.* **2019**, *48*, 1945–1948.
194. Piątkowska, A.; Janus, M.; Szymański, K.; Mozia, S. C, N and S-doped TiO<sub>2</sub> photocatalysts: A Review. *Catalysts* **2021**, *11*, 144. [CrossRef]
195. Asahi, R.; Morikawa, T.; Irie, H.; Ohwaki, T. Nitrogen-Doped Titanium Dioxide as Visible-Light-Sensitive Photocatalyst: Designs, Developments, and Prospects. *Chem. Rev.* **2014**, *114*, 9824–9852. [CrossRef] [PubMed]
196. Zeng, L.; Lu, Z.; Li, M.H.; Yang, J.; Song, W.; Zeng, D.; Xie, C. A modular calcination method to prepare modified N-doped TiO<sub>2</sub> nanoparticle with high photocatalytic activity. *Appl. Catal. B* **2016**, *183*, 308–316. [CrossRef]

197. Bianchi, C.L.; Cappelletti, G.; Ardizzone, S.; Gialanella, S.; Naldoni, A.; Oliva, C.; Pirola, C. N-doped TiO<sub>2</sub> from TiCl<sub>3</sub> for photodegradation of air pollutants. *Catal. Today* **2009**, *144*, 31–36. [CrossRef]
198. Lin, Y.-M.; Tseng, Y.-H.; Huang, J.-H.; Chao, C.C.; Chen, C.-C.; Wang, A.I. Photocatalytic Activity for Degradation of Nitrogen Oxides over Visible Light Responsive Titania-Based Photocatalysts. *Environ. Sci. Technol.* **2006**, *40*, 1616–1621. [CrossRef]
199. Khan, T.T.; Bari, G.A.M.R.; Kang, H.-J.; Lee, T.-G.; Park, J.-W.; Hwang, H.J.; Hossain, S.M.; Mun, J.S.; Suzuki, N.; Fujishima, A.; et al. Synthesis of N-Doped TiO<sub>2</sub> for Efficient Photocatalytic Degradation of Atmospheric NO<sub>x</sub>. *Catalysts* **2021**, *11*, 109. [CrossRef]
200. Dong, F.; Wang, H.Q.; Wu, Z.B. One-step “green” synthetic approach for mesoporous C-doped titanium dioxide with efficient visible light photocatalytic activity. *J. Phys. Chem. C* **2009**, *113*, 16717–16723. [CrossRef]
201. Bilge, S.; Sinağ, A. TiO<sub>2</sub>/core-shell structured carbon support materials derived from hydrothermal carbonization of waste masks biomass: A green photocatalyst. *Inorg. Chem. Commun.* **2022**, *144*, 109911. [CrossRef]
202. Nu, T.T.V.; Tran, N.H.T.; Truong, P.L.; Truong, P.L.; Phan, B.T.; Dinh, M.T.N.; Dinh, V.-P.; Phan, T.S.; Go, S.; Chang, M.C.; et al. Green synthesis of microalgae-based carbon dots for decoration of TiO<sub>2</sub> nanoparticles in enhancement of organic dye photodegradation. *Environ. Res.* **2022**, *206*, 112631. [CrossRef] [PubMed]
203. Takeda, N.; Iwata, N.; Torimoto, T.; Yoneyama, H. Influence of Carbon Black as an Adsorbent Used in TiO<sub>2</sub> Photocatalyst Films on Photodegradation Behaviors of Propylamide. *J. Catal.* **1998**, *177*, 240–246. [CrossRef]
204. Farjadfar, S.; Ghiaci, M.; Kulinch, S.A.; Wunderlich, W. Efficient photocatalyst for the degradation of cationic and anionic dyes prepared via modification of carbonized mesoporous TiO<sub>2</sub> by encapsulation of carbon dots. *Mater. Res. Bull.* **2022**, *155*, 111963. [CrossRef]
205. Tetteh, E.K.; Rathilal, S. Adsorption and Photocatalytic Mineralization of Bromophenol Blue Dye with TiO<sub>2</sub> Modified with Clinoptilolite/ Activated Carbon. *Catalysts* **2021**, *11*, 7–23. [CrossRef]
206. Jo, W.K.; Kim, J.T. Decomposition of gas-phase aromatic hydrocarbons by applying an annular-type reactor coated with sulfur-doped photocatalyst under visible-light irradiation. *J. Chem. Technol. Biotechnol.* **2010**, *85*, 485–492. [CrossRef]
207. Jo, W.K.; Kang, H.J. Aluminum sheet-based S-doped TiO<sub>2</sub> for photocatalytic decomposition of toxic organic vapors. *Chin. J. Catal.* **2014**, *35*, 1189–1195. [CrossRef]
208. Wang, Y.; Li, J.; Peng, P.; Lu, T.; Wang, L. Preparation of S-TiO<sub>2</sub> photocatalyst and photodegradation of L-acid under visible light. *Appl. Surf. Sci.* **2008**, *254*, 5276–5280. [CrossRef]
209. Khan, R.; Kim, S.W.; Kim, T.-J.; Nam, C.-M. Comparative study of the photocatalytic performance of boron-iron Co-doped and boron-doped TiO<sub>2</sub> nanoparticles. *Mater. Chem. Phys.* **2008**, *112*, 167–172. [CrossRef]
210. Yun, E.-T.; Yoo, H.-Y.; Kim, W.; Kim, H.-E.; Kang, G.; Lee, H.; Lee, S.; Park, T.; Lee, C.; Kim, J.-H.; et al. Visible-light-induced activation of periodate that mimics dye-sensitization of TiO<sub>2</sub>: Simultaneous decolorization of dyes and production of oxidizing radicals. *Appl. Catal. B Environ.* **2017**, *203*, 475–484. [CrossRef]
211. Tian, L.; Xing, L.; Shen, X.; Li, Q.; Ge, S.; Liu, B.; Jie, L. Visible light enhanced Fe–I–TiO<sub>2</sub> photocatalysts for the degradation of gaseous benzene. *Atmos. Pollut. Res.* **2020**, *11*, 179–185. [CrossRef]
212. Wang, J.-C.; Lou, H.-H.; Xu, Z.-H.; Gui, C.-X.; Li, Z.-J.; Jiang, K.; Zhang, Y.-P.; Qu, L.-B.; Shi, W. Natural sunlight driven highly efficient photocatalysis for simultaneous degradation of rhodamine B and methyl orange using I/C codoped TiO<sub>2</sub> photocatalyst. *J. Hazard. Mater.* **2018**, *360*, 356–363. [CrossRef] [PubMed]
213. Zhou, M.; Zhong, X.; Wei, D.; Yang, K.; Chen, Y.; Jia, C.; Li, J. Highly efficient doping of titanium dioxide with sulfur using disulfide-linked macrocycles for hydrogen production under visible light. *Green Chem.* **2022**, *24*, 2557–2566. [CrossRef]
214. Chen, D.M.; Jiang, Z.Y.; Geng, J.Q.; Wang, Q.; Yang, D. Carbon and nitrogen co-doped TiO<sub>2</sub> with enhanced visible-light photocatalytic activity. *Ind. Eng. Chem. Res.* **2007**, *46*, 2741–2746. [CrossRef]
215. Wang, J.; Wang, J.; Wu, X.; Zhang, G. Pt-TiO<sub>2</sub> microspheres with exposed {001} facets for degradation of formaldehyde in air: Formation mechanism and enhanced visible light photocatalytic activity. *Mater. Res. Bull.* **2017**, *96*, 262–269. [CrossRef]
216. Pandian, R.; Natarajan, G.; Dhaipule, N.G.K.; Prasad, A.K.; Kamruddin, M.; Tyagi, A.K. Types of nitrogen incorporation in reactively sputtered titania thin films: Influence on UV-visible, photocatalytic and photoconduction properties. *Thin Solid Film.* **2016**, *616*, 466–476. [CrossRef]
217. Lee, J.Y.; Jo, W.K. Heterojunction-based two-dimensional N-doped TiO<sub>2</sub>/WO<sub>3</sub> composite architectures for photocatalytic treatment of hazardous organic vapor. *J. Hazard. Mater.* **2016**, *314*, 22–31. [CrossRef] [PubMed]
218. Albrbar, A.J.; Djokic, V.; Bjelajac, A.; Kovac, J.; Cirkovic, J.; Mitric, M.; Janackovic, D.; Petrovic, R. Visible-light active mesoporous, nanocrystalline N,S-doped and co-doped titania photocatalysts synthesized by non-hydrolytic sol-gel route. *Ceram. Int.* **2016**, *42*, 16718–16728. [CrossRef]
219. Yang, X.; Qiong, J.; Pang, J.; Yang, Y.; Zheng, S.; Jia, J.; Qin, Z. Hierarchical porous N-TiO<sub>2</sub>/carbon foam composite for enhancement of photodegradation activity under simulated sunlight. *Diam. Relat. Mater.* **2022**, *128*, 109234.
220. Dong, F.; Guo, S.; Wang, H.; Li, X.; Wu, Z. Enhancement of the visible light photocatalytic activity of C-doped TiO<sub>2</sub> nanomaterials prepared by a green synthetic approach. *J. Phys. Chem. C* **2011**, *115*, 13285–13292. [CrossRef]
221. Di Valentin, C.; Pacchioni, G.; Selloni, A. Theory of carbon doping of titanium dioxide. *Chem. Mater.* **2005**, *17*, 6656–6665. [CrossRef]
222. Kavitha, R.; Devi, L.G. Synergistic effect between carbon dopant in titania lattice and surface carbonaceous species for enhancing the visible light photocatalysis. *J. Environ. Chem. Eng.* **2014**, *2*, 857–867. [CrossRef]

223. Wang, Y.; Liu, X.; Guo, L.; Shang, L.; Ge, S.; Song, G.; Naik, N.; Shao, Q.; Lin, J.; Guo, Z. Metal organic framework-derived C-doped ZnO/TiO<sub>2</sub> nanocomposite catalysts for enhanced photodegradation of Rhodamine, B. *J. Colloid Interface Sci.* **2021**, *599*, 566–576. [[CrossRef](#)]
224. Thind, S.S.; Mustapic, C.C.; Wen, J.; Goodwin, C.D.; Chen, A. Facile synthesis of mesoporous carbon nitride and titanium dioxide nanocomposites with enhanced visible light photocatalytic activity. *New J. Chem.* **2017**, *41*, 10542–10549. [[CrossRef](#)]
225. Lei, X.F.; Xue, X.X.; Yang, H.; Chen, C.; Li, X.; Niu, M.C.; Gao, X.Y.; Yang, Y.T. Effect of calcination temperature on the structure and visible-light photocatalytic activities of (N, S and C) co-doped TiO<sub>2</sub> nano-materials. *Appl. Surf. Sci.* **2015**, *332*, 172–180. [[CrossRef](#)]
226. Li, D.; Haneda, H.; Hishita, S.; Ohashi, N. Visible-light-driven nitrogen-doped TiO<sub>2</sub> photocatalysts: Effect of nitrogen precursors on their photocatalysis for decomposition of gas-phase organic pollutants. *Mater. Sci. Eng. B* **2005**, *117*, 67–75. [[CrossRef](#)]
227. Pan, L.; Zou, J.-J.; Wang, S.; Huang, Z.-F.; Zhang, X.; Wang, L. Enhancement of visible-light-induced photodegradation over hierarchical porous TiO<sub>2</sub> by nonmetal doping and water-mediated dye sensitization. *Appl. Surf. Sci.* **2013**, *268*, 252–258. [[CrossRef](#)]
228. Zeng, X.; Sun, X.; Yu, Y.; Wang, H.; Wang, Y. Photocatalytic degradation of flumequine with B/N codoped TiO<sub>2</sub> catalyst: Kinetics, main active species, intermediates and pathways. *Chem. Eng. J.* **2019**, *378*, 122226. [[CrossRef](#)]
229. Li, Y.-F.; Xu, D.; Oh, J.I.; Shen, W.; Li, X.; Yu, Y. Mechanistic study of codoped titania with nonmetal and metal ions: A case of C plus Mo codoped TiO<sub>2</sub>. *ACS Catal.* **2012**, *2*, 391–398. [[CrossRef](#)]
230. Dong, F.; Wang, H.-; Wu, Z.-; Qiu, J. Marked enhancement of photocatalytic activity and photochemical stability of N-doped TiO<sub>2</sub> nanocrystals by Fe<sup>3+</sup>/Fe<sup>2+</sup> surface modification. *J. Colloid Interface Sci.* **2010**, *343*, 200–208. [[CrossRef](#)] [[PubMed](#)]
231. Wu, Y.; Zhang, J.; Xiao, L.; Chen, F. Properties of carbon and iron modified TiO<sub>2</sub> photocatalyst synthesized at low temperature and photodegradation of acid orange 7 under visible light. *Appl. Surf. Sci.* **2010**, *256*, 4260–4268. [[CrossRef](#)]
232. Venkatesan, A.; Al-onazi, W.A.; Elshikh, M.S. Study of synergistic effect of cobalt and carbon codoped with TiO<sub>2</sub> photocatalyst for visible light induced degradation of phenol. *Chemosphere* **2022**, *305*, 135333. [[CrossRef](#)] [[PubMed](#)]
233. Khan, M.S.; Riaz, N.; Shaikh, A.J.; Shah, J.A.; Hussain, J.; Irshad, M.; Awan, S.; Syed, A.; Kallerhoff, J.; Arshad, M. Graphene quantum dot and iron co-doped TiO<sub>2</sub> photocatalysts: Synthesis, performance evaluation and phytotoxicity studies. *Ecotoxicol Environ. Saf.* **2021**, *226*, 112855. [[CrossRef](#)]
234. Hafeez, M.; Afyaz, S.; Khalid, A.; Ahmad, P.; Khandaker, M.U.; Sahibzada, M.U.K.; Ahmad, I.; Khan, J.; Alhumaydhi, F.A.; Emran, B.; et al. Synthesis of cobalt and sulphur doped titanium dioxide photocatalysts for environmental applications. *J. King Saud Univ. Sci.* **2022**, *34*, 102028. [[CrossRef](#)]
235. Wang, H.; Zhang, L.; Chen, Z.; Hu, J.; Li, S.; Wang, Z.; Liu, J.; Wang, X. Semiconductor heterojunction photocatalysts: Design, construction, and photocatalytic performances. *Chem. Soc. Rev.* **2014**, *43*, 5234–5244. [[CrossRef](#)] [[PubMed](#)]
236. Lettieri, S.; Pavone, M.; Fioravanti, A.; Amato, L.S.; Maddalena, P. Charge Carrier Processes and Optical Properties in TiO<sub>2</sub> and TiO<sub>2</sub>-Based Heterojunction Photocatalysts: A Review. *Materials* **2021**, *14*, 1645. [[CrossRef](#)] [[PubMed](#)]
237. Barrocas, B.T.; Ambrozova, N.; Koci, K. Photocatalytic Reduction of Carbon Dioxide on TiO<sub>2</sub> Heterojunction Photocatalysts-A Review. *Materials* **2022**, *15*, 967. [[CrossRef](#)] [[PubMed](#)]
238. Nguyen, T.B.; Doong, R. Heterostructured ZnFe<sub>2</sub>O<sub>4</sub>/TiO<sub>2</sub> nanocomposites with a highly recyclable visible-light-response for bisphenol A degradation. *RSC Adv.* **2017**, *7*, 50006–50016. [[CrossRef](#)]
239. Wang, Y.; Sunarso, J.; Zhao, B.; Ge, C.; Chen, G. One-dimensional BiOBr nanosheets/TiO<sub>2</sub> nanofibers composite: Controllable synthesis and enhanced visible photocatalytic activity. *Ceram. Int.* **2017**, *43*, 15769–15776. [[CrossRef](#)]
240. Hu, Y.; Li, D.; Zheng, Y.; Chen, W.; He, Y.; Shao, Y.; Fu, X.; Xiao, G. BiVO<sub>4</sub>/TiO<sub>2</sub> nanocrystalline heterostructure: A wide spectrum responsive photocatalyst towards the highly efficient decomposition of gaseous benzene. *Appl. Catal. B* **2011**, *104*, 30–36. [[CrossRef](#)]
241. Hunge, Y.M.; Yadav, A.A.; Kang, S.-W.; Kin, H. Photocatalytic degradation of tetracycline antibiotics using hydrothermally synthesized two-dimensional molybdenum disulfide/titanium dioxide composites. *J. Colloid Interface Sci.* **2022**, *606*, 454–463. [[CrossRef](#)]
242. Lu, Y.; Ding, C.; Guo, J.; Gan, W.; Chen, P.; Zhang, M.; Sun, Z. Highly efficient photodegradation of ciprofloxacin by dual Z-scheme Bi<sub>2</sub>MoO<sub>6</sub>/GQDs/TiO<sub>2</sub> heterojunction photocatalysts: Mechanism analysis and pathway exploration. *J. Alloys Compd.* **2022**, *924*, 166533. [[CrossRef](#)]
243. Yang BMa, Z.; Wang, Q.; Yang, J.J. Synthesis and Photoelectrocatalytic Applications of TiO<sub>2</sub>/ZnO/Diatomite Composites. *Catalysts* **2022**, *12*, 268. [[CrossRef](#)]
244. Li, Y.; Xie, W.; Hu, X. Comparison of Dye Photodegradation and its Coupling with Light-to-Electricity Conversion over TiO<sub>2</sub> and ZnO. *Langmuir* **2010**, *26*, 591–597. [[CrossRef](#)]
245. Guo, J.; Li, J.; Yin, A.; Fan, K.; Dai, W. Photodegradation of Rhodamine B on Sulfur Doped ZnO/TiO<sub>2</sub> Nanocomposite Photocatalyst under Visible-light Irradiation. *Chin. J. Chem.* **2010**, *28*, 2144–2150. [[CrossRef](#)]
246. Xu, X.; Li, D. Ligand-Decomposition assistant formation of CdS/TiO<sub>2</sub> hybrid nanostructure with enhanced photocatalytic activity. *J. Alloys Compd.* **2022**, *914*, 165393.
247. Warkhade, S.K.; Zodape, S.P.; Pratap, U.R.; Wankhade, A.V. Wankhade, Rutile TiO<sub>2</sub>/CoSe nanocomposite: An efficient photocatalyst for photodegradation of model organic dyes under visible light irradiation. *J. Mol. Liq.* **2019**, *279*, 434–443. [[CrossRef](#)]
248. Costa, L.N.; Nobre, F.X.; Lobo, A.O.; de Matos, J.M.E. Photodegradation of ciprofloxacin using Z-scheme TiO<sub>2</sub>/SnO<sub>2</sub> nanostructures as photocatalyst, Environmental Nanotechnology. *Environ. Nanotech. Monit. Manag.* **2021**, *16*, 100466.

249. Rajput, R.B.; Jamble, S.N.; Kale, R.B. A review on TiO<sub>2</sub>/SnO<sub>2</sub> heterostructures as a photocatalyst for the degradation of dyes and organic pollutants. *J. Environ. Manag.* **2022**, *307*, 114533. [CrossRef]
250. Yaacob, N.; Sean, G.P.; Nazri, N.A.M.; Ismail, A.F.; Abidin, M.N.Z.; Subramaniam, M.N. Simultaneous oily wastewater adsorption and photodegradation by ZrO<sub>2</sub>-TiO<sub>2</sub> heterojunction photocatalysts. *J. Water Process. Eng.* **2021**, *39*, 101644. [CrossRef]
251. Kim, C.-S.; Shin, J.-W.; An, S.-H.; Jang, H.-D.; Kim, T.-O. Photodegradation of volatile organic compounds using zirconium-doped TiO<sub>2</sub>/SiO<sub>2</sub> visible light photocatalysts. *Chem. Eng. J.* **2012**, *204–206*, 40–47. [CrossRef]
252. Tian, J.; Chen, L.; Yin, Y.; Wang, X.; Dai, J.; Zhu, Z.; Liu, X.; Wu, P. Photocatalyst of TiO<sub>2</sub>/ZnO nano composite film: Preparation, characterization, and photodegradation activity of methyl orange. *Surf. Coat. Technol.* **2009**, *204*, 205–214. [CrossRef]
253. Jing, H.; Gao, Y.; Li, L.; Wang, X.; Pei, W. A new double Z-scheme TiO<sub>2</sub>/ZnO-g-C<sub>3</sub>N<sub>4</sub> nanocomposite with enhanced photodegradation efficiency for Rhodamine B under sunlight. *Environ. Prog. Sustain. Energy* **2022**, e13968-12.
254. Neves, M.C.; Nogueira, J.M.F.; Trindade, T.; Mendonca, M.H.; Monteiro, O.C. Photosensitization of TiO<sub>2</sub> by Ag<sub>2</sub>S and its catalytic activity on phenol photodegradation. *J. Photochem. Photobiol. A* **2009**, *204*, 168–173. [CrossRef]
255. Chen, P.; Cai, Y.; Wang, J.; Wang, K.; Tao, Y.; Xue, J.; Wang, H. Preparation of protonized titanate nanotubes/Fe<sub>3</sub>O<sub>4</sub>/TiO<sub>2</sub> ternary composites and dye self-sensitization for visible-light-driven photodegradation of Rhodamine B. *Powder Technol.* **2018**, *326*, 272–280. [CrossRef]
256. Jing, J.; Li, J.; Feng, J.; Li, W.; Yu, W.W. Photodegradation of quinoline in water over magnetically separable Fe<sub>3</sub>O<sub>4</sub>/TiO<sub>2</sub> composite photocatalysts. *Chem. Eng. J.* **2013**, *219*, 355–360. [CrossRef]
257. Alhaddad, M.; Ismail, A.A.; Alghamdi, Y.G.; Al-Khathami, N.D.; Mohamed, R.M. Co<sub>3</sub>O<sub>4</sub> Nanoparticles Accommodated Mesoporous TiO<sub>2</sub> framework as an Excellent Photocatalyst with Enhanced Photocatalytic Properties. *Opt. Mater.* **2022**, *131*, 112643. [CrossRef]
258. Sun, J.; Wang, Y.; Sun, R.; Dong, S. Photodegradation of azo dye Congo Red from aqueous solution by the WO<sub>3</sub>-TiO<sub>2</sub>/activated carbon (AC) photocatalyst under the UV irradiation. *Mater. Chem. Phys.* **2009**, *115*, 303–308. [CrossRef]
259. Moghni, N.; Boutoumi, H.; Khalaf, H.; Makaoui, N.; Colon, G. Enhanced photocatalytic activity of TiO<sub>2</sub>/WO<sub>3</sub> nanocomposite from sonochemical-microwave assisted synthesis for the photodegradation of ciprofloxacin and oxytetracycline antibiotics under UV and sunlight. *J. Photochem. Photobiol. A* **2022**, *428*, 113848. [CrossRef]
260. Zhang, X.X.; Xiao, Y.G.; Cao, S.S.; Yin, Z.L.; Liu, Z.Q. Ternary TiO<sub>2</sub>@Bi<sub>2</sub>O<sub>3</sub>@TiO<sub>2</sub> hollow photocatalyst drives robust visible-light photocatalytic performance and excellent recyclability. *J. Clean. Prod.* **2022**, *352*, 131560. [CrossRef]
261. Li, L.; Song, J.; Wang, B.; Duan, C.; Wang, R.; Zhang, B. New BiOXs/TiO<sub>2</sub> heterojunction photocatalyst towards efficient degradation of organic pollutants under visible-light irradiation. *Micro Nano Lett.* **2019**, *14*, 911–914.
262. Haghighi, P.; Alijani, S.; Bazyari, A.; Thompson, L.T. Visible light dye degradation over fluorinated mesoporous TiO<sub>2</sub>-WO<sub>3</sub>-Bi<sub>2</sub>O<sub>3</sub>/SiO<sub>2</sub> nanocomposite photocatalyst-adsorbent using immersion well reactor, *Journal of Photochemistry & Photobiology, A. Chemistry* **2022**, *426*, 113790.
263. Zhou, Y.; Shen, F.; Zhang, S.; Zhao, Q.; Xu, Z.; Chen, H. Synthesis of Methyl-Capped TiO<sub>2</sub>-SiO<sub>2</sub> Janus Pickering Emulsifiers for Selective Photodegradation of Water-Soluble Dyes. *ACS Appl. Mater. Interfaces* **2020**, *12*, 29876–29882. [CrossRef] [PubMed]
264. Yaparadne, S.; Tripp, C.P.; Amirbahman, A. Photodegradation of taste and odor compounds in water in the presence of immobilized TiO<sub>2</sub>-SiO<sub>2</sub> photocatalysts. *J. Hazard. Mat.* **2018**, *346*, 208–217. [CrossRef] [PubMed]
265. Qourzal, S.; Barka, N.; Tamimi, M.; Assabbane, A.; Nounah, A.; Ihlal, A.; Ait-Ichou, Y. Sol-gel synthesis of TiO<sub>2</sub>-SiO<sub>2</sub> photocatalyst for β-naphthol photodegradation. *Mater. Sci. Eng. C* **2009**, *29*, 1616–1620. [CrossRef]
266. Kuwahara, Y.; Yamashita, H. Efficient photocatalytic degradation of organics diluted in water and air using TiO<sub>2</sub> designed with zeolites and mesoporous silica materials. *J. Mater. Chem.* **2011**, *21*, 2407–2416. [CrossRef]
267. Gómez, C.M.; Angel, G.D.; Ramos-Ramírez, E.; Rangel-Vazquez, I.; Gonzalez, F.; Arrieta, A.; Vazquez-Zavala, A.; BonillaSanchez, A.; Cantu, M.S. Alumina coating with TiO<sub>2</sub> and its effect on catalytic photodegradation of phenol and p-cresol. *J. Chem. Technol. Biotechnol.* **2016**, *91*, 2211–2220. [CrossRef]
268. Toumazatou, A.; Arfanis, M.K.; Pantazopoulos, P.-A.; Kontos, A.G.; Falaras, P.; Stefanou, N.; Likodimos, V. Slow-photon enhancement of dye sensitized TiO<sub>2</sub> photocatalysis. *Mater. Lett.* **2017**, *197*, 123–126. [CrossRef]
269. Diaz-Angulo, J.; Gomez-Bonilla, I.; Jimenez-Tohapanta, C.; Mueses, M.; Pinzon, M.; Machuca-Martinez, F. Visible-light activation of TiO<sub>2</sub> by dye-sensitization for degradation of pharmaceutical compounds. *Photochem. Photobiol. Sci.* **2019**, *18*, 897–904. [CrossRef]
270. Sengupta, D.; Das, P.; Mondal, B.; Mukherjee, K. Effects of doping, morphology and film-thickness of photo-anode materials for dye sensitized solar cell application—A review. *Renew. Sust. Energ. Rev.* **2017**, *60*, 356–376. [CrossRef]
271. Lü, X.F.; Sun, W.J.; Li, J.; Xu, W.; Zhang, F. Spectroscopic investigations on the simulated solar light induced photodegradation of 4-nitrophenol by using three novel copper(II) porphyrin-TiO<sub>2</sub> photocatalysts. *Spectrochim. Acta A Mol. Biomol. Spectrosc.* **2013**, *111*, 161–168. [CrossRef] [PubMed]
272. Ramasubbu, V.; Ram Kumar, P.; Chellapandi, T.; Madhumitha, G.; Mothi, E.A.; Sahaya, X.S. Zn(II) porphyrin sensitized (TiO<sub>2</sub>@Cd-MOF) nanocomposite aerogel as novel photocatalyst for the effective degradation of methyl orange (MO) dye. *Opt. Mater.* **2022**, *132*, 112558. [CrossRef]
273. Hısır, A.; Karaoglan, G.K.; Avciata, O. Synthesis of tetracarboxy phthalocyanines modified TiO<sub>2</sub> nanocomposite photocatalysts and investigation of photocatalytic decomposition of organic pollutant methylene blue under visible light. *J. Mol. Struct.* **2022**, *1266*, 133498. [CrossRef]

274. Yamazaki, S.; Sonoda, K.; Maruoka, K.; Yamazaki, Y.; Naragino, H.; Honda, K.; Murafuji, T.; Sumimoto, M. Porous TiO<sub>2</sub> adsorbed with squaraine dye as visible-light-responsive photocatalyst. *J. Photoch. Photobio. A* **2021**, *421*, 113543. [[CrossRef](#)]
275. Narayanaswamy, K.; Tiwari, A.; Mondal, I.; Pal, U.; Niveditha, S.; Bhanurakash, K.; Singh, S.P. Dithiafulvalene functionalized diketopyrrolopyrrole based sensitizers for efficient hydrogen production. *Phys. Chem. Chem. Phys.* **2015**, *17*, 13710–13718. [[CrossRef](#)]
276. Tiwari, A.; Mondal, I.; Pal, U. Visible light induced hydrogen production over thiophenothiazine-based dye sensitized TiO<sub>2</sub> photocatalyst in neutral water. *Rsc Adv.* **2015**, *5*, 31415–31421. [[CrossRef](#)]
277. Tiwari, A.; Pal, U. Effect of donor-donor- $\pi$ -acceptor architecture of triphenylamine-based organic sensitizers over TiO<sub>2</sub> photocatalysts for visible-light-driven hydrogen production. *Int. J. Hydrogen Energy* **2015**, *40*, 9069–9079. [[CrossRef](#)]
278. Samuel, J.J.; Yam, F.K. Photocatalytic degradation of methylene blue under visible light by dye sensitized titania. *Mater. Res. Express* **2020**, *7*, 015051. [[CrossRef](#)]
279. Ranjit, K.T.; Willner, I. Iron(III) Phthalocyanine-Modified Titanium Dioxide: A Novel Photocatalyst for the Enhanced Photodegradation of Organic Pollutants. *J. Phys. Chem. B* **1998**, *102*, 9397–9403. [[CrossRef](#)]
280. Dinooop lal, S.; Jose, T.S.; Rajesh, C.; Puthukkara, P.A.R.; Unnikrishnan, K.S.; Arun, K.J. Accelerated photodegradation of polystyrene by TiO<sub>2</sub>-polyaniline photocatalyst under UV radiation. *Eur. Polym. J.* **2021**, *153*, 110493. [[CrossRef](#)]
281. Das, A.; Adak, M.K.; Mahata, N.; Biswas, B. Wastewater treatment with the advent of TiO<sub>2</sub> endowed photocatalysts and their reaction kinetics with scavenger effect. *J. Mol. Liq.* **2021**, *338*, 116479. [[CrossRef](#)]
282. Marin, M.L.; Santos-Juanes, L.; Arques, A.; Amat, A.M.; Miranda, M.A. Organic Photocatalysts for the Oxidation of Pollutants and Model Compounds. *Chem. Rev.* **2012**, *112*, 1710–1750. [[CrossRef](#)] [[PubMed](#)]
283. Dong, S.; Feng, J.; Fan, M.; Pi, Y.; Hu, L.; Han, X.; Liu, M.; Sun, J.; Sun, J. Recent developments in heterogeneous photocatalytic water treatment using visible light-responsive photocatalysts: A review. *RSC Adv.* **2015**, *5*, 14610–14630. [[CrossRef](#)]
284. Rancaño, L.; Rivero, M.J.; Mueses M, Á.; Ortiz, I. Comprehensive Kinetics of the Photocatalytic Degradation of Emerging Pollutants in a LED-Assisted Photoreactor. S-Metolachlor as Case Study. *Catalysts* **2021**, *11*, 48. [[CrossRef](#)]
285. Zhao, W.; Dai, J.; Liu, F.; Bao, J.; Wang, Y.; Yang, Y.; Yang, Y.; Zhao, D. Photocatalytic oxidation of indoor toluene: Process risk analysis and influence of relative humidity, photocatalysts, and VUV irradiation. *Sci. Total Environ.* **2012**, *438*, 201–209. [[CrossRef](#)]
286. Zhong, L.; Haghghat, F.; Lee, C.-S.; Lakdawala, N. Performance of ultraviolet photocatalytic oxidation for indoor air applications: Systematic experimental evaluation. *J. Hazard. Mater.* **2013**, *261*, 130–138. [[CrossRef](#)]
287. Zhang, G.; Sun, Z.; Duan, Y.; Ma, R.; Zhang, S. Synthesis of nano-TiO<sub>2</sub> /diatomite composite and its photocatalytic degradation of gaseous formaldehyde. *Appl. Surf. Sci.* **2017**, *412*, 105–112. [[CrossRef](#)]
288. Ao, C.H.; Lee, S.C.; Yu, J.Z.; Xu, J.H. Photodegradation of formaldehyde by photocatalyst TiO<sub>2</sub>: Effects on the presences of NO, SO<sub>2</sub> and VOCs. *Appl. Catal. B* **2004**, *54*, 41–50. [[CrossRef](#)]
289. Li, Q.; Zhang, S.; Xia, W.; Jiang, X.; Huang, Z.; Wu, X.; Zhao, H.; Yuan, C.; Shen, H.; Jing, G. Surface design of g-C<sub>3</sub>N<sub>4</sub> quantum dot-decorated TiO<sub>2</sub>(001) to enhance the photodegradation of indoor formaldehyde by experimental and theoretical investigation. *Ecotoxicol. Environ. Saf.* **2022**, *234*, 113411. [[CrossRef](#)]
290. Song, Y.; Du, H.; Wu, H.; Shi, L.; Yu, D.; Jia, R.; Chitpakdee, C.; Namuangruk, S.; Huang, L. Photodeposition of alloyed Au-Pt nanoparticles on TiO<sub>2</sub> for the enhanced catalytic oxidation of HCHO at room temperature. *J. Alloys Compd.* **2022**, *896*, 163140. [[CrossRef](#)]
291. Lan, Z.; Yu, Y.; Li, H.; Zhang, L.; Gao, Y. Thermal catalytic mechanism for the metal ions(Cu, in, Pd and Pt) modified TiO<sub>2</sub> on degradation of HCHO. *Mater. Sci. Semicond. Process.* **2021**, *123*, 105547. [[CrossRef](#)]
292. Korologos, C.A.; Nikolaki, M.D.; Zerva, C.N.; Philippopoulos, C.L.; Pouloupoulos, S.G. Photocatalytic oxidation of benzene, toluene, ethylbenzene and m-xylene in the gas-phase over TiO<sub>2</sub>-based catalysts. *J. Photoch. Photobio. A* **2012**, *244*, 24–31. [[CrossRef](#)]
293. Rao, Z.; Xie, X.; Wang, X.; Mahmood, A.; Tong, S.; Ge, M.; Sun, J. Defect Chemistry of Er<sup>3+</sup>-Doped TiO<sub>2</sub> and Its Photocatalytic Activity for the Degradation of Flowing Gas-Phase VOCs. *J. Phys. Chem. C* **2019**, *123*, 12321–12334. [[CrossRef](#)]
294. Rao, Z.; Shi, G.; Wang, Z.; Mahmood, A.; Xie, X.; Sun, J. Photocatalytic degradation of gaseous VOCs over Tm<sup>3+</sup>-TiO<sub>2</sub>: Revealing the activity enhancement mechanism and different reaction paths. *Chem. Eng. J.* **2020**, *395*, 125078. [[CrossRef](#)]
295. Mahmood, A.; Shi, G.; Wang, Z.; Rao, Z.; Xiao, W.; Xie, X.; Sun, J. Carbon quantum dots-TiO<sub>2</sub> nanocomposite as an efficient photocatalyst for the photodegradation of aromatic ring-containing mixed VOCs: An experimental and DFT studies of adsorption and electronic structure of the interface. *J. Hazard. Mater.* **2021**, *401*, 123402. [[CrossRef](#)] [[PubMed](#)]
296. Gohin, M.; Allain, E.; Chemin, N.; Maurin, I. Sol-gel nanoparticulate mesoporous films with enhanced self-cleaning properties. *J. Photoch. Photobiol. A* **2010**, *216*, 142–148. [[CrossRef](#)]
297. Stefano, C.; Mirko, F.; Francesca, M.; Enrico, D. A review on membrane distillation in process engineering: Design and exergy equations, materials and wetting problems. *Front. Chem. Sci. Eng.* **2022**, *16*, 592–613.
298. Thambiliyagodage, C. Activity enhanced TiO<sub>2</sub> nanomaterials for photodegradation of dyes—A review. *Environ. Nanotechnol. Monit. Manag.* **2021**, *16*, 100592. [[CrossRef](#)]
299. Nur Alam, S.M.; Sultana, M.; Atol, M. A review on the development of elemental and codoped TiO<sub>2</sub> photocatalysts for enhanced dye degradation under UV-vis irradiation. *J. Water Process. Eng.* **2022**, *47*, 102728.
300. Zangeneh, H.; Zinatizadeh AA, L.; Habibi, M.; Akia, M.; Isa, M.H. Photocatalytic oxidation of organic dyes and pollutants in wastewater using different modified titanium dioxides: A comparative review. *J. Ind. Eng. Chem.* **2015**, *26*, 1–36. [[CrossRef](#)]

301. Kite, S.V.; Kadam, A.N.; Sathe, D.J.; Patil, S.; Mali, S.S.; Hong, C.K.; Lee, S.-W.; Garadkar, K.M. Nanostructured TiO<sub>2</sub> Sensitized with MoS<sub>2</sub> Nanoflowers for Enhanced Photodegradation Efficiency toward Methyl Orange. *ACS Omega*. **2021**, *6*, 17071–17085. [[CrossRef](#)]
302. Boczar, D.; Łęcki, T.; Skompska, M. Visible-light driven Fe<sub>x</sub>O<sub>y</sub>/TiO<sub>2</sub>/Au photocatalyst—Synthesis, characterization and application for methyl orange photodegradation. *J. Electronal. Chem.* **2020**, *859*, 113829. [[CrossRef](#)]
303. Kader, S.; Al-Mamun, M.R.; Suhan, M.B.K.; Shuchi, S.B.; Islam, M.S. Enhanced photodegradation of methyl orange dye under UV irradiation using MoO<sub>3</sub> and Ag doped TiO<sub>2</sub> photocatalysts. *Environ. Technol. Inno.* **2022**, *27*, 102476. [[CrossRef](#)]
304. Wang, S.; Zhou, S. Photodegradation of methyl orange by photocatalyst of CNTs/P-TiO<sub>2</sub> under UV and visible-light irradiation. *J. Hazard. Mater.* **2011**, *185*, 77–85. [[CrossRef](#)] [[PubMed](#)]
305. Zainal, Z.; Hui, L.K.; Hussein, M.Z.; Abdullah, A.H.; Hamadneh, I.R. Characterization of TiO<sub>2</sub>–Chitosan/Glass photocatalyst for the removal of a monoazo dye via photodegradation–adsorption process. *J. Hazard. Mater.* **2009**, *164*, 138–145. [[CrossRef](#)]
306. Zhang, Q.; Yu, L.; Yang, B.; Xu, C.; Diao, G.; Xu, C.; Zhang, W.; Xu, Q.; Diao, G. Magnetic Fe<sub>3</sub>O<sub>4</sub>@Ru-doped TiO<sub>2</sub> nanocomposite as a recyclable photocatalyst for advanced photodegradation of methylene blue in simulated sunlight. *Chem. Phys. Lett.* **2021**, *774*, 138609. [[CrossRef](#)]
307. Samsudin MF, R.; Sufian, S.; Bashiri, R.; Mohmed, N.M.; Siang, L.T.; Ramli, R.M. Optimization of photodegradation of methylene blue over modified TiO<sub>2</sub>/BiVO<sub>4</sub> photocatalysts: Effects of total TiO<sub>2</sub> loading and different type of co-catalyst. *Mater. Today Proc.* **2018**, *5*, 21710–22171. [[CrossRef](#)]
308. Dassanayake, R.S.; Rajakaruna, E.; Abidi, N. Preparation of aerochitin-TiO<sub>2</sub> composite for efficient photocatalytic degradation of methylene blue. *J. Appl. Polym. Sci.* **2018**, *135*, 45908. [[CrossRef](#)]
309. Li, C.; Sun, Z.; Xue, Y.; Yao, G.; Zheng, S. A facile synthesis of g-C<sub>3</sub>N<sub>4</sub>/TiO<sub>2</sub> hybrid photocatalysts by sol–gel method and its enhanced photodegradation towards methylene blue under visible light. *Adv. Powder Technol.* **2016**, *27*, 330–337. [[CrossRef](#)]
310. Ge, Y.; Luo, H.; Huang, J.; Zhang, Z. Visible-light-active TiO<sub>2</sub> photocatalyst for efficient photodegradation of organic dyes. *Opt. Mater.* **2021**, *115*, 111058. [[CrossRef](#)]
311. Wafi, M.A.E.; Ahmed, M.A.; Abdel-Samad, H.S.; Medien, H.A.A. Exceptional removal of methylene blue and p-aminophenol dye over novel TiO<sub>2</sub>/RGO nanocomposites by tandem adsorption-photocatalytic processes. *Mater. Sci. Energy Technol.* **2022**, *5*, 217–231. [[CrossRef](#)]
312. Chandhini, M.; Saad, A.; Eldhose, I. Statistical analysis of photodegradation of methylene blue dye under natural sunlight. *Opt. Mater.* **2021**, *122*, 111809.
313. Liu, J.; Zuo, S.; Yu, L.; Yu, Y.; Li, B.; Chen, P. Visible light photodegradation of methylene blue by AgBr–TiO<sub>2</sub>/SiO<sub>2</sub>@Fe<sub>3</sub>O<sub>4</sub> magnetic photocatalysts. *Particuology* **2013**, *11*, 728–731. [[CrossRef](#)]
314. Fu, P.; Luan, Y.; Dai, X. Preparation of TiO<sub>2</sub> photocatalyst anchored on activated carbon fibers and its photodegradation of methylene blue. *China Part.* **2004**, *2*, 76–80. [[CrossRef](#)]
315. Wang, H.; Zhou, D.; Shen, S.; Wan, J.; Zheng, X.; Yu, L.; Phillips, D.L. The photocatalytic activity and degradation mechanism of methylene blue over copper(ii) tetra(4-carboxyphenyl) porphyrin sensitized TiO<sub>2</sub> under visible light irradiation. *RSC Adv.* **2014**, *4*, 28978–28986. [[CrossRef](#)]
316. Sun, Q.; Xu, Y. Evaluating Intrinsic Photocatalytic Activities of Anatase and Rutile TiO<sub>2</sub> for Organic Degradation in Water. *J. Phys. Chem. C* **2010**, *114*, 18911–18918. [[CrossRef](#)]
317. Bai, Y.; Mora-Seró, I.; Angelis, F.D.; Bisquert, J.; Wang, P. Titanium Dioxide Nanomaterials for Photovoltaic Applications. *Chem. Rev.* **2014**, *114*, 10095–10130. [[CrossRef](#)]
318. Mousavi, M.; GhasemiNovel, J.B. Novel visible-light-responsive Black-TiO<sub>2</sub>/CoTiO<sub>3</sub> Z-scheme heterojunction photocatalyst with efficient photocatalytic performance for the degradation of different organic dyes and tetracycline. *J. Taiwan Inst. Chem. E* **2021**, *121*, 168–183. [[CrossRef](#)]
319. Ruzimuradova, O.; Sharipova, K.; Yarbekova, A.; Saidov, K.; Hojamberdiev, M.; Prasad, R.M.; Cherkashinin, G.; Riedel, R. A facile preparation of dual-phase nitrogen-doped TiO<sub>2</sub>–SrTiO<sub>3</sub> macroporous monolithic photocatalyst for organic dye photodegradation under visible light. *J. Eur. Ceram. Soc.* **2015**, *35*, 1815–1821. [[CrossRef](#)]
320. Zhu, Y.; Yang, S.; Cai, J.; Meng, M.; Li, X. A facile synthesis of Ag<sub>x</sub>Au<sub>1–x</sub>/TiO<sub>2</sub> photocatalysts with tunable surface plasmon resonance (SPR) frequency used for RhB photodegradation. *Mater. Lett.* **2015**, *154*, 163–166. [[CrossRef](#)]
321. Mousavi, M.; Soleimani, M.; Hamzehloo, M.; Badiiei, A.; Ghasemi, J.B. Photocatalytic degradation of different pollutants by the novel gCN-NS/Black-TiO<sub>2</sub> heterojunction photocatalyst under visible light: Introducing a photodegradation model and optimization by response surface methodology (RSM). *Mater. Chem. Phys.* **2021**, *258*, 123912. [[CrossRef](#)]
322. Mourão, H.A.J.L.; Malagutti, A.R.; Ribeiro, C. Synthesis of TiO<sub>2</sub>-coated CoFe<sub>2</sub>O<sub>4</sub> photocatalysts applied to the photodegradation of atrazine and rhodamine B in water. *Appl. Catal. A Gen.* **2010**, *382*, 284–292. [[CrossRef](#)]
323. Asiltürk, M.; Sener, S.; Sener, E. Preparation, Characterization and Photocatalytic Activities of TiO<sub>2</sub>-coated Activated Carbon Catalysts for Rhodamine B Photodegradation. *Bull. Korean Chem. Soc.* **2015**, *36*, 455–463.
324. Liu, K.; Zhu, L.; Li, N.; Sun, Y.; Li, H.; Zhu, X. Solvothermal synthesis of mesoporous slabstone-like TiO<sub>2</sub> and its photodegradation preference in a methyl orange-rhodamine B mixture solution. *Cryst. Res. Technol.* **2012**, *47*, 1088–1094. [[CrossRef](#)]
325. Guo, J.; Yuan, S.; Jiang, W.; Yue, H.; Cui, Z.; Liang, B. Adsorption and photocatalytic degradation behaviors of rhodamine dyes on surface-fluorinated TiO<sub>2</sub> under visible irradiation. *RSC Adv.* **2016**, *6*, 4090–4100. [[CrossRef](#)]

326. Lian, Z.; Wei, C.; Gao, B.; Yang, X.; Chan, Y.; Wang, J.; Chen, G.Z.; Koh, K.S.; Shi, Y.; Yan, Y.; et al. Synergetic treatment of dye contaminated wastewater using microparticles functionalized with carbon nanotubes/titanium dioxide nanocomposites. *RSC Adv.* **2020**, *10*, 9210–9225. [[CrossRef](#)] [[PubMed](#)]
327. Mohamed Reda, M.; Ismail Adel, A.; Kadi Mohammad, W.; Bahnmann Detlef, W. A comparative study on mesoporous and commercial TiO<sub>2</sub> photocatalysts for photodegradation of organic pollutants. *J. Photochem. Photobiol. A* **2018**, *367*, 66–73. [[CrossRef](#)]
328. Chen, F.; He, A.; Wang, Y.; Yu, W.; Chen, H.; Geng, F.; Li, Z.; Zhou, Z.; Liang, Y.; Fu, J.; et al. Efficient photodegradation of PFOA using spherical BiOBr modified TiO<sub>2</sub> via hole-remained oxidation mechanism. *Chemosphere* **2022**, *298*, 134176. [[CrossRef](#)] [[PubMed](#)]
329. Xia, Y.; Li, F.; Jiang, Y.; Xia, M.; Xue, B.; Li, Y. Interface actions between TiO<sub>2</sub> and porous diatomite on the structure and photocatalytic activity of TiO<sub>2</sub>-diatomite. *Appl. Surf. Sci.* **2014**, *303*, 290–296. [[CrossRef](#)]
330. Yang, H.; Yang, J. Photocatalytic degradation of rhodamine B catalyzed by TiO<sub>2</sub> films on a capillary column. *RSC Adv.* **2018**, *8*, 11921–11929. [[CrossRef](#)] [[PubMed](#)]
331. Bui, V.H.; Vu, T.K.; To, H.T.; Negishi, N. Application of TiO<sub>2</sub>-ceramic/UVA photocatalyst for the photodegradation of sulfamethoxazole. *Sustain. Chem. Pharm.* **2022**, *26*, 100617. [[CrossRef](#)]
332. Ke, T.; Shen, S.; Yang, K.; Lin, D. In situ fabrication of Bi<sub>2</sub>O<sub>3</sub>/C<sub>3</sub>N<sub>4</sub>/TiO<sub>2</sub>@C photocatalysts for visible-light photodegradation of sulfamethoxazole in water. *Appl. Surf. Sci.* **2022**, *580*, 152302. [[CrossRef](#)]
333. Gong, H.; Chu, W. Photodegradation of Sulfamethoxazole with a Recyclable Catalyst. *Ind. Eng. Chem. Res.* **2015**, *54*, 12763–12769. [[CrossRef](#)]
334. Akter, S.; Islam Md, S.; Kabir Md, H. UV/TiO<sub>2</sub> photodegradation of metronidazole, ciprofloxacin and sulfamethoxazole in aqueous solution: An optimization and kinetic study. *Arab. J. Chem.* **2022**, *15*, 103900. [[CrossRef](#)]
335. Urda, A.; Radu, T.; Socaci, C. Evaluation of N-doped graphene role in the visible-light driven photodegradation of sulfamethoxazole by a TiO<sub>2</sub>-silver-graphene composite. *J. Photochem. Photobiol. A* **2022**, *425*, 113701. [[CrossRef](#)]
336. Yuan, R.; Zhu, Y.; Zhou, B.; Hu, J. Photocatalytic oxidation of sulfamethoxazole in the presence of TiO<sub>2</sub>: Effect of matrix in aqueous solution on decomposition mechanisms. *Chem. Eng. J.* **2019**, *359*, 1527–1536. [[CrossRef](#)]
337. Mertah, O.; Gómez-Avilés, A.; Kherbeche, A.; Belver, C.; Bedia, J. Peroxymonosulfate enhanced photodegradation of sulfamethoxazole with TiO<sub>2</sub>@CuCo<sub>2</sub>O<sub>4</sub> catalysts under simulated solar light. *J. Environ. Chem. Eng.* **2022**, *10*, 108438. [[CrossRef](#)]
338. Amouhadi, E.; Aliyan, H.; Aghaei, H.; Fazaali, R.; Richeson, D. Photodegradation and mineralization of metronidazole by a novel quadripartite SnO<sub>2</sub>@TiO<sub>2</sub>/ZrTiO<sub>4</sub>/ZrO<sub>2</sub> photocatalyst: Comprehensive photocatalyst characterization and kinetic study. *Mater. Sci. Semicond. Process.* **2022**, *143*, 106560. [[CrossRef](#)]
339. Abbasi-Asl, H.; Sabzehmeidani, M.M.; Ghaedi, M. Efficient degradation of metronidazole antibiotic by TiO<sub>2</sub>/Ag<sub>3</sub>PO<sub>4</sub>/g-C<sub>3</sub>N<sub>4</sub> ternary composite photocatalyst in a continuous flow-loop photoreactor. *J. Environ. Chem. Eng.* **2021**, *9*, 105963. [[CrossRef](#)]
340. Zhang, Y.; Chu, W. Enhanced degradation of metronidazole by cobalt doped TiO<sub>2</sub>/sulfite process under visible light. *Sep. Purif. Technol.* **2022**, *291*, 120900. [[CrossRef](#)]
341. Tran, M.L.; Fu, C.-C.; Juang, R.-S. Effects of water matrix components on degradation efficiency and pathways of antibiotic metronidazole by UV/TiO<sub>2</sub> photocatalysis. *J. Mol. Liq.* **2019**, *276*, 32–38. [[CrossRef](#)]
342. Wang, D.; Luo, H.; Liu, L.; Wei, W.; Li, L. Adsorption characteristics and degradation mechanism of metronidazole on the surface of photocatalyst TiO<sub>2</sub>: A theoretical study. *Appl. Surf. Sci.* **2019**, *478*, 896–905. [[CrossRef](#)]
343. Evgenidou, E.; Chatzialisata, Z.; Tsevis, A. Photocatalytic degradation of a mixture of eight antibiotics using Cu-modified TiO<sub>2</sub> photocatalysts: Kinetics, mineralization, antimicrobial activity elimination and disinfection. *J. Environ. Chem. Eng.* **2021**, *9*, 105295. [[CrossRef](#)]
344. Dudziak, S.; Bielan, Z.; Kubica, P.; Zielinska-Jurek, A. Optimization of carbamazepine photodegradation on defective TiO<sub>2</sub>-based magnetic photocatalyst. *J. Environ. Chem. Eng.* **2021**, *9*, 105782. [[CrossRef](#)]
345. Tashkandi, N.Y.; Albukhari, S.M.; Ismail, A.A. Mesoporous TiO<sub>2</sub> enhanced by anchoring Mn<sub>3</sub>O<sub>4</sub> for highly efficient photocatalyst toward photo-oxidation of ciprofloxacin. *Opt. Mater.* **2022**, *127*, 112274. [[CrossRef](#)]
346. Zhang, X.; Chen, H.; Liu, S.; Zhang, B.; Zhu, H.; Chen, H.; Chen, B.; Chen, L. Preparation of TiO<sub>2</sub>-graphitized carbon composite photocatalyst and their degradation properties for tetracycline antibiotics. *J. Mol. Struct.* **2022**, *1270*, 133897. [[CrossRef](#)]
347. Guo, J.; Gan, W.; Ding, C.; Lu, Y.; Li, J.; Qi, S.; Zhang, M.; Sun, Z. Black phosphorus quantum dots and Ag nanoparticles co-modified TiO<sub>2</sub> nanorod arrays as powerful photocatalyst for tetracycline hydrochloride degradation: Pathways, toxicity assessment, and mechanism insight. *Sep. Purif. Technol.* **2022**, *297*, 121454. [[CrossRef](#)]
348. Bui, H.T.; Thuan, D.V.; Huong, P.T.; Nguyen, K.D.; Nguyen, M.V.; Chu, T.T.H.; Le, Q.V.; Jitae, K.; Devanesan, S.; AlSalhi, M.S.; et al. Enhanced photocatalytic H<sub>2</sub> evolution and photodegradation of antibiotic tetracycline in wastewater by TiO<sub>2</sub>@Ti<sub>3</sub>C<sub>2</sub>. *Int. J. Hydrogen Energy* **2022**. [[CrossRef](#)]
349. Arevalo-Perez, J.C.; Cruz-Romero, D.; Cordero-García, A.; Lobato-García, C.E.; Aguilar-Elguezabal, A.; Torres-Torres, J.G. Photodegradation of 17  $\alpha$ -methyltestosterone using TiO<sub>2</sub>-Gd<sup>3+</sup> and TiO<sub>2</sub>-Sm<sup>3+</sup> photocatalysts and simulated solar radiation as an activation source. *Chemosphere* **2020**, *249*, 126497. [[CrossRef](#)]
350. Awfa, D.; Ateia, M.; Fujii, M.; Johnson, M.S.; Yoshimura, C. Photodegradation of pharmaceuticals and personal care products in water treatment using carbonaceous-TiO<sub>2</sub> composites: A critical review of recent literature. *Water Res.* **2018**, *142*, 26–45. [[CrossRef](#)]

351. Mouele, E.S.M.; Myo, T.Z.M.; Kyaw, H.H.; Tijani, J.O.; Dinu, M.; Pana, I.; Ouardi, Y.E.; Al-Sabahi, J.; Al-Belushi, M.; Sosnin, E.; et al. Degradation of Sulfamethoxazole by Double Cylindrical Dielectric Barrier Discharge System combined with Ti/C-N-TiO<sub>2</sub> supported Nanocatalyst. *J. Hazard. Mater. Adv.* **2022**, *5*, 100051. [[CrossRef](#)]
352. Wu, S.; Lin, Y.; Hu, Y.H. Strategies of tuning catalysts for efficient photodegradation of antibiotics in water environments: A review. *J. Mater. Chem. A* **2021**, *9*, 2592–2611. [[CrossRef](#)]